Functionals of fractional Brownian motion and the three arcsine laws

Tridib Sadhu [1] and Kay Jörg Wiese [2]

[1] *Department of Theoretical Physics, Tata Institute of Fundamental Research, Dr. Homi Bhabha Road, Mumbai 400005, India*

[2] *Laboratoire de Physique de l'Ecole normale supérieure, ENS, Université PSL, CNRS, Sorbonne Université, Université Paris-Diderot, Sorbonne Paris Cité, 24 rue Lhomond, 75005 Paris, France*

(Received 3 June 2021; accepted 30 September 2021; published 15 November 2021)

Fractional Brownian motion is a non-Markovian Gaussian process indexed by the Hurst exponent $H \in (0, 1)$, generalizing standard Brownian motion to account for anomalous diffusion. Functionals of this process are important for practical applications as a standard reference point for nonequilibrium dynamics. We describe a perturbation expansion allowing us to evaluate many nontrivial observables analytically: We generalize the celebrated three *arcsine laws* of standard Brownian motion. The functionals are: (i) the fraction of time the process remains positive, (ii) the time when the process last visits the origin, and (iii) the time when it achieves its maximum (or minimum). We derive expressions for the probability of these three functionals as an expansion in $\varepsilon = H - \frac{1}{2}$, up to second order. We find that the three probabilities are different, except for $H = \frac{1}{2}$, where they coincide. Our results are confirmed to high precision by numerical simulations.

DOI: 10.1103/PhysRevE.104.054112

I. INTRODUCTION

A. Fractional Brownian motion

In the theory of stochastic processes, fractional Brownian motion (fBm) plays as important a role as standard Brownian motion [1–4]. It was introduced [5,6] to incorporate anomalous diffusive transport [7], which is abundant in nature but not describable by standard Brownian motion. Fractional Brownian motion has several key mathematical structures to qualify it as the most fundamental stochastic process for anomalous diffusion: translation invariance in both time and space (stationarity), invariance under rescaling, and Gaussianity [8]. The current mathematical formulation of fBm was given by Mandelbrot and Van Ness [6] to describe correlated time-series in natural processes. It is defined as a Gaussian stochastic process X_t with $X_0 = 0$, mean $\langle X_t \rangle = 0$, and covariance

$$\langle X_t X_s \rangle = t^{2H} + s^{2H} - |t - s|^{2H}. \tag{1}$$

The parameter $H \in (0, 1)$ is the Hurst exponent. An example is given in Fig. 1. Standard Brownian motion corresponds to $H = \frac{1}{2}$ where the covariance reduces to $\langle X_t X_s \rangle = 2 \min(s, t)$.

Fractional Brownian motion is important as it successfully models a variety of natural processes [1,2]: A tagged particle in single-file diffusion ($H = 0.25$) [9–13], the integrated current in diffusive transport ($H = 0.25$) [14], polymer translocation through a narrow pore ($H \simeq 0.4$) [15–17], anomalous diffusion [18], values of the log return of a stock ($H \simeq 0.6$ to 0.8) [19–22], hydrology ($H \simeq 0.72$ to 0.87) [23,24], a tagged monomer in a polymer chain ($H = 0.25$) [25], solar flare activity ($H \simeq 0.57$ to 0.86) [26], the price of electricity in a liberated market ($H \simeq 0.41$) [27], telecommunication networks ($H \simeq 0.78$ to 0.86) [28], telomeres inside the nucleus of human cells ($H \simeq 0.18$ to 0.35) [29], subdiffusion of lipid granules in yeast cells [30], and diffusion inside crowded fluids ($H \simeq 0.4$) [31], are few such examples. Due to the simplicity of its definition, fBm has a fundamental importance, as well as a multitude of potential applications. The pressing questions are how the celebrated properties of standard Brownian motion generalize for fBm, and how can one analyze them? In this paper we aim to address some of these questions.

The anomalous diffusion in fBm comes from the long-range correlations in time, which makes the process non-Markovian, i.e., its increments are not independent, unless $H = \frac{1}{2}$; this can be seen from the correlation of increments,

$$\langle dX_t dX_s \rangle \simeq 2H(2H - 1)(t - s)^{2(H-1)} dt^2, \tag{2}$$

for $t > s \gg dt$ and $dX_t \equiv X_{t+dt} - X_t$. The positivity of correlations for $H > \frac{1}{2}$ means that the process is correlated and the paths appear to be more regular than for standard Brownian motion. The converse holds for $H < \frac{1}{2}$, where increments are anticorrelated, making the process rough on short scales. This can be seen in Fig. 1 for the sample trajectory of a fBm generated in our computer simulation, using the same random numbers for the Fourier modes, which renders the resulting curves comparable.

The non-Markovian dynamics makes a theoretical analysis of fBm difficult. Until now, few exact results are available in the literature [32–34]. In this paper, we describe a systematic theoretical approach to fBm, by constructing a perturbation theory in

$$\varepsilon = H - \tfrac{1}{2} \tag{3}$$

around the Markovian dynamics. We describe this approach with a focus on observables that are functionals of the fBm trajectory X_t, and thereby depend on the entire history of the process. The fraction of time X_t remains positive, the area

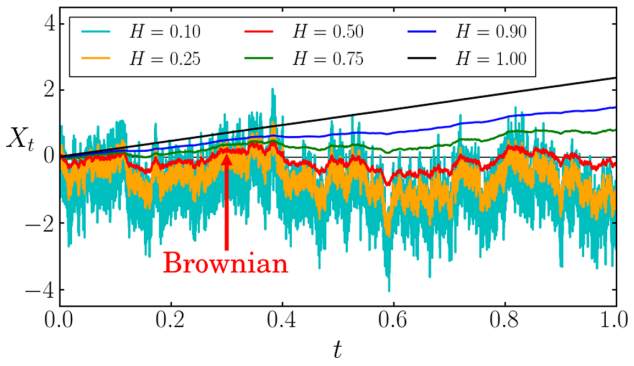

FIG. 1. Sample trajectories of an fBm corresponding to different Hurst exponent (H). Anticorrelation of increments for $H < \frac{1}{2}$ can be seen from larger fluctuations of the trajectories. In comparison, smoother trajectories for $H > \frac{1}{2}$ reflect positive correlations, which become a straight line for $H \to 1$.

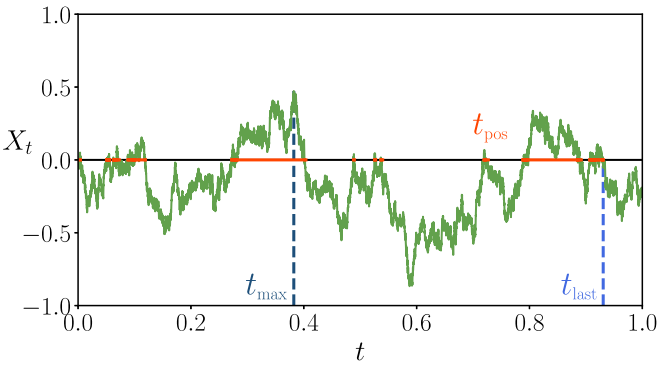

FIG. 2. The three observables $t_{\rm pos}$, $t_{\rm last}$, and $t_{\rm max}$ for a stochastic process starting at the origin. For the standard Brownian motion, all three have the same cumulative probability distribution expressed in terms of arcsine function [42–45].

under X_t, the position of the last maximum, or the time where X_t reaches its maximum are examples of such functionals.

Functionals of stochastic processes are a topic of general interest [35–38]. Beside their relevance in addressing practical problems, they appear in path-ensemble generalizations of traditional statistical mechanics [39,40]. Beyond equilibrium statistical mechanics, the dynamics plays a crucial role in the statistical theory of nonequilibrium systems. Observables that are functionals of a stochastic trajectory, e.g., entropy production, empirical work, integrated current, or activity, are relevant dynamical observables for a thermodynamic description of nonequilibrium systems [41].

The statistics of functionals is nontrivial already for Markovian processes, and is much harder for non-Markovian ones like fBm. In our work, we overcome the inherent difficulty of the non-Markovian dynamics of fBm by using a perturbation expansion around standard Brownian motion ($H = \frac{1}{2}$), which is a Markovian process. This allows us to use many tricks available for Brownian motion, such as the method of images.

B. The three arcsine laws

We illustrate this approach by considering a generalization of a famous result for standard Brownian motion: the three arcsine laws [42–45]. This result is about the following three functionals of a Brownian motion B_t starting from the origin $B_0 = 0$, and evolving during time T (see Fig. 2):

(i) the total duration $t_{\rm pos}$ when the process is positive,
(ii) the last time $t_{\rm last}$ the process visits the origin, and
(iii) the time $t_{\rm max}$ it achieves its maximum (or minimum).

Remarkably, all three functionals have the same probability distribution as a function of $\vartheta := t/T$, given by [42–45]

$$p(\vartheta) = \frac{1}{\pi\sqrt{\vartheta(1-\vartheta)}}\,. \tag{4}$$

As the cumulative distribution contains an arcsine function, these laws are commonly referred to as the *first, second*, and *third* arcsine laws. These laws apply quite generally to Markov processes, i.e., processes where the increments are uncorrelated [43]. Their counterintuitive form with a divergence at $\vartheta = 0$ and $\vartheta = 1$ has sparked a lot of interest, and they are considered among the most important results for stochastic processes. Recent studies led to many extensions, in constrained Brownian motion [46–48], for general stochastic processes [49–54], and even in higher dimensions [55–57]. The laws are realized in a plethora of real-world examples, from finance [58,59] to competitive team sports [60].

Using our perturbative approach, we show how the three arcsine laws generalize for fBm. Our results show that unlike for standard Brownian motion, all three functionals have different probability distributions, which coincide only when $\varepsilon = 0$, i.e., for Brownian motion. As for two of the laws the difference is first seen at second order in ε, we have to develop the technology beyond what was done at leading order [61–68]. Using our perturbation results up to second order, and a scaling ansatz, we propose expressions for all three probability densities. These expressions agree well with our numerical results, even for large values of ε, i.e., including the full range of Hurst exponents reported in the literature cited above [9–30]. A short account of our main results was reported in Ref. [69].

This article is organized in the following order: In Sec. II we discuss basics of an fBm and introduce the perturbation expansion of the action. As a consistency check we derive the free propagator for an fBm in Sec. III, which is checked against the exact result. In the rest of the sections we discuss the three functionals for the arcsine law. In Sec. IV, we summarize our main analytical results for the generalization of the arcsine laws for an fBm, and we compare them with our numerical simulations. How these results are derived is first sketched in Sec. V and thoroughly discussed in later sections. Many algebraic details and a description of our numerical algorithm are given in the Appendices.

II. PERTURBATION THEORY

A. The action to second order in ε

Our analysis is based on a perturbation expansion of the action for an fBm trajectory around standard Brownian motion ($H = \frac{1}{2}$). This expansion was discussed and used earlier in Refs. [61–69] at linear order. Here, we give additional details

at second order, which is essential to show the difference between the generalizations of the three arcsine laws.

An ensemble of trajectories for fBm in a time window $[0, T]$ is characterized by the Gaussian action

$$S[X_t] = \frac{1}{2}\int_0^T dt_1 \int_0^T dt_2 X_{t_1} G(t_1, t_2) X_{t_2}, \tag{5}$$

with covariance $G^{-1}(t_1, t_2) = \langle X_{t_1} X_{t_2}\rangle$ as given in Eq. (1). The probability of a trajectory, up to a normalization, is given by

$$P[X_t] \sim e^{-S[X_t]}. \tag{6}$$

For $H = \frac{1}{2}$ one recovers the Feynman-Kac formula [70] for standard Brownian motion.

Writing $H = \frac{1}{2} + \varepsilon$ and expanding Eq. (5) in powers of ε we obtain (a derivation is in Appendix A)

$$S = \frac{1}{D}\left[S_0 - \frac{\varepsilon}{2} S_1 + \varepsilon^2 S_2 + \cdots\right], \tag{7}$$

where

$$S_0 = \frac{1}{4}\int_0^T dt\, \dot{x}(t)^2, \tag{8a}$$

$$S_1 = \int_0^T dr_1 \int_{r_1+\omega}^T dr_2\, \frac{\dot{x}(r_1)\dot{x}(r_2)}{r_2 - r_1}, \tag{8b}$$

$$S_2 = \frac{1}{2}\int_0^T dr_1 \int_{r_1+\omega}^T dr_2\, \dot{x}(r_1)\dot{x}(r_2)\left[\int_0^{r_1-\omega} \frac{ds}{(r_1 - s)(r_2 - s)} + \int_{r_2+\omega}^T \frac{ds}{(s - r_1)(s - r_2)}\right]. \tag{8c}$$

The prefactor, the diffusion constant, reads

$$D \equiv D(\varepsilon, \omega) = e^{\varepsilon\, 2(1+\ln\omega) - \varepsilon^2\, 2(1-\frac{\pi^2}{6}) + \mathcal{O}(\varepsilon^3)}. \tag{9}$$

The small-time (ultraviolet) cutoff $\omega > 0$ is introduced to regularize the integrals in the action. Our final results are in the limit of $\omega \to 0$, and independent of ω. The second-order term in the exponential in Eq. (9) is independent of ω, since from dimensional arguments $D \sim \omega^{\varepsilon}$. An alternative expression for the second order term of the action was first reported in our earlier work [69].

Remark. To keep our formulas simple, we explicitly write the ultraviolet cutoff in Eqs. (8b) and (8c) only for integrals which would otherwise diverge.

B. Integral representation of the action and normal-ordered form of the weight

For our explicit calculations we use an alternative representation of Eqs. (8b) and (8c):

$$S_1 = \int_0^\Lambda dy \int_0^T dr_1 \int_{r_1}^T dr_2\, \dot{x}(r_1)\dot{x}(r_2) e^{y(r_1 - r_2)}, \tag{10a}$$

and

$$S_2 = \frac{1}{2}\int_0^\Lambda dy_1 \int_0^\Lambda dy_2 \int_0^T dr_1 \int_{r_1}^T dr_2\, \dot{x}(r_1)\dot{x}(r_2) \times \left[\int_0^{r_1} ds\, e^{-y_1(r_1 - s) - y_2(r_2 - s)} + \int_{r_2}^T ds\, e^{-y_1(s - r_1) - y_2(s - r_2)}\right], \tag{10b}$$

where the ultraviolet cutoff ω in time is replaced by an upper limit Λ for the y variables. A vanishing ω is equivalent to $\Lambda \to \infty$, which is always taken in the final results.

Their relation can be inferred as follows: for small ω

$$\int_\omega^\infty \frac{dt}{t} e^{-st} \simeq -\ln(s\,\omega) - \gamma_{\mathrm{E}} + \mathcal{O}(\omega), \tag{11}$$

where $\gamma_{\mathrm{E}} = 0.57721\ldots$ is the Euler constant. However, the integral representation for large Λ reads

$$\int_0^\Lambda dy \int_0^\infty dt\, e^{-ts - ty} \simeq \ln\left(\frac{\Lambda}{s}\right) + \mathcal{O}(\Lambda^{-1}). \tag{12}$$

Demanding that they agree, we get

$$\Lambda = \frac{1}{\omega} e^{-\gamma_{\mathrm{E}}}. \tag{13}$$

In Sec. III we further check Eq. (13) by constructing the free diffusion propagator for fBm. In terms of Λ, Eq. (9) reads

$$D = e^{\varepsilon\, 2(1 - \ln\Lambda - \gamma_{\mathrm{E}}) - \varepsilon^2\, 2(1 - \frac{\pi^2}{6}) + \mathcal{O}(\varepsilon^3)}. \tag{14}$$

Remark. Keeping in mind the ultraviolet cutoff ω present in Eqs. (8b) and (8c), integrals arising from Eq. (10) are interpreted such that

$$\int_{r_1}^T dr_2\, \delta(r_2 - r_1) := \lim_{\omega\to 0} \int_{r_1+\omega}^T dr_2\, \delta(r_2 - r_1) = 0. \tag{15}$$

This convention for the expression of the action is used throughout our analysis.

Remark. A subtle technical point is that at second order for perturbation of the probability in Eq. (6) one encounters a term

$$\frac{S_1^2}{8D^2} = \frac{1}{8D^2}\int_0^T dr_1 \int_{r_1+\omega}^T dr_2\, \frac{\dot{x}(r_1)\dot{x}(r_2)}{r_2 - r_1} \times \int_0^T dr_3 \int_{r_3+\omega}^T dr_4\, \frac{\dot{x}(r_3)\dot{x}(r_4)}{r_4 - r_3}. \tag{16}$$

For the integration range, pairs of time indices coincide and contracting these corresponding pairs of $\dot{x}$ using the action S_0 generates the following terms (see later discussion in Sec. VI C and Appendix M):

$$\frac{S_1^2}{8D^2} \longrightarrow \begin{cases} \frac{1}{4D}\int_{r_1<r_2,r_4} & \frac{\dot{x}(r_2)}{r_2 - r_1}\frac{\dot{x}(r_4)}{r_4 - r_1}, \\ \frac{1}{4D}\int_{r_3<r_1<r_2} & \frac{\dot{x}(r_2)}{r_2 - r_1}\frac{\dot{x}(r_3)}{r_1 - r_3}, \\ \frac{1}{4D}\int_{r_1<r_2<r_4} & \frac{\dot{x}(r_1)}{r_2 - r_1}\frac{\dot{x}(r_4)}{r_4 - r_2}, \\ \frac{1}{4D}\int_{r_1,r_3<r_2} & \frac{\dot{x}(r_1)}{r_2 - r_1}\frac{\dot{x}(r_3)}{r_2 - r_3}, \end{cases}$$

where the cutoffs in the integrations are implicit and the right arrow indicates contraction of a pair of $\dot{x}$. (Contracting all four $\dot{x}$ gives a constant entering into the normalization of

the probability, thus ignored.) The four terms come, in the given order, from the contraction of $\dot{x}(r_1)\dot{x}(r_3)$, $\dot{x}(r_1)\dot{x}(r_4)$, $\dot{x}(r_2)\dot{x}(r_3)$, and $\dot{x}(r_2)\dot{x}(r_4)$ in Eq. (16). They have the same structure as those of S_2 in Eq. (8c), and we can group them together: the first contracted term in Eq. (17) cancels the first term of Eq. (8c), the fourth contracted term in Eq. (17) cancels the last term in Eq. (8c) (note that S_2 comes with a minus sign in the expansion, and the points r_1 and r_2 are ordered); the remaining two contracted terms are identical and can be incorporated into a redefinition of S_2 as discusses below.

These cancellations make it advantageous to exclude self-contractions, i.e., the terms on the r.h.s. of Eq. (17), from e^{-S}, which in field theory is noted as a *normal-ordered* [71] weight,

$$e^{-S} \longrightarrow :e^{-\mathcal{S}^{(\mathrm{n})}}: \tag{17}$$

In this normal-ordered form, the second-order term S_2 is replaced by

$$\mathcal{S}_2^{(\mathrm{n})} = \frac{1}{2}\int_0^\Lambda dy_1 \int_0^\Lambda dy_2 \int_0^T dr_1 \int_{r_1}^T dr_2 \dot{x}(r_1)\dot{x}(r_2) \times \int_{r_1}^{r_2} ds\, e^{-y_1(r_1-s)-y_2(r_2-s)}, \tag{18}$$

(cutoffs are implicit). Using the normal-ordered weight makes our calculations simple and elegant. However, to keep our calculation accessible for a nonspecialist, we present our analysis using the weight in Eq. (10). We shall mention at relevant stages of the calculation which can be simplified using normal ordered weight.

III. THE FREE FBM PROPAGATOR

In this section, we verify the perturbation expansion in Eqs. (7)–(10) by deriving a known result about the propagator of an fBm. The probability for an fBm, starting at $X_0 = 0$, to be at $X_T = m$ at time T is given by

$$\mathcal{G}_H(m,T) = \frac{e^{-\frac{m^2}{4T^{2H}}}}{\sqrt{4\pi T^{2H}}}, \tag{19}$$

which is straightforward to see for the Gaussian process with covariance Eq. (1).

In terms of the action in Eq. (5), the same propagator can be expressed as

$$\mathcal{G}_H(m,T) = \frac{W_H(m,T)}{N_T}, \tag{20}$$

where

$$W_H(m,T) = \int_{x(0)=0}^{x(T)=m} \mathcal{D}[x] e^{-S[x]} \tag{21a}$$

and normalization

$$N_T = \int_{-\infty}^{\infty} dm W_H(m,T). \tag{21b}$$

Eq. (19) can be derived from Eq. (20) using the perturbation expansion (7). For this, we Taylor expand Eq. (19) in ε as

$$\mathcal{G}_H(m,T) = \mathcal{G}(m,T) + \varepsilon\, 2T(\ln T)\partial_m^2 \mathcal{G}(m,T) + \varepsilon^2\left[2(T\ln T)^2\partial_m^4\mathcal{G}(m,T) + 2T(\ln T)^2\partial_m^2\mathcal{G}(m,T)\right] + \cdots, \tag{22}$$

where $\mathcal{G}(m,T)$ (without the subscript H) is the propagator for standard Brownian motion ($H = \frac{1}{2}$) with unit diffusivity. In this section, we restrict our analysis to second order in ε, which is enough to verify formulas (8)–(10). An all-orders analysis is deferred to Appendix C.

Using Eqs. (7) and (14) in Eq. (21) we get

$$W_H(m,T) = W_0(m,T) + \varepsilon\, W_1(m,T) + \varepsilon^2 W_2(m,T) + \cdots,$$

where

$$W_0(m,T) = \int_{x(0)=0}^{x(T)=m} \mathcal{D}[x] e^{-\frac{S_0}{D}}, \tag{23a}$$

$$W_1(m,T) = \frac{1}{2}\int_{x(0)=0}^{x(T)=m} \mathcal{D}[x] e^{-\frac{S_0}{D}} S_1, \tag{23b}$$

$$W_2(m,T) = \int_{x(0)=0}^{x(T)=m} \mathcal{D}[x] e^{-\frac{S_0}{D}}\left[\frac{S_1^2}{8} - (1-\gamma_{\mathrm{E}}-\ln\Lambda)S_1 - S_2\right]. \tag{23c}$$

The second term comes from the order-ε contribution to the diffusion constant (14) inserted into Eq. (7).

Each term in the expansion of W_H can now be evaluated as an average with a Brownian measure of diffusivity D. The path integral measure $\mathcal{D}[x]$ is defined such that the leading term

$$W_0(m,T) = Z_T(0,m) := \frac{e^{-\frac{m^2}{4DT}}}{\sqrt{4\pi DT}} \tag{24}$$

is the normalized propagator $Z_T(0,m)$ for standard Brownian motion with diffusivity D, starting from $x = 0$ at $t = 0$, and ending in $x = m$ at $t = T$. (For $D = 1$, $Z_T(0,m) \equiv \mathcal{G}(m,T)$ in Eq. (22).)

For the linear-order term in Eq. (23b) we use Eq. (10a) and the identity (M11) derived in Appendix M to obtain

$$\int_{x(0)=0}^{x(T)=m} \mathcal{D}[x]\dot{x}(r_1)\dot{x}(r_2) e^{-\frac{S_0}{D}} = \Delta(r_1-r_2) Z_T(0,m), \tag{25}$$

$$\Delta(r_1-r_2) := 2^2 D^2 \partial_m^2 + 2D\,\delta(r_1-r_2). \tag{26}$$

Using the convention in Eq. (15) we get

$$W_1(m,T) = f_1(T) D^2\, 2\, \partial_m^2 Z_T(0,m), \tag{27}$$

$$f_1(T) = \int_0^\Lambda dy \int_0^T dr_1 \int_{r_1}^T dr_2 e^{-y(r_2-r_1)} \simeq T[\ln(T\Lambda e^{\gamma_{\mathrm{E}}}) - 1] + \mathcal{O}(\Lambda^{-1}). \tag{28}$$

For the quadratic term in Eq. (23c) we use Wick's theorem to obtain

$$\int_{x(0)=0}^{x(T)=m} \mathcal{D}[x]\dot{x}(r_1)\dot{x}(r_2)\dot{x}(r_3)\dot{x}(r_4)e^{-\frac{S_0}{D}} = \left(\sum_{\sigma} \Delta(r_{\sigma(1)}-r_{\sigma(2)})\Delta(r_{\sigma(3)}-r_{\sigma(4)})\right) Z_T(0,m), \tag{29}$$

where σ denotes the set of all pairs. Then, using Eqs. (10b) and (15) leads to

$$W_2(m,T) = 2f_1^2(T)D^4\partial_m^4 Z_T(0,m) + [f_5(T)D - 4(1-\gamma_{\rm E}-\ln\Lambda)f_1(T) - 2f_3(T)] \times D^2\partial_m^2 Z_T(0,m) + \tfrac{1}{2}f_6(T)D^2 Z_T(0,m). \tag{30}$$

Here

$$f_5(T) = \int_0^\Lambda dy_1 \int_0^\Lambda dy_2 \int_0^T dr_1 \times \int_{r_1}^T dr_2 \int_0^T dr_3 \int_{r_3}^T dr_4 e^{y_1(r_1-r_2)+y_2(r_3-r_4)} \times [\delta(r_1-r_3)+\delta(r_2-r_4)+\delta(r_1-r_4)+\delta(r_3-r_2)],$$

which simplifies to

$$f_5(T) = 2\int_0^\Lambda dy_1 \int_0^\Lambda dy_2 \int_0^T dr_1 \int_{r_1}^T dr_2 \int_0^T ds\, e^{-y_1|s-r_1|-y_2|s-r_2|}. \tag{31a}$$

The remaining terms are

$$f_3(T) = \int_0^\Lambda dy_1 \int_0^\Lambda dy_2 \int_0^T dr_1 \int_{r_1}^T dr_2 \times \left\{\int_0^{r_1} ds + \int_{r_2}^T ds\right\} e^{-y_1|s-r_1|-y_2|s-r_2|}, \tag{31b}$$

$$f_6(T) = \int_0^\Lambda dy_1 \int_0^\Lambda dy_2 \int_0^T dr_1 \int_{r_1}^T dr_2\, e^{-(y_1+y_2)(r_2-r_1)}. \tag{31c}$$

In a similar calculation, the normalization in Eq. (21) is obtained from Eqs. (24), (27), and (30) as

$$N_T = 1 + \varepsilon^2 \tfrac{1}{2} f_6(T)D^2 + \mathcal{O}(\varepsilon^3).$$

Note that the linear-order term vanishes.

Altogether, from Eq. (20) we get

$$\mathcal{G}_H(m,T) = Z_T(0,m) + \varepsilon\, 2f_1(T)D^2\partial_m^2 Z_T(0,m) + \varepsilon^2\{2f_1^2(T)D^4\partial_m^4 Z_T(0,m) + [f_5(T)D - 2f_3(T) - 4(1-\gamma_{\rm E}-\ln\Lambda)f_1(T)]D^2\partial_m^2 Z_T(0,m)\} + \mathcal{O}(\varepsilon^3). \tag{32}$$

To see that Eq. (32) agrees with Eq. (22) we use Eq. (14) in Eq. (24) and write

$$Z_T(0,m) = \mathcal{G}(m,T) + \varepsilon\, 2(1-\gamma_{\rm E}-\ln\Lambda)T\partial_m^2\mathcal{G}(m,T) + \varepsilon^2\left[2\left((1-\gamma_{\rm E}-\ln\Lambda)^2 - 1 + \frac{\pi^2}{6}\right)T\partial_m^2\mathcal{G}(m,T) + 2(1-\gamma_{\rm E}-\ln\Lambda)^2T^2\partial_m^4\mathcal{G}(m,T)\right] + \cdots.$$

Substituting the above expression of $Z_T(0,m)$ in Eq. (32) and then using Eq. (14) yields

$$\mathcal{G}_H(m,T) = \mathcal{G}(m,T) + \varepsilon\, 2TK_1^2\partial_m^2\mathcal{G}(m,T) + \varepsilon^2[2T^2K_1^2\partial_m^4\mathcal{G}(m,T) + 2TK_2\partial_m^2\mathcal{G}(m,T)] + \cdots, \tag{33}$$

where

$$K_1 = \frac{f_1(T)}{T} + 1 - \gamma_{\rm E} - \ln\Lambda, \tag{34}$$

and

$$K_2 = \frac{f_5(T)-2f_3(T)}{2T} + 2(1-\gamma_{\rm E}-\ln\Lambda)\frac{f_1(T)}{T} + (1-\gamma_{\rm E}-\ln\Lambda)^2 - 1 + \frac{\pi^2}{6}. \tag{35}$$

It is then easy to see from the expression of $f_1(T)$ in Eq. (28) and

$$\frac{1}{2}f_5(T) - f_3(T) = \int_0^\Lambda dy_1 \int_0^\Lambda dy_2 \int_0^T dr_1 \int_{r_1}^T dr_2 \times \int_{r_1}^{r_2} ds e^{-y_1(s-r_1)-y_2(r_2-s)} \simeq T\left\{[\ln T - (1-\gamma_{\rm E}-\ln\Lambda)]^2 + 1 - \frac{\pi^2}{6}\right\} \tag{36}$$

for large Λ, that Eq. (33) agrees with Eq. (22).

Remark. The asymptotics of the integral in Eq. (36) is numerically verified in Mathematica, with results shown in Fig. 3.

Remark. The analog of the integral in Eq. (36) with ultraviolet cutoff ω in time is

$$\int_0^{T-2\omega} dr_1 \int_{r_1+2\omega}^T dr_2 \int_{r_1+\omega}^{r_2-\omega} ds\, \frac{1}{(s-r_1)(r_2-s)}.$$

As a consistency check we verified that for small ω, and using the identification Eq. (13), the integral yields the asymptotics in Eq. (36).

Remark. In our derivation of Eq. (22) using Eq. (7) we interchanged the small-ε and large-Λ limits. Agreement of the final result in Eq. (22) shows that this step is justified. We assume the same property in our perturbation analysis in the observables of the three arcsine laws.

Remark. The analysis would be simpler with the normal-ordered action in Eq. (17), because then terms f_5 and f_6 in Eq. (30) vanish.

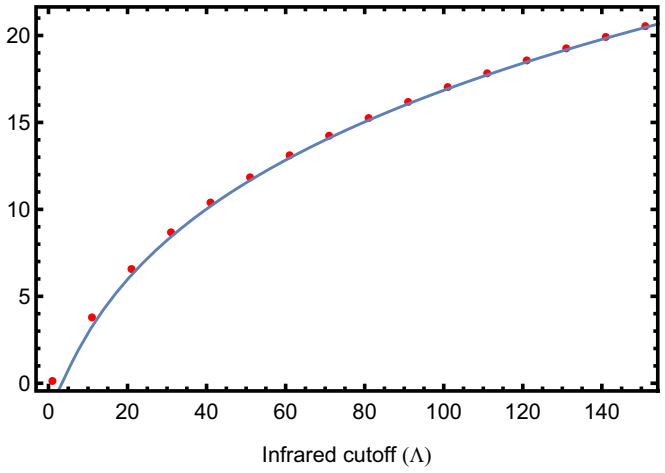

FIG. 3. A comparison of the integral in Eq. (36) (indicated by red points) with its asymptotic (indicated by solid line) for large Λ and $T = 1$.

IV. A GENERALIZATION OF THE THREE ARCSINE LAWS

Unlike for standard Brownian motion, the probabilities for the three observables $t_{\rm last}$, $t_{\rm max}$, and $t_{\rm pos}$ all differ. Self-affinity of an fBm (invariance under rescaling of space with T^H) means that the three probabilities are a function of the rescaled variable $\vartheta = t/T$ (t being $t_{\rm last}$, $t_{\rm max}$, $t_{\rm pos}$). They can be written as

$$p_{\rm last}(\vartheta) = \frac{\mathcal{N}_{\rm last}}{\pi\, \vartheta^H (1-\vartheta)^{1-H}}\, {\rm e}^{\mathcal{F}^{\rm last}(\vartheta,H)}, \tag{37}$$

$$p_{\rm max}(\vartheta) = \frac{\mathcal{N}_{\rm max}}{\pi\, [\vartheta(1-\vartheta)]^H}\, {\rm e}^{\mathcal{F}^{\rm max}(\vartheta,H)}, \tag{38}$$

$$p_{\rm pos}(\vartheta) = \frac{\mathcal{N}_{\rm pos}}{\pi\, [\vartheta(1-\vartheta)]^H}\, {\rm e}^{\mathcal{F}^{\rm pos}(\vartheta,H)}. \tag{39}$$

The divergences in the prefactor of the exponential terms are predicted using a scaling argument (discussed in Sec. IV B) for $\vartheta \to 0$ and $\vartheta \to 1$. They are linked to earlier results about the persistence exponent $\Theta = 1 - H$ [32,33,61]. The terms $\mathcal{F}$ in the exponential are nontrivial and *remain finite over the full range of* ϑ. We use the convention that the integral of each $\mathcal{F}$ function over ϑ vanishes, which together with the normalization $\int_0^1 d\vartheta\, p(\vartheta) = 1$ fixes the constants $\mathcal{N}$.

For $H = \frac{1}{2}$, all three $\mathcal{F}$ functions vanish, $H = 1 - H$, and the expressions (37) to (39) reduce to the same well-known result of standard Brownian motion ("arcsine law"). For $H \neq \frac{1}{2}$, they can be written as a perturbation expansion in $\varepsilon = H - \frac{1}{2}$,

$$\mathcal{F}^{\rm last}(\vartheta, H) = \varepsilon\, \mathcal{F}_1^{\rm last}(\vartheta) + \varepsilon^2 \mathcal{F}_2^{\rm last}(\vartheta) + \cdots, \tag{40a}$$

$$\mathcal{F}^{\rm max}(\vartheta, H) = \varepsilon\, \mathcal{F}_1^{\rm max}(\vartheta) + \varepsilon^2 \mathcal{F}_2^{\rm max}(\vartheta) + \cdots, \tag{40b}$$

$$\mathcal{F}^{\rm pos}(\vartheta, H) = \varepsilon\, \mathcal{F}_1^{\rm pos}(\vartheta) + \varepsilon^2 \mathcal{F}_2^{\rm pos}(\vartheta) + \cdots. \tag{40c}$$

For the leading-order terms we find

$$\mathcal{F}_1^{\rm last}(\vartheta) = 0, \tag{41a}$$

and

$$\mathcal{F}_1^{\rm max}(\vartheta) = \mathcal{F}_1^{\rm pos}(\vartheta) = 2 - \frac{\pi^2}{2} + \psi\left(\sqrt{\frac{\vartheta}{1-\vartheta}}\right), \tag{41b}$$

with

$$\psi(x) = \frac{2}{x}\arctan(x) + 2\,x \arctan\left(\frac{1}{x}\right). \tag{41c}$$

This is the simplest form we found. Alternative expressions were given in Refs. [62–64,66], using that $\arctan(x) + \arctan(\frac{1}{x}) = \frac{\pi}{2}$. Yet another equivalent form is given in Eq. (6) of [69]. We note that the expression (41b) is symmetric under $\vartheta \to 1 - \vartheta$. This can be understood from the symmetry of the problem. We do not have an intuitive understanding of the equality of $\mathcal{F}_1^{\rm pos}$ and $\mathcal{F}_1^{\rm max}$, while the vanishing of $\mathcal{F}_1^{\rm last}$ in Eq. (41) can easily be understood from perturbation theory [66].

Expressions for the subleading terms $\mathcal{F}_2$ can be written as integrals, which are hard to evaluate analytically. For $t_{\rm last}$, it is given up to an additive constant by

$$\mathcal{F}_2^{\rm last}(\vartheta) = \int_0^\infty \frac{dy_1 dy_2}{y_1^2 y_2^2}\, \Psi^{\rm last}\left(y_1, y_2, \frac{1-\vartheta}{\vartheta}\right), \tag{42a}$$

where $\Psi^{\rm last}(y_1, y_2, z)$ is symmetric in (y_1, y_2) and given by

$$\begin{aligned}\Psi^{\rm last}(y_1, y_2, z) = {} & 2\sqrt{(1+y_1+y_2)z} \\ & \times (1 - \sqrt{1+y_1} - \sqrt{1+y_2} \\ & + \sqrt{1+y_1+y_2})(\sqrt{z} - \Theta(z-y_1)\sqrt{z-y_1} \\ & - \Theta(z-y_2)\sqrt{z-y_2} \\ & + \Theta(z-y_1-y_2)\sqrt{z-y_1-y_2}),\end{aligned} \tag{42b}$$

with $\Theta(x)$ being the Heaviside step function. An alternative formula for $\mathcal{F}_2^{\rm last}$ was reported in our earlier work [69]. Expressions for $\mathcal{F}_2^{\rm max}$ and $\mathcal{F}_2^{\rm pos}$ are cumbersome and given later.

In order that the reader can use our results, we give simple but rather precise approximations for the results obtained after numerical integration.

$$\begin{aligned}\mathcal{F}_2^{\rm last}(\vartheta) \simeq {} & -17.92401 + 13.30207\sqrt{\vartheta} \\ & - 2.16604\sqrt{1-\vartheta} + 8.30059\vartheta + 11.59529\vartheta^{\frac{3}{2}} \\ & + 13.23121(1-\vartheta)^{\frac{3}{2}} - 10.74274\vartheta^2,\end{aligned} \tag{43}$$

$$\begin{aligned}\mathcal{F}_2^{\rm max}(\vartheta) \simeq {} & -0.431001 + 1.69259[\vartheta(1-\vartheta)]^{\frac{1}{2}} \\ & - 1.93367[\vartheta(1-\vartheta)] + 1.3572[\vartheta(1-\vartheta)]^{\frac{3}{2}} \\ & - 0.33995[\vartheta(1-\vartheta)]^2,\end{aligned} \tag{44}$$

$$\begin{aligned}\mathcal{F}_2^{\rm pos}(\vartheta) \simeq {} & -0.842235 + 1.76479[\vartheta(1-\vartheta)]^{\frac{1}{2}} \\ & + 3.70810[\vartheta(1-\vartheta)] - 9.71973[\vartheta(1-\vartheta)]^{\frac{3}{2}} \\ & + 7.40511[\vartheta(1-\vartheta)]^2.\end{aligned} \tag{45}$$

These approximate functions were reported in our earlier work [69]. These are estimated respecting symmetries in the problem, i.e., that $\mathcal{F}_2^{\rm pos}(\vartheta)$ and $\mathcal{F}_2^{\rm max}(\vartheta)$ are symmetric under the exchange of $\vartheta \to 1 - \vartheta$ while $\mathcal{F}_2^{\rm last}(\vartheta)$ is not.

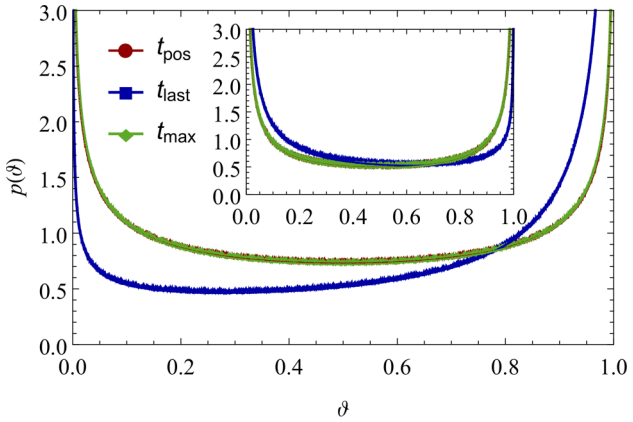

FIG. 4. Numerical simulation results for the probability of the three observables t_{last}, t_{max}, and t_{pos} for an fBm with $H = 0.33$. The inset shows the probabilities for $H = 0.66$. Note that the distributions of t_{pos} and t_{max} are almost indistinguishable.

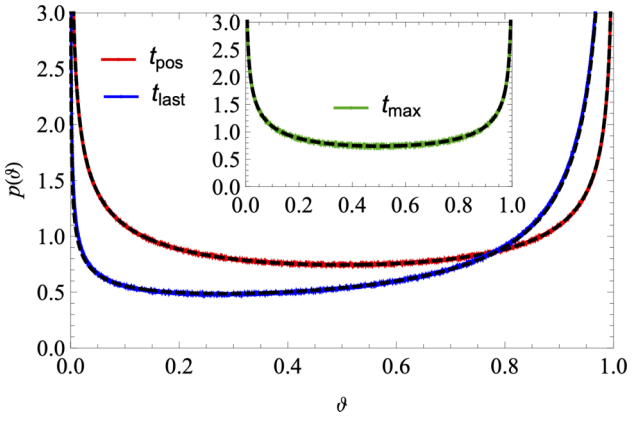

FIG. 5. A comparison of the data shown in Fig. 4 with their theoretical formula (37)–(39). The dashed lines are for theoretical results. The distribution $p_{max}(\vartheta)$ is shown in the inset as it is almost indistinguishable from the distribution $p_{pos}(\vartheta)$.

Remark. We stated above that $p_{pos}(\vartheta)$ and $p_{max}(\vartheta)$ are symmetric around $\vartheta = \frac{1}{2}$, while $p_{last}(\vartheta)$ is not (except for $H = \frac{1}{2}$). Symmetry of the first two probabilities is due to the observation that x_t and $X_T - x_{T-t}$ have the same law. For p_{last} the asymmetry is easy to see from the almost-straight-line trajectories for $H \simeq 1$ in Fig. 1, which makes $\vartheta = 0$ the most probable value. This is reflected in the small-ϑ divergence of the distribution (37) in the limit of $H \to 1$.

A. Comparison with numerical results

An efficient implementation of fBm on a computer is nontrivial due to its long-range correlations in time. For this paper, we use the Davis-Harte algorithm [72,73], which generates sample trajectories drawn from a Gaussian probability with covariance (1) in a time of order $N \ln(N)$, given N equally spaced discretization points. Details of this algorithm are given in Appendix D. Interestingly, for the first-passage time, recently an algorithm was introduced which grows as $\ln(N)^3$, albeit accepting a small error probability [68,74,75], allowing for even more precise estimates.

Results for the three probabilities from our computer simulations are shown in figure 4 for $H = 0.33$. They are obtained by averaging over 5×10^9 sample trajectories, each generated with 2^{13} discrete-time steps. The two distributions $p_{max}(\vartheta)$ and $p_{pos}(\vartheta)$ are almost indistinguishable, as predicted in their theoretical expressions in Eqs. (38) and (39). These numerical results were first reported in our earlier work [69].

Figure 4 also shows that $p_{last}(\vartheta)$ behaves markedly differently from the other two distributions; especially, it is asymmetric under the exchange $\vartheta \to 1 - \vartheta$. This asymmetry in exponents is reversed around $H = \frac{1}{2}$, as shown in the inset of figure 4. This can be seen in the scaling form in Eq. (37).

A comparison of numerical data for $H = 0.33$ with their corresponding theoretical result in Eqs. (37)–(39) are shown in Fig. 5. They are in excellent agreement. Deviations are visible for higher values of H as shown in Fig. 6 for a set of increasing values of $H \geqslant \frac{1}{2}$. We see a perfect agreement between theoretical and numerical results for $H = \frac{1}{2}$, (i.e., $\varepsilon = 0$). The agreement is very good for small $\varepsilon = H - \frac{1}{2}$, but deviations can be seen as ε is increased beyond $|\varepsilon| \approx 0.25$, i.e., $H \leqslant 0.25$ or $H \geqslant 0.75$.

The difference between p_{last} and p_{max} first appears in the second-order term $\mathcal{F}_2$ in Eq. (40). In Fig. 7 we plot our theoretical results of $\mathcal{F}_2(\vartheta)$ alongside the results from computer simulations. This give a finer verification of our theory. To illustrate this procedure, we use Eq. (39) to define

$$\mathcal{F}^{pos}_{2,\varepsilon}(\vartheta) := \frac{1}{\varepsilon}\left[\frac{1}{\varepsilon}\ln\left(p_{pos}(\vartheta)\frac{[\vartheta(1-\vartheta)]^H}{\mathcal{N}}\right) - \mathcal{F}^{pos}_1(\vartheta)\right]. \tag{46}$$

Then, $\mathcal{F}^{pos}_{2,\varepsilon}(\vartheta) = \mathcal{F}^{pos}_2(\vartheta) + \mathcal{O}(\varepsilon)$ and it contains all terms in the exponential in Eq. (39) except $\mathcal{F}^{pos}_1(\vartheta)$. We can further improve this estimate by observing that the subleading term in $\mathcal{F}^{pos}_{2,\varepsilon}(\vartheta)$ is odd in ε. Define

$$\overline{\mathcal{F}}^{pos}_{2,\varepsilon}(\vartheta) := \tfrac{1}{2}\left[\mathcal{F}^{pos}_{2,\varepsilon}(\vartheta) + \mathcal{F}^{pos}_{2,-\varepsilon}(\vartheta)\right], \tag{47}$$

then $\overline{\mathcal{F}}^{pos}_{2,\varepsilon}(\vartheta)$ differs from the theoretical $\mathcal{F}^{pos}_2(\vartheta)$ by order ε^2 or higher, for small ε, equivalent to an order ε^4 correction to $p_{last}(\vartheta)$.

A comparison of $\overline{\mathcal{F}}^{pos}_{2,\varepsilon}(\vartheta)$ extracted from numerical simulations of $p_{pos}(\vartheta)$ to the theoretical result of $\mathcal{F}^{pos}_2(\vartheta)$ is shown in Fig. 7 for $\varepsilon = \pm\frac{1}{6}$ (i.e., for $H = \frac{2}{3}$ and $\frac{1}{3}$). The figure also contains a similar comparison for $\mathcal{F}^{last}_2(\vartheta)$ and $\mathcal{F}^{max}_2(\vartheta)$, with their corresponding numerical results. One sees the excellent agreement between results from our theory and numerical simulations. We remind that these are *sub-sub-leading* corrections, almost indiscernible in the probability density $p(\vartheta)$ shown on Fig. 5.

An important observation from Fig. 7 is that for all three observables $\mathcal{F}_2(\vartheta)$ is finite in the entire range of ϑ. We note that the amplitude of $\mathcal{F}^{last}_2(\vartheta)$ is about ten times larger than $\mathcal{F}^{pos}_2(\vartheta)$ and $\mathcal{F}^{max}_2(\vartheta)$. The former also shows the largest deviations from our theoretical result, especially for $\vartheta \to 0$. These indicate the presence of subleading terms of order ε^4, or higher in p.

The difference between $p_{pos}(\vartheta)$ and $p_{max}(\vartheta)$ first appears at second order in perturbation theory. To underline that

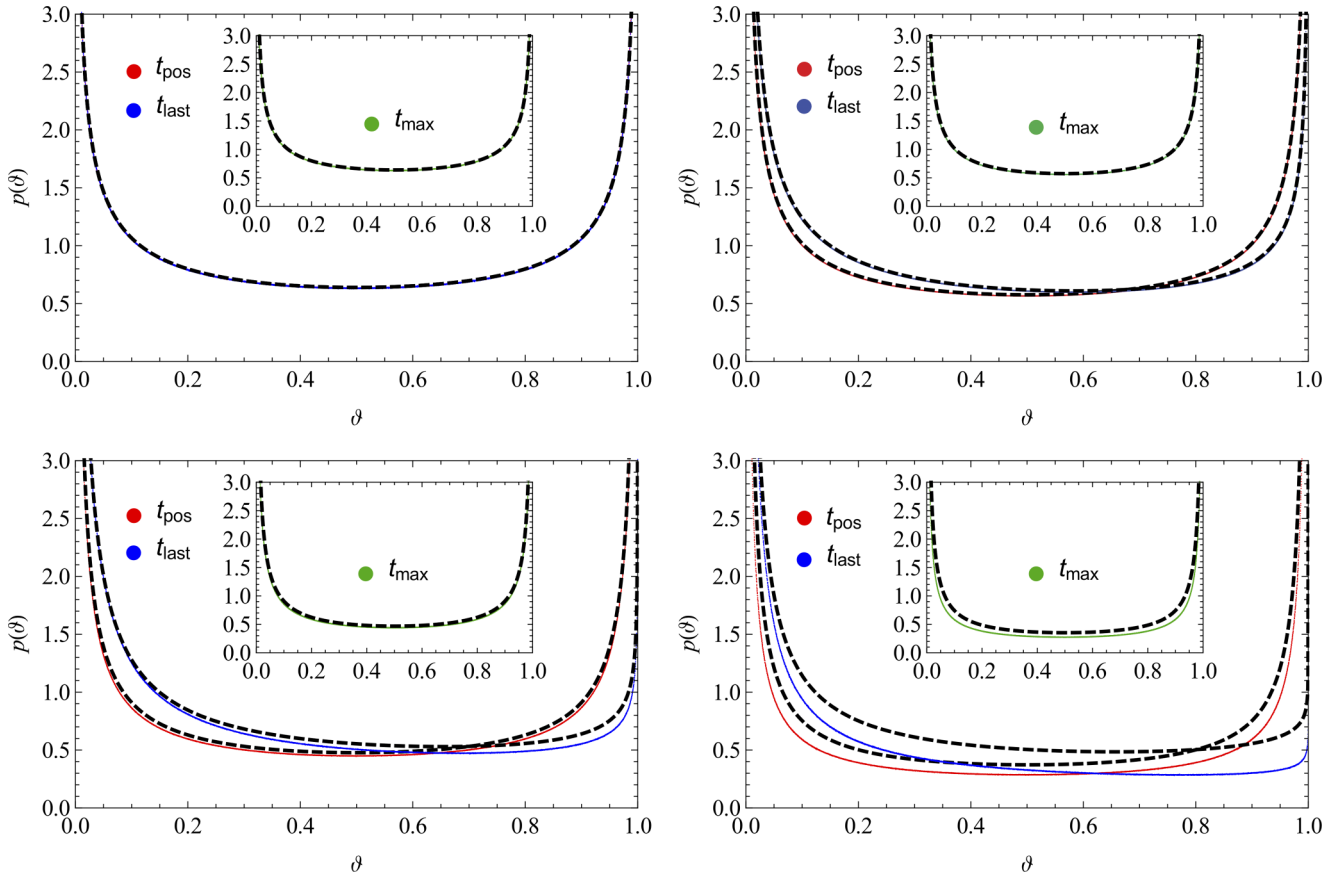

FIG. 6. A comparison of the theoretical formulas in Eqs. (37)–(39) with their corresponding numerical simulation result of an fBm at diffrent values of $H \geqslant \frac{1}{2}$: $H = 0.5$, 0.6, 0.75 and 0.9. The dashed lines are the theoretical results, the continuous lines the numerical results. These numerical results were first reported in our earlier work [69].

$\mathcal{F}_2^{\rm pos}(\vartheta)$ and $\mathcal{F}_2^{\rm max}(\vartheta)$ in Eqs. (44) and (45) are distinct functions, we show in Fig. 8 their difference

$$\delta\mathcal{F}_2(\vartheta) = \mathcal{F}_2^{\rm max}(\vartheta) - \mathcal{F}_2^{\rm pos}(\vartheta) = \lim_{\varepsilon\to 0}\frac{1}{\varepsilon^2}\ln\left(\frac{p_{\rm max}(\vartheta)}{p_{\rm pos}(\vartheta)}\right). \quad (48)$$

The theoretical result of the difference shows excellent agreement with the numerical data for $\overline{\mathcal{F}}_{2,\varepsilon}^{\rm max}(\vartheta) - \overline{\mathcal{F}}_{2,\varepsilon}^{\rm pos}(\vartheta)$ defined following the same conventions as in Eq. (47). This proves that the laws for $t_{\rm max}$ and $t_{\rm pos}$ are indeed different. Larger fluctuations in Figs. 7 and 8 compared to similar figures in our earlier work [69] are due to difference in their sample sizes.

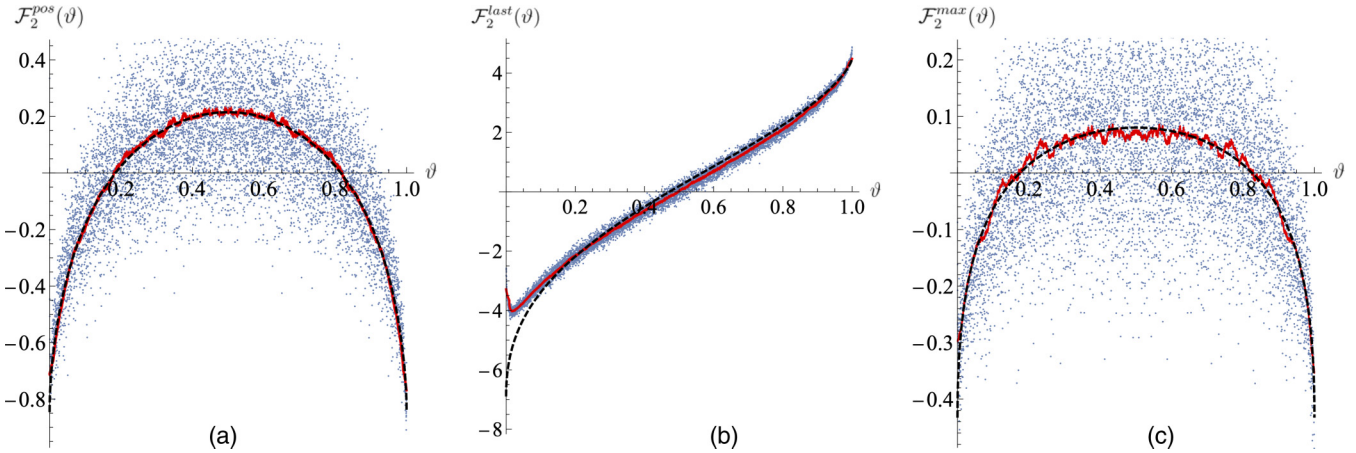

FIG. 7. A comparison of the three $\mathcal{F}_2(\vartheta)$ obtained analytically (black dashed lines) and their measurement using Eq. (47) with $\varepsilon = \pm\frac{1}{6}$. From left to right the figures correspond to $\mathcal{F}_2$ for (*a*) positive time, (*b*) time for the last visit to the origin, and (*c*) time for the maximum. The scattered dots are the raw data from trajectories of $N = 2^{13}$ time steps, averaged over $\sim 10^9$ samples, which are coarse grained by a factor of 100 to give the red curve. The apparent chopping of the data is due to the plot range of the figure.

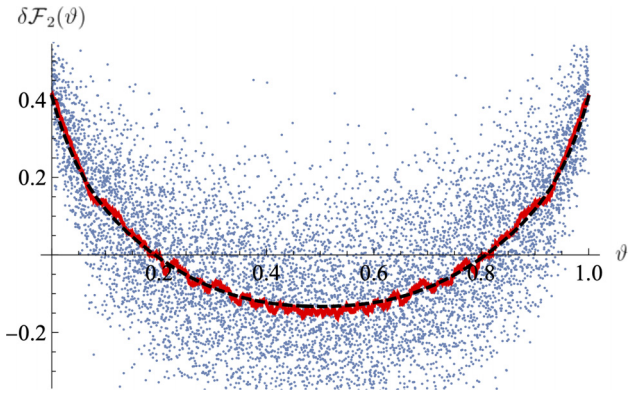

FIG. 8. The difference $\delta\mathcal{F}_2(\vartheta) = \mathcal{F}_2^{\max}(\vartheta) - \mathcal{F}_2^{\rm pos}(\vartheta)$ using the same conventions as in Fig. 7. This plot quantifies the difference between the distribution of $t_{\max}$ and $t_{\rm pos}$. The apparent chopping of the data is due to the plot range of the figure.

B. Scaling analysis

The prefactor of the exponential in Eqs. (37)–(39) can be predicted using scaling arguments. The simplest one is $p_{\rm last}(\vartheta)$, which is the probability that the fBm is at the origin at time ϑ and does not return for the remaining time $1-\vartheta$. (We put the total time $T=1$, s.t. $\vartheta = t$.) The probability for the first part of the event scales as ϑ^{-H}, see Eq. (19). The second part scales as $\vartheta^{-\theta}$, where $\theta = 1-H$ is the persistent exponent [32,33,61]. Combining the two gives the prefactor in Eq. (37).

The scaling argument for $p_{\max}(\vartheta)$ is more involved, and was first discussed in Refs. [61,64,66]. One starts with the relation

$$\mathcal{P}_T(m) = \frac{d\mathcal{S}_T(m)}{dm}, \tag{49}$$

where $\mathcal{P}_T(m)$ is the probability for the position of the maximum m for an fBm in a time interval T started at the origin; $\mathcal{S}_T(m)$ is the survival probability up to time T for an fBm started at $m>0$, in presence of an absorbing wall at the origin. Self-affinity of an fBm suggests the scaling form

$$\mathcal{P}_T(m) = \frac{1}{T^H} g_1\left(\frac{m}{T^H}\right); \quad \mathcal{S}_T(m) = g_2\left(\frac{m}{T^H}\right), \tag{50}$$

which leads to

$$g_1(x) = g_2'(x). \tag{51}$$

To be consistent with the result for the persistence exponent [32,33], one must have $g_2(x) \sim x^{\frac{\theta}{H}}$ for small x. This leads to $g_1(x) \sim x^{\frac{\theta}{H}-1}$, equivalent to

$$\mathcal{P}_T(m) \sim \frac{m^{\frac{\theta}{H}-1}}{T^\theta} \quad \text{for small m.} \tag{52}$$

To relate to the distribution $P_T(t_{\max})$ of $t_{\max}$ we use that at small $t_{\max}$ the maximum m is also small and $m \sim t_{\max}^H$. This leads to

$$P_T(t_{\max}) = \mathcal{P}_T(m)\frac{dm}{dt_{\max}} \sim \frac{1}{t_{\max}}\left(\frac{t_{\max}}{T}\right)^\theta. \tag{53}$$

Substituting $\theta = 1-H$ one gets

$$P_T(t_{\max}) \sim \frac{1}{T}\left(\frac{t_{\max}}{T}\right)^{-H}, \tag{54}$$

and equivalently

$$p_{\max}(\vartheta) = T\,P_T(\vartheta\,T) \sim \vartheta^{-H} \quad \text{for small } \vartheta. \tag{55}$$

Using the symmetry of the probability $p_{\max}(\vartheta)$ under $\vartheta \to 1-\vartheta$ one gets $(1-\vartheta)^{-H}$ for $\vartheta \to 1$. This gives the prefactor in Eq. (38).

A similar argument relating to the persistent exponent [76] can be constructed for the distribution of $t_{\rm pos}$. For $t_{\rm pos} \ll T$, probability $P_T(t_{\rm pos})$ for an fBm to remain positive of net $t_{\rm pos}$ time, relates to persistence probability for the fBm to stay negative for most of its total duration T. This means, for $1 \ll t_{\rm pos} \ll T$,

$$P_T(t_{\rm pos}) \sim T^{-\theta}, \tag{56}$$

with the persistent exponent θ. For this T-dependence to be consistent with the rescaled probability $P_T(\vartheta\,T) = \frac{1}{T}p_{\rm pos}(\vartheta)$, one must have

$$p_{\rm pos}(\vartheta) \sim \vartheta^{\theta-1} \quad \text{for } \vartheta \to 0, \tag{57}$$

giving the small ϑ divergence in Eq. (39). The symmetry under $\vartheta \to 1-\vartheta$ gives the divergence near $\vartheta \to 1$.

C. Comparison to an exact result

In Ref. [12] the first few moments of $t_{\rm pos}$ were calculated analytically for an fBm of $H = \frac{1}{4}$. It is straightforward to generalize this analysis for arbitrary H. For the fraction of positive time $\vartheta = t_{\rm pos}/T$, we obtain the first three moments: $\langle\vartheta\rangle = \frac{1}{2}$ (obvious from the symmetry of the distribution),

$$\langle\vartheta^2\rangle = \frac{1}{4} + \frac{1}{2\pi}\int_0^1 dr\, \arcsin R(r), \tag{58a}$$

$$\langle\vartheta^3\rangle = \frac{1}{8} + \frac{3}{4\pi}\int_0^1 dr\, \arcsin R(r), \tag{58b}$$

where

$$R(r) = \frac{1}{2r^H}[1 + r^{2H} - (1-r)^{2H}]. \tag{58c}$$

It is hard to determine higher moments. The problem maps to the calculation of orthant probability that all coordinates of a multivariate Gaussian of zero mean is positive. A closed form solution of the orthant probability is still unsolved [77].

A perturbation expansion of Eq. (58) in $\varepsilon = H - \frac{1}{2}$ gives

$$\langle\vartheta^2\rangle = \frac{3}{8} + \frac{\varepsilon}{4}(\ln 4 - 1) + \frac{\varepsilon^2}{24}(6\ln^2 4 - \pi^2) + \cdots, \tag{59a}$$

$$\langle\vartheta^3\rangle = \frac{5}{16} + \frac{3\varepsilon}{8}(\ln 4 - 1) + \frac{\varepsilon^2}{16}(6\ln^2 4 - \pi^2) + \cdots. \tag{59b}$$

Terms up to linear order are reproduced using our perturbation result Eq. (39). The ε^2 order terms (0.0693 for $\langle\vartheta^2\rangle$ and 0.1040 for $\langle\vartheta^3\rangle$) obtained using the numerical approximation Eq. (45) agree with the exact result in Eq. (59) up to the third decimal place. [This is a 0.2% disagreement, as apposed to a 40% disagreement if $\mathcal{F}_2^{\rm pos}$ is ignored in Eq. (40c).]

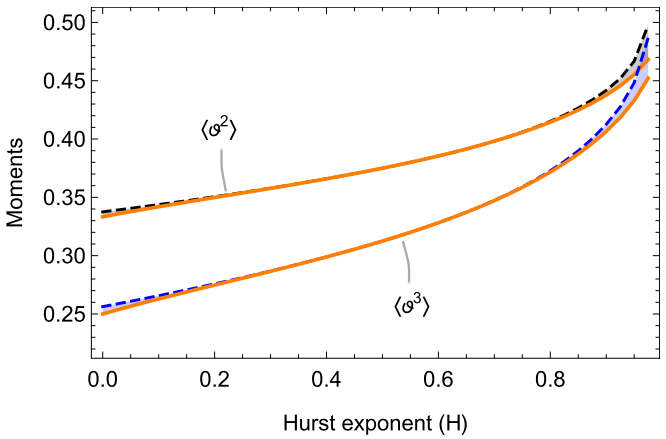

FIG. 9. Second and third moment for the fraction of positive time $\vartheta = t_{\rm pos}/T$ as a function of the Hurst exponent H. The solid lines are the exact result in Eq. (58), whereas the dashed lines denote their result obtained using Eq. (39) with $\mathcal{F}^{\rm pos}$ in Eq. (40) up to second order. The difference is noticeable for H far from $\frac{1}{2}$, indicating corrections from higher-order terms in Eq. (40).

A comparison of the exact result for the moments with their results obtained using Eq. (39) is shown in Fig. 9.

V. OVERVIEW OF THEORETICAL ANALYSIS

Before we present details of the derivation for Eqs. (37)–(39), we give an overview of our approach. Our calculation is done using a double Laplace transformation $\mathcal{D}$ for the probability $P_T(\tau)$, defined by

$$\widetilde{P}(\lambda, s) = \underset{T\to s}{\mathscr{D}_{\tau\to\lambda}} \odot P_T(\tau), \tag{60}$$

with

$$\underset{T\to s}{\mathscr{D}_{\tau\to\lambda}} \odot P_T(\tau) := \int_0^\infty dT \int_0^T d\tau\; e^{-sT-\lambda\tau}\; P_T(\tau). \tag{61}$$

For the rescaled probability $p(\vartheta) := T\,P_T(\vartheta\,T)$ and its Laplace transform

$$\widetilde{p}(\kappa) = \int_0^\infty d\vartheta\; e^{-\kappa\,\vartheta}\, p(\vartheta), \tag{62}$$

the $\mathscr{D}$-transformation gives

$$\widetilde{P}(\lambda, s) = \frac{1}{s}\widetilde{p}\left(\frac{\lambda}{s}\right), \quad \text{with} \quad \widetilde{p}(\kappa) = \int_0^1 d\vartheta\; \frac{p(\vartheta)}{1+\kappa\,\vartheta}. \tag{63}$$

Complex analysis using the residue theorem gives the corresponding inverse transformation (see Appendix E for a derivation),

$$p(\vartheta) = \frac{1}{2\pi\,i} \lim_{\delta\to 0^+} \frac{\widetilde{p}\left(-\frac{1}{\vartheta} - i\delta\right) - \widetilde{p}\left(-\frac{1}{\vartheta} + i\delta\right)}{\vartheta}. \tag{64}$$

Equivalently, one can write

$$p(\vartheta) = \frac{1}{2\pi\,i} \lim_{\phi\to\pi^-} \left[\kappa\;\widetilde{p}(\kappa) - \kappa^\star \widetilde{p}(\kappa^\star)\right]_{\kappa=\frac{e^{i\phi}}{\vartheta}}, \tag{65}$$

where the limit is taken from ϕ below π, and the star ($\star$) denotes complex conjugation.

The analysis can be simplified by considering the form of results in Eqs. (37)–(39) expected from scaling arguments. We write

$$p(\vartheta) = \frac{e^{\mathcal{F}(\vartheta,H)-(H-\frac{1}{2})\mathcal{R}(\vartheta)}}{\pi\sqrt{\vartheta(1-\vartheta)}}, \tag{66}$$

with $\mathcal{R}(\vartheta) = \ln\frac{\vartheta}{(1-\vartheta)}$ for $t_{\rm last}$ and $\mathcal{R}(\vartheta) = \ln\vartheta(1-\vartheta)$ for $t_{\rm max}$ and $t_{\rm pos}$. [In writing Eq. (66) the normalization constant $\mathcal{N}$ from Eqs. (37)–(39) is absorbed in $\mathcal{F}$.] Then, from Eqs. (65) and (66) we write

$$\widetilde{p}(\kappa) = \frac{e^{\widetilde{\mathcal{F}}(\kappa,H)}}{\sqrt{1+\kappa}}, \tag{67}$$

such that

$$e^{\mathcal{F}(\vartheta,H)-(H-\frac{1}{2})\mathcal{R}(\vartheta)} = \mathcal{K}^{-1}_{\kappa\to\vartheta} \odot e^{\widetilde{\mathcal{F}}(\kappa,H)}. \tag{68}$$

Here we define the transformation

$$\mathcal{K}^{-1}_{\kappa\to\vartheta} \odot f(\kappa) \equiv \lim_{\phi\to\pi-} \mathscr{R}\left[f\left(\frac{e^{i\phi}}{\vartheta}\right)\right], \tag{69}$$

with $\mathscr{R}$ denoting the real part.

In our derivation of the probabilities in Eqs. (37)–(39), we first calculate $\widetilde{\mathcal{F}}(\kappa, H)$, and then use Eq. (68) to obtain $\mathcal{F}(\vartheta, H)$. To do this order by order in a perturbation expansion in $\varepsilon = H - \frac{1}{2}$, write

$$\widetilde{\mathcal{F}}(\kappa, H) = \varepsilon\;\widetilde{\mathcal{F}}_1(\kappa) + \varepsilon^2\widetilde{\mathcal{F}}_2(\kappa) + \mathcal{O}(\varepsilon^3). \tag{70a}$$

Using this expansion in Eq. (68) we get Eq. (40) with

$$\mathcal{F}_1(\vartheta) = \mathcal{R}(\vartheta) + \mathcal{K}^{-1}_{\kappa\to\vartheta} \odot \widetilde{\mathcal{F}}_1(\kappa), \tag{70b}$$

$$\mathcal{F}_2(\vartheta) = -\tfrac{1}{2}[\mathcal{F}_1(\vartheta) - \mathcal{R}(\vartheta)]^2 + \mathcal{K}^{-1}_{\kappa\to\vartheta} \odot \left[\widetilde{\mathcal{F}}_2(\kappa) + \tfrac{1}{2}\widetilde{\mathcal{F}}_1(\kappa)^2\right]. \tag{70c}$$

Remark. For completeness and for verification purposes, let us write the inverse transformation of Eq. (69),

$$\mathcal{K}_{\vartheta\to k} \odot f(\vartheta) := \frac{1}{\pi}\int_0^1 d\vartheta\; \frac{\sqrt{1+\kappa}}{1+\kappa\,\vartheta}\,\frac{f(\vartheta)}{\sqrt{\vartheta(1-\vartheta)}}. \tag{71}$$

A list of the used inverse $\mathcal{K}$-transforms is given in Appendix F.

Remark. From the normalization condition $\int_0^1 d\vartheta\; p(\vartheta) = 1$ one can see in Eq. (63) that $\widetilde{p}(0) = 1$ and therefore in Eq. (67),

$$\widetilde{\mathcal{F}}(\kappa, H) = 0 \quad \text{for } \kappa = 0. \tag{72}$$

Remark. There are two reasons for performing our analysis using Laplace transform. The first is that convolutions in time are factorized, the second that integrations over space can be done over the Laplace-transformed propagator, but not the propagator in time. This will become clear in the analysis in the following sections.

VI. DISTRIBUTION OF TIME $t_{\rm last}$ FOR THE LAST VISIT TO THE ORIGIN

The analysis for the distribution of $t_{\rm last}$ is the simplest among the three observables, and we present it first. The

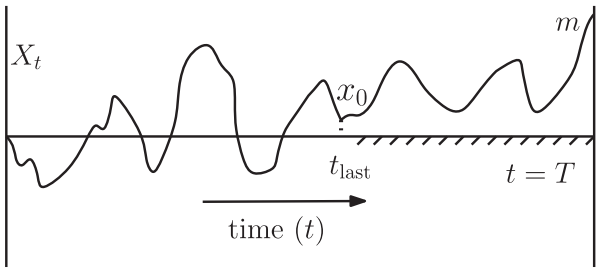

FIG. 10. A schematic of an fBm trajectory contributing to the time $t_{\rm last}$ of last visit to the origin. The striped line indicates an absorbing boundary.

probability of $t_{\rm last} = \tau$ for an fBm in a time window $[0, T]$ can be determined by

$$P_T(t_{\rm last} = \tau) = \frac{W(\tau, T)}{N(T)} \quad \text{for } x_0 \to 0, \tag{73}$$

where $W(\tau, T)$ is *twice* the weight of fBm trajectories that start at $X_0 = 0$, pass through $X_\tau = x_0 > 0$, and remain positive for the rest of the time (see Fig. 10 for an illustration). Note that the factor of 2 accounts for the possibility that the final position is either $m > 0$, or $m < 0$. Here $N(T)$ is the normalization

$$N(T) = \int_0^T d\tau W(\tau, T). \tag{74}$$

(To keep notations simple, we avoid explicit reference to x_0, unless necessary.)

Formally, we write

$$W(\tau, T) = 2\int_0^\infty dm \int_{x(0)=0}^{x(T)=m} \mathcal{D}[x]\, \delta[x(\tau) - x_0] \times \prod_{t=\tau}^{T} \Theta[x(t)]\, e^{-S}. \tag{75}$$

The perturbative expansion in Eq. (7) of the action leads to a similar expansion for W, given by

$$W(\tau, T) = W_0(\tau, T) + \varepsilon W_1(\tau, T) + \varepsilon^2 W_2(\tau, T) + \dots \tag{76}$$

with

$$W_0(\tau, T) = 2\int_0^\infty dm\, \langle\langle 1\rangle\rangle_m, \tag{77}$$

$$W_1(\tau, T) = \int_0^\infty dm \left\langle\!\!\left\langle \frac{S_1}{D} \right\rangle\!\!\right\rangle_m, \tag{78}$$

$$W_2(\tau, T) = \int_0^\infty dm \left\langle\!\!\left\langle \frac{S_1^2}{4D^2} - 2\frac{S_2}{D} \right\rangle\!\!\right\rangle_m. \tag{79}$$

The double-angular brackets denote (for $m > 0$) the average over trajectories as sketched in Fig. 10 with a standard Brownian measure,

$$\langle\langle O[x]\rangle\rangle_m := \int_{x(0)=0}^{x(T)=m} \mathcal{D}[x]\delta(x(\tau) - x_0) \times \prod_{t=\tau}^{T} \Theta[x(t)]\, e^{-\frac{S_0}{D}} O[x(t)]. \tag{80}$$

This definition of double-angular brackets is specific to the trajectories used here, its definition in other sections will include the corresponding boundary conditions needed there.

A. Zeroth-order term

In terms of the free Brownian propagator Eq. (24) and the propagator in the presence of an absorbing wall,

$$Z_t^+(x_1, x_2) = \int_{x(0)=x_1}^{x(t)=x_2} \mathcal{D}[x] \prod_{r=0}^{t} \Theta[x(r)] e^{-\frac{S_0}{D}}, \tag{81}$$

we write Eq. (77) as

$$W_0(\tau, T) = 2\int_0^\infty dm\, Z_\tau(0, x_0)\, Z_{T-\tau}^+(x_0, m). \tag{82}$$

Its double Laplace transformation Eq. (61) denoted by

$$\widetilde{W}_0(\lambda, s) = \mathscr{D}_{\tau\to\lambda\ T\to s} \odot W_0(\tau, T) \tag{83}$$

is

$$\widetilde{W}_0(\lambda, s) = 2\int_0^\infty dm\, \widetilde{Z}_{s+\lambda}(0, x_0)\, \widetilde{Z}_s^+(x_0, m). \tag{84}$$

Here $\widetilde{Z}_s$ and $\widetilde{Z}_s^+$ are the Laplace transforms of Z_t and Z_t^+, given by

$$\widetilde{Z}_s(x_1, x_2) = \int_0^\infty dt\, e^{-st}\, Z_t(x_1, x_2) = \frac{e^{-\sqrt{\frac{s}{D}}|x_1 - x_2|}}{2\sqrt{sD}}, \tag{85a}$$

and

$$\widetilde{Z}_s^+(x_1, x_2) = \int_0^\infty dt\, e^{-st}\, Z_t^+(x_1, x_2) = \frac{e^{-\sqrt{\frac{s}{D}}|x_1 - x_2|} - e^{-\sqrt{\frac{s}{D}}|x_1 + x_2|}}{2\sqrt{sD}}. \tag{85b}$$

Using these results in Eq. (84) and evaluating the integral for small x_0 we get [see Eq. (L5)]

$$\widetilde{W}_0(s\kappa, s) \simeq \frac{x_0}{Ds} \times \frac{1}{\sqrt{1 + \kappa}}. \tag{86}$$

Remark. The factorization in Eq. (84) results from the identity

$$\mathscr{D}_{\substack{\tau\to\lambda \\ T\to s}} \odot [g(\tau) f(T - \tau)] = \widetilde{g}(s + \lambda)\, \widetilde{f}(s), \tag{87}$$

where $\widetilde{g}(s)$ and $\widetilde{f}(s)$ are the Laplace transforms of $g(t)$ and $f(t)$, respectively.

Remark. From Eq. (86) it is straightforward to verify the arcsine-law Eq. (4) for Brownian motion. One can use $D = 1$ for $\varepsilon = 0$ in Eq. (86), and verify that $W_0(\vartheta T, T) \simeq x_0[\pi T\sqrt{\vartheta(1 - \vartheta)}]^{-1}$. Then, Eqs. (73) and (74) lead to the distribution Eq. (4).

B. Linear order: One-loop diagrams

Using S_1 from Eq. (10a) we explicitly write Eq. (78) as

$$W_1(\tau, T) = \frac{1}{D}\int_0^\infty dm \int_0^\Lambda dy \int_0^T dr_1 \int_{r_1}^T dr_2 \times e^{y(r_1 - r_2)}\, \langle\langle \dot{x}(r_1)\dot{x}(r_2)\rangle\rangle_m. \tag{88}$$

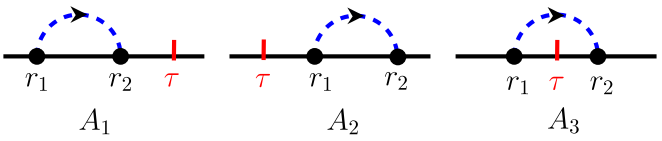

FIG. 11. One-loop diagrams: a graphical representation of the terms in Eq. (89a) for the linear order in our perturbation expansion. For all diagrams $r_1 < r_2$, staying on the same side of τ as indicated. The dashed lines indicate coupling between points r_1 and r_2 with $r_1 < r_2$ (indicated by an arrowhead) and a coupling strength $e^{y(r_1-r_2)}$. The solid disks indicate the 'charge' $\dot{x}(r_1)$ and $\dot{x}(r_2)$ for the associated points. A similar convention will be used for diagrams in later parts of our analysis.

For convenience we use a graphical representation of the expression in Eq. (88). We write the amplitude in three parts, according to the relative order of times r_1, r_2, and τ, as illustrated in the one-loop diagrams in Fig. 11.

Remark. Diagrams in Fig. 11 consists of couplings between a single pair of points, resulting in the y integral in Eq. (88). In analogy with field theory, we refer to them as one-loop diagrams, with y representing the loop-variable to be integrated over. In Sec. VI C, i.e., at second order, amplitudes involve couplings between two pairs, resulting into two y integrations, and therefore referred to as two-loop diagrams.

Following our convention for the diagrams in Fig. 11 we write Eq. (88) as

$$W_1 = A_1 + A_2 + A_3, \tag{89a}$$

with

$$A_1(\tau, T) = \frac{1}{D}\int_0^\infty dm \int_0^\Lambda dy\, J_\tau(0, x_0; -y, y)\, Z^+_{T-\tau}(x_0, m), \tag{89b}$$

$$A_2(\tau, T) = \frac{1}{D}\int_0^\infty dm \int_0^\Lambda dy\, Z_\tau(0, x_0)\, J^+_{T-\tau}(x_0, m; -y, y), \tag{89c}$$

$$A_3(\tau, T) = \frac{1}{D}\int_0^\infty dm \int_0^\Lambda dy\, J_\tau(0, x_0; -y) \times e^{-y\tau} J^+_{T-\tau}(x_0, m; y). \tag{89d}$$

We defined

$$J_t(u, v; y_1, \ldots, y_n) := \int_{0<r_1<\cdots<r_n}^{t} \prod_{i=1}^{n} e^{-y_i r_i} \int_{x(0)=u}^{x(t)=v} \mathcal{D}[x]\dot{x}(r_1)\cdots\dot{x}(r_n) e^{-\frac{S_0}{D}} \tag{90}$$

and its analog J^+ in the presence of an absorbing wall at $x = 0$. The integral over time in Eq. (90) is interpreted as in Eq. (15), i.e., with an ultraviolet cutoff Λ on y.

Using Eq. (87) we write the double Laplace transform Eq. (61) of the diagrams A_i in terms of Laplace transforms of Z and Z^+ in Eq. (85), as well as Laplace transforms for J and J^+. Expressions are obtained in Appendix N and summarized here,

$$\widetilde{A}_1(\lambda, s) = \frac{1}{D}\int_0^\infty dm \int_0^\Lambda dy\, \widetilde{J}_{s+\lambda}(0, x_0; -y, y)\, \widetilde{Z}^+_s(x_0, m),$$

$$\widetilde{A}_2(\lambda, s) = \frac{1}{D}\int_0^\infty dm \int_0^\Lambda dy\, \widetilde{Z}_{s+\lambda}(0, x_0)\, \widetilde{J}^+_s(x_0, m; -y, y).$$

Using Eqs. (85), (N8), and (N13) gives, for small x_0,

$$\widetilde{A}_1(s\kappa, s) \simeq -\frac{x_0}{Ds} \times \frac{\widetilde{\mathcal{A}}(1+\kappa)}{\sqrt{1+\kappa}},$$

$$\widetilde{A}_2(s\kappa, s) \simeq \frac{x_0}{Ds} \times \frac{\widetilde{\mathcal{A}}(1)}{\sqrt{1+\kappa}},$$

with

$$\widetilde{\mathcal{A}}(z) = \int_0^{\Lambda/s} \frac{dy}{y^2}(\sqrt{z+y} - \sqrt{z})^2. \tag{91}$$

A similar analysis for A_3 in Eq. (89d), using Eqs. (N1) and (N5), shows that the corresponding double Laplace transform $\widetilde{A}_3 \sim x_0^2$, for small x_0. As a result, the double Laplace transform of $W_1(\tau, T)$ defined in analogy to Eq. (83) reads, for small x_0,

$$\widetilde{W}_1(s\kappa, s) \simeq \frac{x_0}{Ds} \times \frac{\widetilde{\mathcal{A}}(1) - \widetilde{\mathcal{A}}(1+\kappa)}{\sqrt{1+\kappa}}. \tag{92}$$

Remark. The reason for $\widetilde{A}_3$ to vanish as x_0^2 or faster, for small x_0, can be understood from a simple observation. In the limit of $x_0 \to 0$, $J_t(0, x_0; y_1, \ldots, y_n)$ in Eq. (90) vanishes for odd n. One way to see this is by noting that, in the limit of $x_0 \to 0$, for each trajectory with a certain $\dot{x}(r)$, there is a mirror trajectory $-\dot{x}(r)$, with equal probability. In comparison, $J^+(x_0, m; y_1, \ldots, y_n)$ vanishes for $x_0 \to 0$ because of the absorbing boundary. This means that in Eq. (89d), both J and J^+ are at least of order x_0, and therefore $\widetilde{A}_3 \sim x_0^2$, to the least. We shall see later that for a similar reason the amplitudes of the two-loop diagrams B and C in Fig. 14 are of order x_0^2, for small x_0.

Remark. We shall see that these diagrams A_1, A_2, and A_3 contribute to the propagator W_1 in Eq. (89a), thus to the scaling prefactor in Eq. (37), but they do not feed into the exponential term $\mathcal{F}^{\text{last}}$.

C. Quadratic order: Two-loop diagrams

Using Eq. (10) we explicitly write the terms in Eq. (79) as

$$\int_0^\infty dm \left\langle\left\langle \frac{S_1^2}{4D^2} \right\rangle\right\rangle_m = \frac{1}{4D^2}\int_0^\infty dm \int_0^\Lambda dy_1 dy_2 \int_0^T dr_1 \int_{r_1}^T dr_2 \int_0^T dr_3 \int_{r_3}^T dr_4 \times e^{y_1(r_1-r_2)}\, e^{y_2(r_3-r_4)} \langle\langle \dot{x}(r_1)\dot{x}(r_2)\dot{x}(r_3)\dot{x}(r_4)\rangle\rangle_m \tag{93}$$

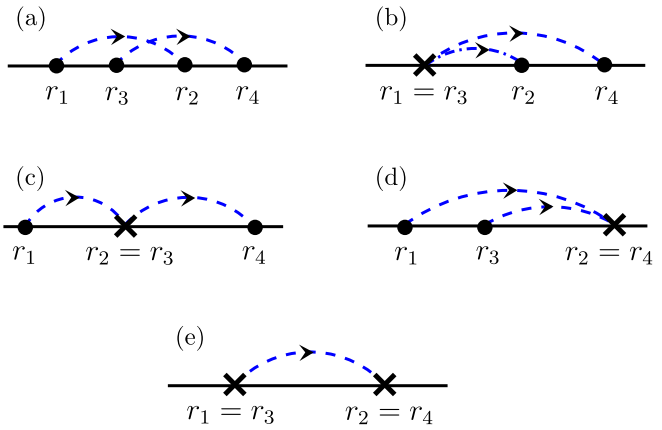

FIG. 12. A diagrammatic representation for the amplitude in Eq. (93) where all orders of time are allowed keeping $r_2 > r_1$ and $r_4 > r_3$ (as indicated by an arrowhead). We write the amplitude Eq. (93) in five parts according to the contraction of times (indicated by cross). In panel (a) none of the times are equal (contracted). In panels (b, c, d) two times are contracted and in panel (e) all four times are contracted.

and

$$\int_0^\infty dm \left\langle\left\langle \frac{2S_2}{D} \right\rangle\right\rangle_m = \frac{1}{D}\int_0^\infty dm \int_0^\Lambda dy_1 dy_2 \times \int_0^T dr_1 \int_{r_1}^T dr_2 \left[\int_0^{r_1} ds\, e^{-y_1(r_1-s)-y_2(r_2-s)} + \int_{r_2}^T ds\, e^{-y_1(s-r_1)-y_2(s-r_2)} \right] \langle\langle \dot{x}(r_1)\dot{x}(r_2)\rangle\rangle_m. \tag{94}$$

A graphical illustration of the amplitudes in Eqs. (93) and (94) is shown in Figs. 12 and 13, respectively. Similar to the conventions in Fig. 11, a dashed line indicates an interaction between points r_i and r_j with an amplitude $e^{y(r_i-r_j)}$. The solid disks indicate the field derivative $\dot{x}(r_i)$ at point r_i. For a contracted point, indicated by a cross, the associated amplitude is $2D$. A reason for this will be clear shortly. Empty points in Fig. 13 have an amplitude 1.

We shall see that among these diagrams, only diagrams (a) and (c) contribute at the second order. This can be directly seen using the normal-ordered weight in Eq. (17). Here, we explicitly show why this happens.

We find that the amplitudes of diagrams (b) and (b′) are equal, as are those of (d) and (d′). To see this we use that under Wick contraction between $\dot{x}(r_1)$ and $\dot{x}(r_3)$

$$\langle\langle \dot{x}(r_1)\dot{x}(r_2)\dot{x}(r_3)\dot{x}(r_4)\rangle\rangle_m \to 2D\, \langle\langle \dot{x}(r_2)\dot{x}(r_4)\rangle\rangle_m. \tag{95}$$

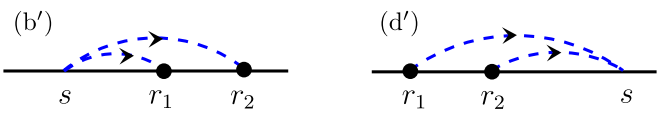

FIG. 13. A diagrammatic representation of the formula in Eq. (94) where for (b′) $s < r_1 < r_2$ and for (d′) $r_1 < r_2 < s$.

(A similar result holds for contraction of any pair of times.) One can see this as a consequence of $\delta(r_i - r_j)$ term in Eq. (M8), and its analog in presence of an absorbing boundary. Using the result Eq. (95) in Eq. (93) for diagram (b) we write its amplitude as

$$\frac{1}{2D}\int_0^\infty dm \int_0^\Lambda dy_1 dy_2 \int_0^T dr_1 \int_{r_1}^T dr_2 \int_{r_1}^T dr_4 \times e^{y_1(r_1-r_2)} e^{y_2(r_1-r_4)} \langle\langle \dot{x}(r_2)\dot{x}(r_4)\rangle\rangle_m = \frac{1}{D}\int_0^\infty dm \int_0^\Lambda dy_1 dy_2 \int_0^T dr_2 \int_{r_2}^T dr_4 \int_0^{r_2} dr_1 \times e^{y_1(r_1-r_2)} e^{y_2(r_1-r_4)} \langle\langle \dot{x}(r_2)\dot{x}(r_4)\rangle\rangle_m.$$

Following a relabeling of the dummy variables r we see that the integral is equal to the amplitude of diagram (b′) from Eq. (94) and Fig. 13. A similar analysis shows equal amplitude for diagrams (d) and (d′).

The amplitude of diagram (e), where all four times are contracted, is proportional to W_0 in Eq. (77), which can be seen by using

$$\langle\langle \dot{x}(r_1)\dot{x}(r_2)\dot{x}(r_3)\dot{x}(r_4)\rangle\rangle_m \to 4D^2 \langle\langle 1\rangle\rangle_m, \tag{96}$$

when all four points are contracted. This means that the contribution of diagram (e) can be included in the normalization Eq. (37), and therefore ignored.

Considering the contribution of the diagrams in Figs. 12 and 13, resulting into Eq. (79), we see that the relevant contribution for W_2 comes from the two-loop diagrams (a) and (c) in Fig. 12. Considering the relative position of the loops with respect to τ, we write the amplitude W_2 as a sum of the following ten diagrams:

$$\begin{aligned} W_2 &= a + c \\ &= (E_1 + E_2) + A + D + (C_1 + C_2) \\ &\quad + (B_1 + B_2) + (G_1 + G_2). \end{aligned} \tag{97}$$

This is shown in Fig. 14. Explicit formulas of their amplitudes are given in Appendix G. We shall see that among these diagrams, only diagram D contributes to the nontrivial term $\mathcal{F}^{\text{last}}$ in Eq. (37), whereas the remaining diagrams contribute to the power-law prefactor only.

Here, we present the double Laplace transformation Eq. (61) of the amplitude of these diagrams, for small x_0 limit. Their derivation is similar to those of the amplitude of zeroth and linear order terms in Eqs. (86) and (92). We defer their explicit calculation to the Appendix G.

For small x_0, we get

$$\widetilde{D}(s\kappa, s) \simeq \frac{x_0}{Ds} \times \frac{\widetilde{\mathcal{D}}(1+\kappa)}{\sqrt{1+\kappa}}, \tag{98}$$

with

$$\widetilde{\mathcal{D}}(z) = -2\int_0^{\Lambda/s} \frac{dy_1 dy_2}{y_1^2 y_2^2} \sqrt{z}\sqrt{1+y_1+y_2} \times (\sqrt{1+y_1+y_2} - \sqrt{1+y_1} - \sqrt{1+y_2} + 1) \times (\sqrt{z+y_1+y_2} - \sqrt{z+y_1} - \sqrt{z+y_2} + \sqrt{z}). \tag{99}$$

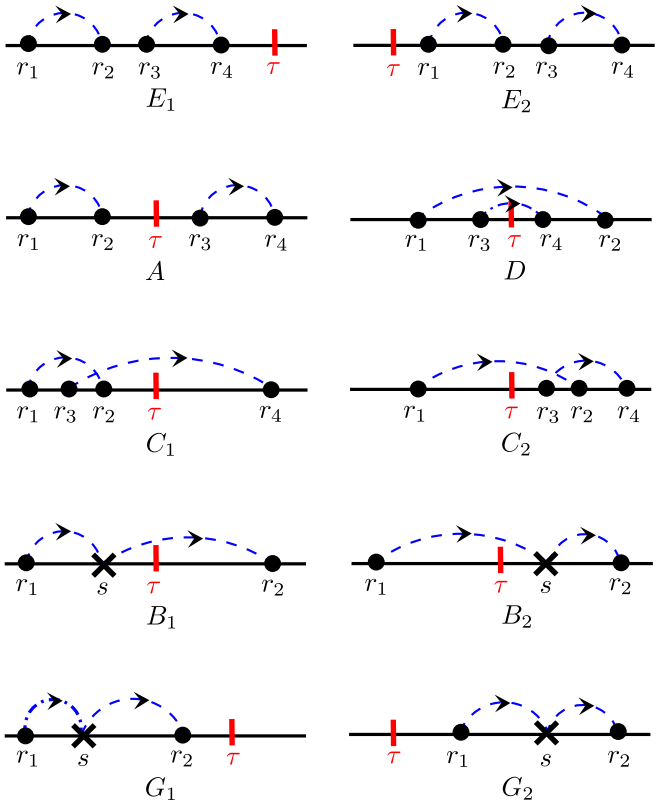

FIG. 14. Two-loop diagrams for the quadratic order term W_2 in Eq. (79). The diagrams are categorized according to relative position of the loops with respect to τ. For diagram E_1, the times $r_1 < r_2 < \tau$ and $r_3 < r_4 < \tau$, excluding cases where any two times are equal (contracted). Similar convention is adopted for the diagrams E_2, A, D, and C, where $r_1 < r_2$, $r_3 < r_4$, and their relative position with τ indicated in the diagrams. For diagrams B and G we consider, $r_2 > s > r_1$ being on the same side of τ as indicated. A solid disk denotes a "charge" $\dot{x}(r)$ for the associated point r, and a cross denotes a "charge" $2D$. A dashed line indicates coupling between points r_i and r_j with a coupling strength $e^{y(r_i-r_j)}$.

The amplitude of the diagrams B and C is of order x_0^2 for small x_0,

$$\widetilde{B}(s\kappa, s) \simeq \widetilde{C}(s\kappa, s) \sim x_0^2. \tag{100}$$

This can be seen from the argument given in the remark below Eq. (92). Their explicit derivation is in Appendix G 2 d.

The amplitude for the remaining diagrams is of order x_0, and given as follows. For small x_0,

$$\widetilde{E}_1(s\kappa, s) + \widetilde{E}_2(s\kappa, s) \simeq \frac{x_0}{s} \times \frac{\widetilde{\mathcal{E}}(1+\kappa) + \widetilde{\mathcal{E}}(1)}{D\sqrt{1+\kappa}}, \tag{101}$$

where

$$\begin{aligned}\widetilde{\mathcal{E}}(z) = &-\frac{1}{2}\int_0^{\Lambda/s} \frac{dy_1 dy_2}{y_1^2 y_2^2}\{(z+y_1)(z+y_2) \\ &+ \sqrt{z}\,(\sqrt{z} - \sqrt{z+y_1} - \sqrt{z+y_2})[\sqrt{z+y_1} \\ &\times (\sqrt{z} - \sqrt{z+y_1}) + \sqrt{z+y_2}(\sqrt{z} - \sqrt{z+y_2}) \\ &+ (\sqrt{z} - \sqrt{z+y_1} - \sqrt{z+y_2})^2 \\ &- 2(\sqrt{z+y_1+y_2} - \sqrt{z+y_1} - \sqrt{z+y_2} + \sqrt{z})^2]\}.\end{aligned} \tag{102}$$

Similarly, for small x_0,

$$\widetilde{A}(s\kappa, s) \simeq -\frac{x_0}{s} \times \frac{\widetilde{\mathcal{A}}(1+\kappa)\widetilde{\mathcal{A}}(1)}{D\sqrt{1+\kappa}}, \tag{103}$$

with Eq. (91), and

$$\widetilde{G}_1(s\kappa, s) + \widetilde{G}_2(s\kappa, s) \simeq \frac{x_0}{s} \times \frac{\widetilde{\mathcal{G}}(1+\kappa) + \widetilde{\mathcal{G}}(1)}{D\sqrt{1+\kappa}}, \tag{104}$$

where

$$\begin{aligned}\widetilde{\mathcal{G}}(z) = &\int_0^{\Lambda/s} \frac{dy_1 dy_2}{y_1^2 y_2^2} \\ &\times \left[\frac{(\sqrt{z+y_2} - \sqrt{z})^2 y_1^2 - (\sqrt{z+y_1} - \sqrt{z})^2 y_2^2}{(y_1 - y_2)}\right].\end{aligned} \tag{105}$$

Considering the amplitude of these two-loop diagrams in Eq. (97) we get the double Laplace transform Eq. (61) of $W_2(\tau, T)$ in Eq. (79). For small x_0 it reads

$$\begin{aligned}\widetilde{W}_2(s\kappa, s) \simeq &\frac{x_0}{s D\sqrt{1+\kappa}}[\widetilde{\mathcal{E}}(1+\kappa) + \widetilde{\mathcal{E}}(1) \\ &- \widetilde{\mathcal{A}}(1+\kappa)\widetilde{\mathcal{A}}(1) + \widetilde{\mathcal{D}}(1+\kappa) \\ &+ \widetilde{\mathcal{G}}(1+\kappa) + \widetilde{\mathcal{G}}(1)].\end{aligned} \tag{106}$$

D. Result for $\mathcal{F}^{\text{last}}(\kappa, H)$

From the results in Eqs. (86), (92), and (106) we obtain the double Laplace transform Eq. (61) of $W(\tau, T)$ in Eq. (76) in an exponential form,

$$\widetilde{W}(s\kappa, s) = \mathscr{D}_{\tau\to s\kappa\ T\to s} \odot W(\tau, T) \simeq \frac{x_0}{s} \times \frac{e^{\widetilde{\mathcal{W}}(\kappa)}}{\sqrt{1+\kappa}}, \tag{107}$$

Here x_0 is small, and we used D in Eq. (14) to explicitly write the exponential term $\widetilde{\mathcal{W}} = \varepsilon\widetilde{\mathcal{W}}_1 + \varepsilon^2\widetilde{\mathcal{W}}_2 + \cdots$, with

$$\widetilde{\mathcal{W}}_1(\kappa) = \widetilde{\mathcal{A}}(1) - \widetilde{\mathcal{A}}(1+\kappa) + 2(\ln\Lambda + \gamma_{\mathrm{E}} - 1), \tag{108a}$$

$$\begin{aligned}\widetilde{\mathcal{W}}_2(\kappa) = &\widetilde{\mathcal{E}}(1+\kappa) + \widetilde{\mathcal{E}}(1) + \widetilde{\mathcal{D}}(1+\kappa) \\ &- \widetilde{\mathcal{A}}(1+\kappa)\widetilde{\mathcal{A}}(1) + \widetilde{\mathcal{G}}(1+\kappa) + \widetilde{\mathcal{G}}(1) \\ &- \frac{1}{2}[\widetilde{\mathcal{A}}(1) - \widetilde{\mathcal{A}}(1+\kappa)]^2 + 2\left[1 - \frac{\pi^2}{6}\right].\end{aligned} \tag{108b}$$

To relate to the exponential form in Eq. (67) we note that the Laplace transform of N_T in Eq. (74) is

$$\widetilde{N}(s) = \widetilde{W}(0, s). \tag{109}$$

The simple s-dependence in Eq. (107) (for $\Lambda \to \infty$) makes it easy to invert the Laplace transform, giving

$$N(T) \simeq x_0\, e^{\widetilde{\mathcal{W}}(0)} \quad \text{for small } x_0. \tag{110}$$

This means, for small x_0, $N(T) \equiv N$ is independent of T, and the double Laplace transform of $P_T(\tau)$ in Eq. (73) is

$$\widetilde{P}(\lambda, s) \simeq \frac{\widetilde{W}(\lambda, s)}{N} \quad \text{for small } x_0. \tag{111}$$

Then, using Eq. (107) and comparing with Eqs. (63) and (67) gives

$$\widetilde{\mathcal{F}}^{\rm last}(\kappa, H) = \widetilde{\mathcal{W}}(\kappa) - \widetilde{\mathcal{W}}(0), \tag{112}$$

which we shall need to determine $\mathcal{F}(\vartheta, H)$ in Eq. (68). The leading terms in its perturbation expansion Eq. (70a) is given by

$$\widetilde{\mathcal{F}}_1^{\rm last}(\kappa) = \widetilde{\mathcal{A}}(1) - \widetilde{\mathcal{A}}(1+\kappa), \tag{113a}$$

$$\widetilde{\mathcal{F}}_2^{\rm last}(\kappa) = [\widetilde{\mathcal{D}}(1+\kappa) - \widetilde{\mathcal{D}}(1)] + \big\{\widetilde{\mathcal{E}}(1+\kappa) + \widetilde{\mathcal{G}}(1+\kappa) - \tfrac{1}{2}\widetilde{\mathcal{A}}^2(1+\kappa) - \big[\widetilde{\mathcal{E}}(1) + \widetilde{\mathcal{G}}(1) - \tfrac{1}{2}\widetilde{\mathcal{A}}^2(1)\big]\big\}. \tag{113b}$$

We have numerically verified that, for $\Lambda \to \infty$,

$$\widetilde{\mathcal{E}}(z) + \widetilde{\mathcal{G}}(z) - \frac{1}{2}\widetilde{\mathcal{A}}^2(z) = [1 + \ln(2)]^2 - \frac{5\pi^2}{12}. \tag{114}$$

Therefore, the only nonvanishing contribution for $\Lambda \to \infty$ comes from the diagram D, leading to

$$\widetilde{\mathcal{F}}_2^{\rm last}(\kappa) = \widetilde{\mathcal{D}}(1+\kappa) - \widetilde{\mathcal{D}}(1). \tag{115}$$

Remark. We see that Eq. (112) is consistent with the condition Eq. (72). Moreover, we shall see that the integrals in Eq. (113a) and Eq. (115) converge in the $\Lambda \to \infty$ limit, as one would expect for our theory to be correct.

Remark. Note that in Eq. (108) the contribution from diffusion constant D in Eq. (14) is constant, which cancels in Eq. (112). This is expected as the distribution of $t_{\rm last}$ is independent of the diffusion constant, whereas as a distribution involving space would depend on D. The same applies for the distribution of $t_{\rm max}$ and $t_{\rm pos}$.

For the leading-order term Eq. (113a), explicitly carrying out the integral in Eq. (91) in the limit of $\Lambda \to \infty$, we get

$$\widetilde{\mathcal{F}}_1^{\rm last}(\kappa) = \ln(1+\kappa), \tag{116}$$

whose $\mathcal{K}^{-1}$-transformation is [see Eq. (F4)]

$$\mathcal{K}^{-1}_{\kappa\to\vartheta} \odot \widetilde{\mathcal{F}}_1^{\rm last}(\kappa) = -\ln\tfrac{\vartheta}{(1-\vartheta)} = -\mathcal{R}^{\rm last}(\vartheta). \tag{117}$$

Using the result Eq. (70b) for $t_{\rm last}$ gives the leading-order result in Eq. (41a).

For the second-order term in Eq. (70c) we use Eq. (115), Eq. (41a), and

$$\mathcal{K}^{-1}_{\kappa\to\vartheta} \odot \widetilde{\mathcal{F}}_1^{\rm last}(\kappa)^2 = \mathcal{R}^{\rm last}(\vartheta)^2 - \pi^2 \tag{118}$$

[using the identity Eq. (F5)] to write

$$\mathcal{F}_2^{\rm last}(\vartheta) = \mathcal{K}^{-1}_{\kappa\to\vartheta} \odot [\widetilde{\mathcal{D}}(1+\kappa) - \widetilde{\mathcal{D}}(1)] - \frac{\pi^2}{2}, \tag{119}$$

where we use linearity of the operator $\mathcal{K}^{-1}$.

The integral for $\widetilde{\mathcal{D}}(z)$ in Eq. (99) is convergent in the limit of $\Lambda \to \infty$, but it is hard to evaluate analytically. The expression for $\mathcal{F}_2^{\rm last}(\vartheta)$ in Eq. (42) is obtained [78] by exchanging the order of $\mathcal{K}^{-1}_{\kappa\to\vartheta}$ transformation and the y-integrals in Eqs. (119) and (99). (For several other examples like in Eqs. (113a) and (117) where integration can be explicitly carried out, we have verified that this exchange of order gives the correct result.) The resulting function $\mathcal{F}_2^{\rm last}(\vartheta)$ in Eq. (42) is plotted in Fig. 15 along with a polynomial estimation given in Eq. (43). The expression Eq. (42) is in good agreement with our computer simulation result in Fig. 7.

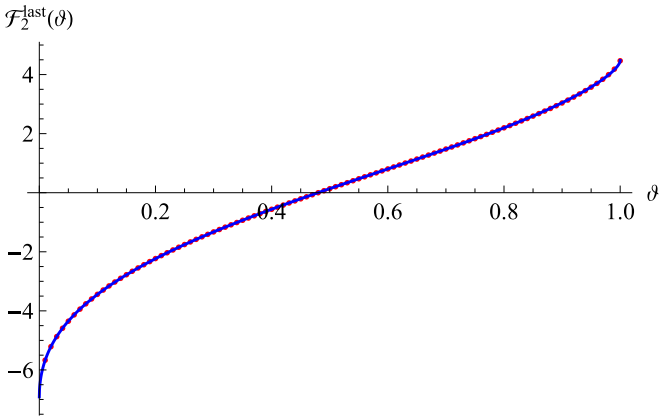

FIG. 15. The dotted points (colored red) show results of numerical integration for $\mathcal{F}_2^{\rm last}(\vartheta)$ in Eq. (42). The solid line is the polynomial fit in Eq. (43), which gives a good estimation for $\mathcal{F}_2^{\rm last}(\vartheta)$.

VII. DISTRIBUTION OF THE TIME $t_{\rm max}$ WHEN THE FBM ATTAINS MAXIMUM

The probability for an fBm, starting at $X_0 = 0$ and evolving till time T, to attain its maximum at time $t_{\rm max} = \tau$ can be expressed as

$$P_T(t_{\rm max} = \tau) = \frac{W(\tau, T)}{N(T)}. \tag{120}$$

Here $W(\tau, T)$ is the weight of all contributing trajectories, and $N(T)$ is the corresponding normalization. We use the same notations as in Sec. VI. Note, however, that the definition of these quantities (W, N, etc.) is specific to the problem in this section.

Noting the symmetry of the problem (illustrated in Fig. 16), we write

$$W(\tau, T) = \int_0^\infty dm_1 \int_0^\infty dm_2 \int_{x(0)=m_1}^{x(T)=m_2} \mathcal{D}[x] \times \delta(x(\tau) - x_0) \prod_{t=0}^{T} \Theta[x(t)] e^{-S[x]}. \tag{121}$$

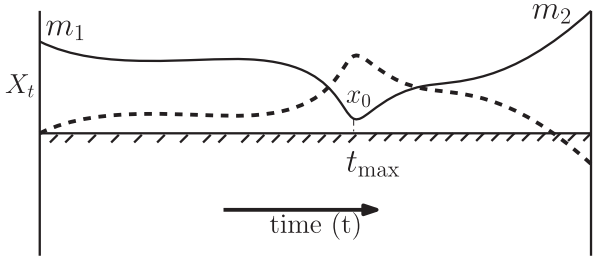

FIG. 16. The dark solid curve is a schematic of paths X_t for Eq. (121), where the stripped line indicates an absorbing boundary at the origin. For $x_0 \to 0$, there is an one-to-one correspondence with an fBm path (indicated by dashed curve) that contributes for the process to attain its maximum m_1 at time $t_{\rm max}$.

The probability density $P_T(\tau)$ in Eq. (120) is obtained by taking the limit of $x_0 \to 0$. (Like in the previous section, we do not write any explicit reference to x_0, unless necessary.)

The perturbation expansion Eq. (7) of the fBm action S leads to an expansion of W similar to Eq. (76) with

$$W_0(\tau, T) = \int_0^\infty dm_1 \int_0^\infty dm_2 \, \langle\langle 1 \rangle\rangle_{(m_1,m_2)}, \tag{122}$$

$$W_1(\tau, T) = \int_0^\infty dm_1 \int_0^\infty dm_2 \left\langle\!\!\left\langle \frac{S_1}{2D} \right\rangle\!\!\right\rangle_{(m_1,m_2)}, \tag{123}$$

$$W_2(\tau, T) = \int_0^\infty dm_1 \int_0^\infty dm_2 \left\langle\!\!\left\langle \frac{S_1^2}{8D^2} - \frac{S_2}{D} \right\rangle\!\!\right\rangle_{(m_1,m_2)}. \tag{124}$$

By the double-angular brackets we denote

$$\langle\langle O[x] \rangle\rangle_{(m_1,m_2)} := \int_{x(0)=m_1}^{x(T)=m_2} \mathcal{D}[x] \delta\big(x(\tau) - x_0\big) \prod_{t=0}^{T} \Theta[x(t)] \, e^{-\frac{S_0}{D}} O[x(t)]. \tag{125}$$

Here, both $m_1 \geqslant 0$ and $m_2 \geqslant 0$, and the average is over trajectories sketched in Fig. 16 with the standard Brownian measure. Note that this definition is different from the one in Eq. (80), due to the different boundary conditions employed there. We will now in turn study averages at different orders, expressed in terms of the Brownian propagator Eq. (81) in presence of an absorbing wall. This is similar to the analysis of $t_{\rm last}$ in the previous Sec. VI.

A. Zeroth order

Similar to Eq. (84), we write the double Laplace transformation of Eq. (122) as

$$\widetilde{W}_0(\lambda, s) = \int_0^\infty dm_1 \int_0^\infty dm_2 \, \widetilde{Z}^+_{s+\lambda}(m_1, x_0) \, \widetilde{Z}^+_s(x_0, m_2).$$

Using Eq. (85) and integrating, it is easy to see that for small x_0,

$$\widetilde{W}_0(s\kappa, s) \simeq \frac{x_0^2}{Ds} \times \frac{1}{\sqrt{1+\kappa}}. \tag{126}$$

The leading nonvanishing term is of order x_0^2, and its amplitude is same as in Eq. (86). This gives the well-known arcsine-law Eq. (4) for $t_{\rm max}$.

B. Linear order: One-loop diagrams

Similar to Eq. (89a) we write W_1 in Eq. (123) in three parts according to the order of (r_1, r_2, τ). Their diagrammatic representation is similar to the one-loop diagrams in Fig. 11, but their amplitude is different. They are given by

$$A_1(\tau, T) = \frac{1}{2D} \int_0^\infty dm_1 dm_2 \int_0^\Lambda dy \times J^+_\tau(m_1, x_0; -y, y) Z^+_{T-\tau}(x_0, m_2), \tag{127a}$$

$$A_2(\tau, T) = \frac{1}{2D} \int_0^\infty dm_1 dm_2 \int_0^\Lambda dy \times Z^+_\tau(m_1, x_0) J^+_{T-\tau}(x_0, m_2; -y, y), \tag{127b}$$

$$A_3(\tau, T) = \frac{1}{2D} \int_0^\infty dm_1 dm_2 \int_0^\Lambda dy \times J^+_\tau(m_1, x_0; -y) J^+_{T-\tau}(x_0, m_2; y) \, e^{-y\tau}. \tag{127c}$$

The function J^+_t is the counterpart of Eq. (90) in presence of an absorbing wall at the origin. Their double Laplace transform Eq. (61) gives

$$\widetilde{A}_1(\lambda, s) = \frac{1}{2D} \int_0^\infty dm_1 dm_2 \int_0^\Lambda dy \times \widetilde{J}^+_{s+\lambda}(m_1, x_0; -y, y) \widetilde{Z}^+_s(x_0, m_2), \tag{128a}$$

$$\widetilde{A}_2(\lambda, s) = \frac{1}{2D} \int_0^\infty dm_1 dm_2 \int_0^\Lambda dy \times \widetilde{Z}^+_{s+\lambda}(m_1, x_0) \widetilde{J}^+_s(x_0, m_2; -y, y), \tag{128b}$$

$$\widetilde{A}_3(\lambda, s) = \frac{1}{2D} \int_0^\infty dm_1 dm_2 \int_0^\Lambda dy \times \widetilde{J}^+_{s+\lambda+y}(m_1, x_0; -y) \widetilde{J}^+_s(x_0, m_2; y). \tag{128c}$$

These integrals can be evaluated explicitly using the results in Appendices L and N, specifically Eqs. (G3), (L5), and their symmetry properties for evaluating Eqs. (128a), (128b), as well as Eqs. (N6) and (N7) for evaluating Eq. (128c). For small x_0, we get

$$\widetilde{A}_1(s\kappa, s) \simeq \frac{x_0^2}{Ds} \times \frac{\widetilde{\mathcal{A}}(1+\kappa)}{\sqrt{1+\kappa}}, \tag{129}$$

$$\widetilde{A}_2(s\kappa, s) \simeq \frac{x_0^2}{Ds} \times \frac{\widetilde{\mathcal{A}}(1)}{\sqrt{1+\kappa}}, \tag{130}$$

$$\widetilde{A}_3(s\kappa, s) \simeq \frac{x_0^2}{Ds} \times \frac{\widetilde{\mathcal{A}}_3(1+\kappa)}{\sqrt{1+\kappa}}, \tag{131}$$

with $\widetilde{\mathcal{A}}(z)$ defined in Eq. (91) and

$$\widetilde{\mathcal{A}}_3(z) = -2 \int_0^{\Lambda/s} \frac{dy}{y^2} (\sqrt{z+y} - \sqrt{z})(\sqrt{1+y} - 1). \tag{132}$$

Summing all three contributions we get the double Laplace transform Eq. (61) of the linear-order term $W_1(\tau, T)$ in Eq. (123). It reads, for small x_0,

$$\widetilde{W}_1(s\kappa, s) \simeq \frac{x_0^2}{sD} \times \frac{\widetilde{\mathcal{A}}(1+\kappa) + \widetilde{\mathcal{A}}(1) + \widetilde{\mathcal{A}}_3(1+\kappa)}{\sqrt{1+\kappa}}. \tag{133}$$

We note the simplification

$$\widetilde{\mathcal{A}}(z) + \widetilde{\mathcal{A}}(1) + \widetilde{\mathcal{A}}_3(z) = \int_0^{\Lambda/s} \frac{dy}{y^2} [(\sqrt{z+y} - \sqrt{z}) - (\sqrt{1+y} - 1)]^2. \tag{134}$$

C. Quadratic order

Similar to Eq. (97), we find that the second-order term W_2 in Eq. (124) is composed of the two-loop diagrams in Fig. 14. The amplitudes of these diagrams are different for this problem. Here we summarize their result for small x_0. Their derivation is given in Appendix H.

The list below contains the double Laplace transform of all two-loop diagrams. All amplitudes are of order x_0^2 for small

x_0. Note that many diagrams are the same as in the problem of $t_{\rm last}$ in Sec. VI; this may not be surprising as the same power-law corrections for $\vartheta \to 0$ and $\vartheta \to 1$ are also present in the distribution of $t_{\rm last}$.

The list of already calculated diagrams reads ($x_0 \ll 1$):

$$\widetilde{E}_1(s\kappa, s) + \widetilde{E}_2(s\kappa, s) \simeq \frac{x_0^2}{sD} \times \frac{\widetilde{\mathcal{E}}(1+\kappa) + \widetilde{\mathcal{E}}(1)}{\sqrt{1+\kappa}}, \quad (135)$$

with $\widetilde{\mathcal{E}}$ given in Eq. (102).

$$\widetilde{A}(s\kappa, s) \simeq \frac{x_0^2}{sD} \times \frac{\widetilde{\mathcal{A}}(1+\kappa)\widetilde{\mathcal{A}}(1)}{\sqrt{1+\kappa}}, \quad (136)$$

with $\widetilde{\mathcal{A}}(z)$ given in Eq. (91).

$$\widetilde{G}_1(s\kappa, s) + \widetilde{G}_2(s\kappa, s) \simeq \frac{x_0^2}{sD} \times \frac{\widetilde{\mathcal{G}}(1+\kappa) + \widetilde{\mathcal{G}}(1)}{\sqrt{1+\kappa}}, \quad (137)$$

with $\widetilde{\mathcal{G}}(z)$ given in Eq. (105).

The amplitudes of the remaining diagrams are different. We get, for small x_0,

$$\widetilde{D}(s\kappa, s) = \frac{x_0^2}{sD} \times \frac{\widetilde{\mathcal{D}}(1+\kappa)}{\sqrt{1+\kappa}}, \quad (138)$$

with

$$\widetilde{\mathcal{D}}(z) = 2\int_0^{\Lambda/s} \frac{dy_1 dy_2}{y_1^2 y_2^2} \sqrt{z+y_1+y_2}\sqrt{1+y_1+y_2} \times (\sqrt{1+y_1+y_2} - \sqrt{1+y_1} - \sqrt{1+y_2} + 1) \times (\sqrt{z+y_1+y_2} - \sqrt{z+y_1} - \sqrt{z+y_2} + \sqrt{z}). \quad (139)$$

The difference to Eq. (99) is in the first term inside the integrals and the overall sign.

The leading nonvanishing amplitudes of diagrams B and C are of order x_0^2, and unlike in Sec. VI, these diagrams are relevant here. Their Laplace transform, for small x_0 are

$$\widetilde{B}_1(s\kappa, s) + \widetilde{B}_2(s\kappa, s) \simeq \frac{x_0^2}{s} \times \frac{\widetilde{\mathcal{B}}(1+\kappa)}{D\sqrt{1+\kappa}}, \quad (140)$$

where

$$\widetilde{\mathcal{B}}(z) = 2\int_0^{\Lambda/s} \frac{dy_1 dy_2}{y_1^2 y_2^2 (y_1 - y_2)} \left[y_2^2 (\sqrt{z+y_1} - \sqrt{z})(\sqrt{1+y_1} - 1) - y_1^2 (\sqrt{z+y_2} - \sqrt{z})(\sqrt{1+y_2} - 1) \right] \quad (141)$$

and

$$\widetilde{C}_1(s\kappa, s) + \widetilde{C}_2(s\kappa, s) \simeq \frac{x_0^2}{s} \times \frac{[\widetilde{\mathcal{C}}(1,\ 1+\kappa) + \widetilde{\mathcal{C}}(1+\kappa,\ 1)]}{D\sqrt{1+\kappa}}, \quad (142)$$

where

$$\widetilde{\mathcal{C}}(z_1, z_2) = 2\int_0^{\Lambda/s} \frac{dy_1 dy_2}{y_1^2\, y_2^2} (\sqrt{z_1} - \sqrt{z_1+y_1})\sqrt{z_2+y_1} \times (\sqrt{z_2+y_1+y_2} - \sqrt{z_2+y_1} - \sqrt{z_2+y_2} + \sqrt{z_2})^2. \quad (143)$$

From the amplitude of all two-loop diagrams in Eq. (97) we get the double Laplace transform of $W_2(\tau, T)$ in Eq. (124), for small x_0,

$$\widetilde{W}_2(s\kappa, s) \simeq \frac{x_0^2}{sD\sqrt{1+\kappa}} [\widetilde{\mathcal{E}}(1+\kappa) + \widetilde{\mathcal{E}}(1) + \widetilde{\mathcal{A}}(1+\kappa)\widetilde{\mathcal{A}}(1) + \widetilde{\mathcal{D}}(1+\kappa) + \widetilde{\mathcal{C}}(1,\ 1+\kappa) + \widetilde{\mathcal{C}}(1+\kappa,\ 1) + \widetilde{\mathcal{B}}(1+\kappa) + \widetilde{\mathcal{G}}(1+\kappa) + \widetilde{\mathcal{G}}(1)]. \quad (144)$$

D. Result for $\mathcal{F}^{\max}(\kappa, H)$

Taking the results in Eqs. (126), (133), (144), and the expansion Eq. (14) we write in an exponential form analogous to Eq. (107), where, for this problem,

$$\widetilde{\mathcal{W}}_1(\kappa) = \widetilde{\mathcal{A}}(1+\kappa) + \widetilde{\mathcal{A}}(1) + \widetilde{\mathcal{A}}_3(1+\kappa) + 2(\ln\Lambda + \gamma_{\rm E} - 1),$$
$$\widetilde{\mathcal{W}}_2(\kappa) = [\widetilde{\mathcal{E}}(1+\kappa) + \widetilde{\mathcal{E}}(1) + \widetilde{\mathcal{A}}(1+\kappa)\widetilde{\mathcal{A}}(1) + \widetilde{\mathcal{D}}(1+\kappa) + \widetilde{\mathcal{C}}(1,\ 1+\kappa) + \widetilde{\mathcal{C}}(1+\kappa,\ 1) + \widetilde{\mathcal{B}}(1+\kappa) + \widetilde{\mathcal{G}}(1+\kappa) + \widetilde{\mathcal{G}}(1)] - \frac{1}{2}[\widetilde{\mathcal{A}}(1+\kappa) + \widetilde{\mathcal{A}}(1) + \widetilde{\mathcal{A}}_3(1+\kappa)]^2 + 2\left(1 - \frac{\pi^2}{6}\right).$$

The rest of the analysis is very similar to that in Sec. VI D. To leading order we get

$$\widetilde{\mathcal{F}}_1^{\max}(\kappa) = \widetilde{\mathcal{W}}_1(\kappa) - \widetilde{\mathcal{W}}_1(0) = \int_0^{\Lambda/s} \frac{dy}{y^2} (\sqrt{1+\kappa+y} - \sqrt{1+\kappa} - \sqrt{1+y} + 1)^2. \quad (145)$$

Explicitly carrying out the integral in the $\Lambda \to \infty$ limit yields

$$\widetilde{\mathcal{F}}_1^{\max}(\kappa) = -8\ln 2 - (1+\sqrt{1+\kappa})\ln(1+\kappa) + \frac{2}{\sqrt{1+\kappa}}(1+\sqrt{1+\kappa})^2 \ln(1+\sqrt{1+\kappa}). \quad (146)$$

Its inverse transform Eq. (69) is [see Eq. (F8)]

$$\mathcal{K}^{-1}_{\kappa\to\vartheta} \odot \widetilde{\mathcal{F}}_1^{\max}(\kappa) = -8\ln 2 + \psi\left(\sqrt{\frac{\vartheta}{1-\vartheta}}\right) - \ln[\vartheta(1-\vartheta)], \quad (147)$$

with $\psi(x)$ defined in Eq. (41c). Then Eq. (70b) with $\mathcal{R}^{\max}(\vartheta) = \ln[\vartheta(1-\vartheta)]$ gives the leading-order term

$$\mathcal{F}_1^{\max}(\vartheta) = -8\ln 2 + \psi\left(\sqrt{\frac{\vartheta}{1-\vartheta}}\right). \quad (148)$$

The expression in Eq. (148) differs from Eq. (41b) by a constant, which comes from our convention that for the latter the integral over ϑ vanishes.

At second order, we get

$$\begin{aligned}\widetilde{\mathcal{F}}_2^{\max}(\kappa) &= \widetilde{\mathcal{W}}_2(\kappa) - \widetilde{\mathcal{W}}_2(0)\\ &= \{\widetilde{\mathcal{D}}(1+\kappa) - \tfrac{1}{2}\widetilde{\mathcal{A}}_3(1+\kappa)^2 - [\widetilde{\mathcal{D}}(1) - \tfrac{1}{2}\widetilde{\mathcal{A}}_3(1)^2]\}\\ &\quad + \{\widetilde{\mathcal{B}}(1+\kappa) + \widetilde{\mathcal{C}}(1,\ 1+\kappa) + \widetilde{\mathcal{C}}(1+\kappa,\ 1)\\ &\quad - \widetilde{\mathcal{A}}_3(1+\kappa)[\widetilde{\mathcal{A}}(1+\kappa) + \widetilde{\mathcal{A}}(1)]\\ &\quad - [\widetilde{\mathcal{B}}(1) + 2\widetilde{\mathcal{C}}(1,\ 1) - 2\widetilde{\mathcal{A}}_3(1)\widetilde{\mathcal{A}}(1)]\}\\ &\quad + \{\widetilde{\mathcal{E}}(1+\kappa) + \widetilde{\mathcal{G}}(1+\kappa) - \tfrac{1}{2}\widetilde{\mathcal{A}}^2(1+\kappa)\\ &\quad - [\widetilde{\mathcal{E}}(1) + \widetilde{\mathcal{G}}(1) - \tfrac{1}{2}\widetilde{\mathcal{A}}^2(1)]\}. \end{aligned} \tag{149}$$

The terms are written such that each square bracket remains finite for $\Lambda \to \infty$ limit. In fact, we see that the expression in the last square bracket is same as in Eq. (113b) and it vanishes for $\Lambda \to \infty$. Rest two square brackets give $\widetilde{\mathcal{F}}_2^{\max}(\kappa)$ for the $\Lambda \to \infty$.

Remark. We see that for $\kappa = 0$, both $\widetilde{\mathcal{F}}_1^{\max}(\kappa)$ and $\widetilde{\mathcal{F}}_2^{\max}(\kappa)$ vanish, which is consistent with the condition Eq. (72).

From Eq. (70c) and using linearity of the transformation $\mathcal{K}^{-1}_{\kappa\to\vartheta}$ we write

$$\begin{aligned}yes\mathcal{F}_2^{\max}(\vartheta) &= \mathcal{K}^{-1}_{\kappa\to\vartheta} \odot \widetilde{\mathcal{F}}_2^{\max}(\kappa) + \tfrac{1}{2}\{\mathcal{K}^{-1}_{\kappa\to\vartheta} \odot \widetilde{\mathcal{F}}_1^{\max}(\kappa)^2\\ &\quad - [\mathcal{F}_1^{\max}(\vartheta) - \mathcal{R}^{\max}(\vartheta)]^2\}. \end{aligned} \tag{150}$$

Using an identity Eq. (F9) we see that

$$\begin{aligned}&\mathcal{K}^{-1}_{\kappa\to\vartheta} \odot \widetilde{\mathcal{F}}_1^{\max}(\kappa)^2\\ &\quad = \left[\mathcal{F}_1^{\max}(\vartheta) - \mathcal{R}^{\max}(\vartheta)\right]^2 - \psi_2\left(\sqrt{\frac{\vartheta}{1-\vartheta}}\right)^2, \end{aligned} \tag{151}$$

where we define

$$\begin{aligned}\psi_2(x) &= 2\arctan x + x\ln\left(1+\frac{1}{x^2}\right)\\ &\quad - \left[2\arctan\frac{1}{x} + \frac{1}{x}\ln(1+x^2)\right]. \end{aligned} \tag{152}$$

This leads to our result

$$\mathcal{F}_2^{\max}(\vartheta) = \mathcal{K}^{-1}_{\kappa\to\vartheta} \odot \widetilde{\mathcal{F}}_2^{\max}(\kappa) - \frac{1}{2}\psi_2\left(\sqrt{\frac{\vartheta}{1-\vartheta}}\right)^2. \tag{153}$$

(We note that the last term is symmetric in $\vartheta \to 1-\vartheta$.)

It is hard to analytically evaluate the integrals in Eq. (149). Similar to Eq. (119), we determine $\mathcal{F}_2^{\max}(\vartheta)$ by exchanging the order of $\mathcal{K}$-transformation and integration. This gives, up to an additive constant,

$$\begin{aligned}\mathcal{F}_2^{\max}(\vartheta) &= -\frac{1}{2}\psi_2\left(\sqrt{\frac{\vartheta}{1-\vartheta}}\right)^2\\ &\quad + 2\int_0^\infty \frac{dy_1 dy_2}{y_1^2 y_2^2}\ \Psi^{\max}\left(y_1, y_2, \frac{1-\vartheta}{\vartheta}\right), \end{aligned} \tag{154}$$

where $\Psi^{\max}(y_1, y_2, z)$ has a lengthy expression given in the Appendix I. The expression is also given in the supplemental Mathematica notebook [78] for numerical evaluation.

Our result for $\mathcal{F}_2^{\max}(\vartheta)$ in Eq. (153) is plotted in Fig. 17, which agrees well with our computer simulation result in Fig. 7. For this, we evaluated both the $\mathcal{K}^{-1}$-transformation and the y-integration numerically.

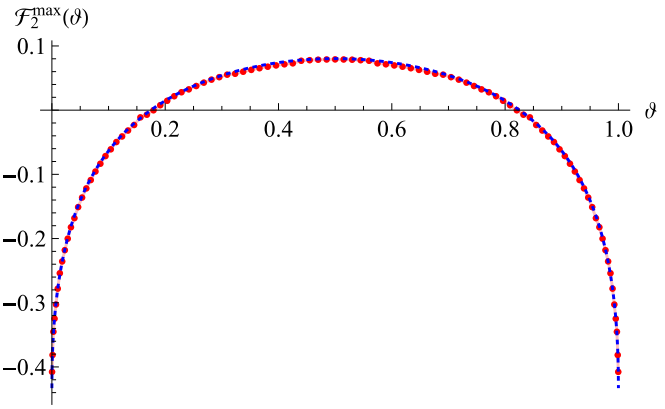

FIG. 17. The dotted points (colored red) show $\mathcal{F}_2^{\max}(\vartheta)$ evaluated by numerical integration from Eq. (153). The solid line is the polynomial in Eq. (44), which gives a good estimation for $\mathcal{F}_2^{\max}(\vartheta)$.

VIII. DISTRIBUTION OF TIME t_{pos} WHERE THE PROCESS IS POSITIVE

This analysis is more involved compared to the analysis for t_{last} and $t_{\max}$. The main reason is that the expressions at second order are very cumbersome, and a lot of ingeniosity is needed to reduce them to a manageable size.

Analogous to Eq. (120), the probability that an fBm, starting at $X_0 = 0$ and evolving until time T, spends time $t_{\text{pos}} = \tau$ being positive ($X_t > 0$), can be expressed as

$$P_T(t_{\text{pos}} = \tau) = \frac{W(\tau, T)}{N(T)}, \tag{155}$$

where $W(\tau, T)$ is the weight of all fBm trajectories contributing to the event and $N(T)$ its normalization. Formally,

$$W(\tau, T) = \int_{-\infty}^{\infty} dm \int_{x(0)=0}^{x(T)=m} \mathcal{D}[x]\,\delta\left\{\tau - \int_0^T dt\ \Theta[x(t)]\right\} e^{-S[x]}, \tag{156}$$

where $\Theta(x)$ is the Heaviside step function. A sketch of such a trajectory is given in Fig. 18. We follow the same notations as in Secs. VI and VII. The definition of the quantities W, N, etc., is modified to measure the positive time.

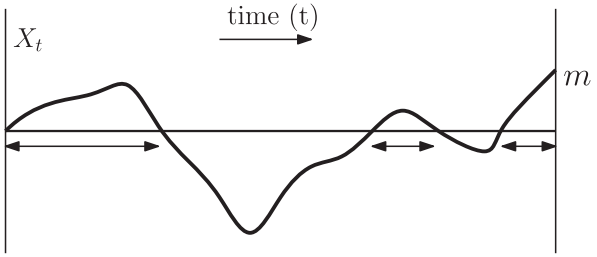

FIG. 18. Schematic of an fBm trajectory leading to positive time t_{pos}. Times spent on the positive side is indicated by double-sided arrow.

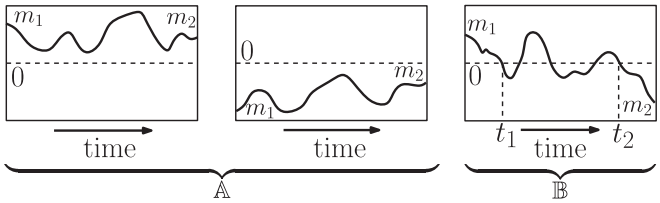

FIG. 19. Different Brownian paths for the conditional propagator in Eq. (160). ($\mathbb{A}$) Includes paths which have never crossed the origin, ($\mathbb{B}$) includes paths which have crossed the origin at least once.

Using the perturbation expansion of the fBm action in Eq. (7) we write Eq. (76), with

$$W_0(\tau,T)=\int_{-\infty}^{\infty} dm\,\langle\langle 1\rangle\rangle_{(0,m)}, \tag{157a}$$

$$W_1(\tau,T)=\int_{-\infty}^{\infty} dm\left\langle\left\langle \frac{S_1}{2D}\right\rangle\right\rangle_{(0,m)}, \tag{157b}$$

$$W_2(\tau,T)=\int_{-\infty}^{\infty} dm\left\langle\left\langle \frac{S_1^2}{8D^2}-\frac{S_2}{D}\right\rangle\right\rangle_{(0,m)}, \tag{157c}$$

where the double-angular brackets denote

$$\langle\langle O[x]\rangle\rangle_{(m_1,m_2)} := \int_{x(0)=m_1}^{x(T)=m_2}\mathcal{D}[x]\,\delta\left\{\tau-\int_0^T dt\,\Theta[x(t)]\right\}e^{-\frac{S_0}{D}}O[x(t)]. \tag{158}$$

This is an average over trajectories with Brownian measure.

A. Conditional propagator

In Secs. VI and VII, the amplitudes in the expansion Eq. (76) are expressed in terms of the free Brownian propagator Z in Eq. (24) and its analog Z^+ in presence of an absorbing wall. For amplitudes Eq. (157), it is natural to express in terms of a conditional Brownian propagator, defined by

$$\mathbb{Z}_T(m_1,m_2|\tau)=\int_{x(0)=m_1}^{x(T)=m_2}\mathcal{D}[x]\,\delta\left\{\tau-\int_0^T dt\,\Theta[x(t)]\right\}e^{-\frac{S_0}{D}}. \tag{159}$$

This gives the weight of all Brownian paths starting at m_1 and ending at m_2 at time T conditioned to spending time τ on the positive half.

To find an explicit expression for the conditional propagator, we write the associated paths into two groups,

$$\mathbb{Z}_T(m_1,m_2|\tau)=\mathbb{A}_T(m_1,m_2|\tau)+\mathbb{B}_T(m_1,m_2|\tau), \tag{160}$$

shown in the Fig. 19. The term $\mathbb{A}$ is nonzero only for $\tau=0$ or T. Using Eq. (81), we write

$$\mathbb{A}_T(m_1,m_2|\tau)=\Theta(m_1)\Theta(m_2)\delta(\tau-T)Z_T^+(m_1,m_2)+\Theta(-m_1)\Theta(-m_2)\delta(\tau)Z_T^+(-m_1,-m_2).$$

Its double Laplace transform can be written with the help of identity Eq. (87) as

$$\widetilde{\mathbb{A}}_s(m_1,m_2|\lambda)=\Theta(m_1)\Theta(m_2)\widetilde{Z}^+_{s+\lambda}(m_1,m_2)+\Theta(-m_1)\Theta(-m_2)\widetilde{Z}^+_s(-m_1,-m_2), \tag{161}$$

where Eq. (85) leads to

$$\widetilde{\mathbb{A}}_s(m_1,m_2|\lambda)=\frac{\Theta(m_1m_2)}{2\sqrt{D[s+\lambda\Theta(m_1)]}}\times\left[e^{-|m_1-m_2|\sqrt{\frac{s+\lambda\Theta(m_1)}{D}}}-e^{-|m_1+m_2|\sqrt{\frac{s+\lambda\Theta(m_1)}{D}}}\right]. \tag{162}$$

The second part of Eq. (160) is defined by (see Fig. 19)

$$\mathbb{B}_T(m_1,m_2|\tau)=\int_0^T dt_1\int_{t_1}^T dt_2\langle\langle\delta(x(t_1))\delta(x(t_2))\rangle\rangle_{(m_1,m_2)}, \tag{163}$$

with τ specified in the average Eq. (158). One can estimate, for example, for $m_1>0$ and $m_2>0$,

$$\langle\langle\delta[x(t_1)]\delta[x(t_2)]\rangle\rangle_{(m_1,m_2)} = \mathcal{N}\,D^2\left[\lim_{x_0\to0}\frac{Z^+_{t_1}(m_1,x_0)}{x_0}\right]\times\mathcal{G}(\tau-t_1-t_2,T-t_1-t_2)\times\left[\lim_{x_0\to0}\frac{Z^+_{t_2}(x_0,m_2)}{x_0}\right] \tag{164}$$

(here D^2 is from dimensional argument), up to a normalization $\mathcal{N}$, where $\mathcal{G}(\tau,T)$ is the weight of Brownian paths starting at the origin and returning there at time T, spending time τ in the positive half.

In general, using identity Eq. (87), we write the double Laplace transform of $\mathbb{B}$ as

$$\widetilde{\mathbb{B}}_s(m_1,m_2|\lambda) = \mathcal{N}\,D^2\,\widetilde{\mathcal{G}}(\lambda,s)\times\left[\lim_{x_0\to0}\frac{\Theta(m_1)\widetilde{Z}^+_{s+\lambda}(m_1,x_0)+\Theta(-m_1)\widetilde{Z}^+_s(-m_1,x_0)}{x_0}\right]\times\left[\lim_{x_0\to0}\frac{\Theta(m_2)\widetilde{Z}^+_{s+\lambda}(x_0,m_2)+\Theta(-m_2)\widetilde{Z}^+_s(x_0,-m_2)}{x_0}\right].$$

The normalization $\mathcal{N}$ to be determined self-consistently, and $\widetilde{\mathcal{G}}(\lambda,s)$ is the double Laplace transform of $\mathcal{G}(\tau,T)$.

We see that

$$\mathcal{G}(\tau,T)=Z_T(0,0)P_{\rm bridge}(\tau,T),$$

where $P_{\rm bridge}(\tau,T)$ is the probability of positive time $t_{\rm pos}=\tau$ for a Brownian bridge of duration T. One can show (a derivation is given in Appendix Q) that for a Brownian bridge, all values of τ are equally probable, and therefore $P_{\rm bridge}(\tau,T)=1/T$. This, along with Eq. (24), gives

$$\widetilde{\mathcal{G}}(\lambda,s)=\frac{\sqrt{s+\lambda}-\sqrt{s}}{\lambda\sqrt{D}}.$$

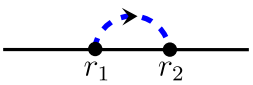

FIG. 20. A one-loop diagram representation of the linear order term Eq. (169) for distribution of positive time. We follow a similar convention as earlier. A dashed line indicates coupling between points (r_1, r_2) (their order indicated by an arrowhead) with a coupling strength $e^{y(r_1-r_2)}$ and a solid disk indicates a 'charge' of amplitude $\dot{x}(r)$ for the associated point r.

Using these results and Eq. (85), we find

$$\widetilde{\mathbb{B}}_s(m_1, m_2|\lambda) = e^{-|m_1|\sqrt{\frac{s+\Theta(m_1)\lambda}{D}}} \times \left[\frac{\sqrt{s+\lambda}-\sqrt{s}}{\lambda\sqrt{D}}\right] e^{-|m_2|\sqrt{\frac{s+\Theta(m_2)\lambda}{D}}}, \quad (165)$$

where we used $\mathcal{N} = 1$, determined using the self-consistency condition that

$$\int_0^T d\tau\ \mathbb{Z}_T(m_1, m_2|\tau) = Z_T(m_1, m_2), \quad (166)$$

for Eq. (160), and equivalently,

$$\widetilde{\mathbb{Z}}_s(m_1, m_2|0) = \widetilde{Z}_s(m_1, m_2) = \frac{e^{-\sqrt{\frac{s}{D}}|m_1-m_2|}}{2\sqrt{sD}},$$

where $\widetilde{\mathbb{Z}}_s(m_1, m_2|\lambda)$ is the Double Laplace transformation Eq. (61) of $\mathbb{Z}_T(m_1, m_2|\tau)$. Results Eqs. (162) and (165) together give

$$\widetilde{\mathbb{Z}}_s(m_1, m_2|\lambda) = \widetilde{\mathbb{A}}_s(m_1, m_2|\lambda) + \widetilde{\mathbb{B}}_s(m_1, m_2|\lambda). \quad (167)$$

This will be used extensively in the following sections.

B. Zeroth-order term

The leading term Eq. (157a) is

$$W_0(\tau, T) = \int_{-\infty}^{\infty} dm\, \mathbb{Z}_T(0, m|\tau).$$

Its double Laplace transform is

$$\widetilde{W}_0(\lambda, s) = \int_{-\infty}^{\infty} dm\ \widetilde{\mathbb{Z}}_s(0, m|\lambda),$$

with $\widetilde{\mathbb{Z}}$ in Eq. (167).

The integration can be evaluated using Eq. (167) with $\widetilde{\mathbb{A}}$ and $\widetilde{\mathbb{B}}$ given in Eqs. (162) and (165). The result is given in Eq. (P3) using which we write

$$\widetilde{W}_0(s\kappa, s) = \frac{1}{s} \times \frac{1}{\sqrt{1+\kappa}}. \quad (168)$$

This is same as for distribution of $t_{\rm last}$ and $t_{\rm max}$, and confirms the arcsine-law Eq. (4).

C. Linear order: One-loop diagram

Using Eq. (10a) we write the linear order term Eq. (157b) as

$$W_1(\tau, T) = \frac{1}{2D}\int_{-\infty}^{\infty} dm \int_0^{\Lambda} dy \int_0^T dr_1 \int_{r_1}^T dr_2 \times e^{y(r_1-r_2)}\ \langle\langle \dot{x}(r_1)\dot{x}(r_2)\rangle\rangle_{(0,m)}, \quad (169)$$

where the integral over time r is interpreted as in Eq. (15). A graphical representation of the amplitude as a one-loop diagram is sketched in Fig. 20.

To evaluate the conditional average in Eq. (169) we use a result for the correlation similar to Eq. (M4). Generalizing the analysis in Appendix M for the conditioned case, we see that for $r_2 > r_1$,

$$\langle\langle \dot{x}(r_1)\dot{x}(r_2)\rangle\rangle_{(m_1,m_2)} = 2^2D^2 \int_0^{r_1} d\tau_1 \int_0^{r_2-r_1} d\tau_2 \int_0^{T-r_2} d\tau_3 \delta(\tau-\tau_1-\tau_2-\tau_3) \int_{-\infty}^{\infty} dx_1\, dx_2\, \mathbb{Z}_{r_1}(m_1, x_1|\tau_1) \times\ \partial_{x_1}\mathbb{Z}_{r_2-r_1}(x_1, x_2|\tau_2)\partial_{x_2}\mathbb{Z}_{T-r_2}(x_2, m_2|\tau_3). \quad (170)$$

This helps us to write $W_1(\tau, T)$ in terms of the conditional propagator $\mathbb{Z}$. By a change of variables and an integration by parts we obtain

$$W_1(\tau, T) = -2D\int_0^{\infty} dt_1 dt_2 dt_3 \int_0^{t_1} d\tau_1 \int_0^{t_2} d\tau_2 \int_0^{t_3} d\tau_3 \delta(T-t_1-t_2-t_3)\ \delta(\tau-\tau_1-\tau_2-\tau_3) \int_0^{\Lambda} dy\, e^{-y\,t_2} \int_{-\infty}^{\infty} dm \times \int_{-\infty}^{\infty} dx_1 dx_2\ \partial_{x_1}\mathbb{Z}_{t_1}(0, x_1|\tau_1)\mathbb{Z}_{t_2}(x_1, x_2|\tau_2)\partial_{x_2}\mathbb{Z}_{t_3}(x_2, m|\tau_3). \quad (171)$$

A double Laplace transform Eq. (61) of the amplitude gives

$$\widetilde{W}_1(\lambda, s) = -2D\int_0^{\Lambda} dy \int_{-\infty}^{\infty} dx_1 dx_2 \partial_{x_1}\widetilde{\mathbb{Z}}_s(0, x_1|\lambda)\widetilde{\mathbb{Z}}_{s+y}(x_1, x_2|\lambda) \int_{-\infty}^{\infty} dm \partial_{x_2}\widetilde{\mathbb{Z}}_s(x_2, m|\lambda), \quad (172)$$

with $\widetilde{\mathbb{Z}}$ defined in Eq. (167).

Using the result Eq. (167) and integrating using integral Eqs. (P7) and (P8), we get

$$\widetilde{W}_1(\kappa\, s, s) = \frac{\widetilde{\mathcal{A}}(1+\kappa)}{s\sqrt{1+\kappa}}, \quad (173)$$

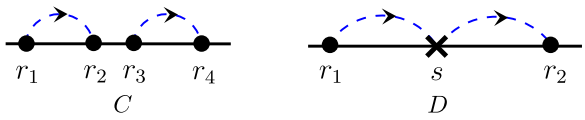

FIG. 21. Two-loop diagrams for the quadratic order term W_2 for the distribution of positive time $t_{\rm pos}$. In this illustration we choose $r_2 > r_1$ and $r_4 > r_3$ for diagram C, whereas $r_1 < s < r_2$ for diagram D. A solid disk denotes a "charge" $\dot{x}(r)$ for the associated point r, whereas a cross denotes a contracted point with a "charge" $2D$.

with

$$\widetilde{\mathcal{A}}(z) = \int_0^{\Lambda/s} \frac{dy}{y^2} [\sqrt{z+y} - \sqrt{z} - \sqrt{1+y} + 1]^2, \tag{174}$$

which by mere coincidence happens to be the same integral as in Eq. (134), although their corresponding diagrams are different.

D. Quadratic order: Two-loop diagrams

Following an analysis similar to that in Sec. VI C, it is straightforward to see that for W_2 in Eq. (157c) contributions come only from the two diagrams shown in Fig. 21,

$$W_2(\tau, T) = C(\tau, T) + D(\tau, T), \tag{175}$$

where the amplitudes are given by

$$C(\tau, T) = \frac{1}{8D^2} \int_{-\infty}^{\infty} dm \int_0^{\Lambda} dy_1 dy_2 \int_0^T dr_1 \int_{r_1}^T dr_2 \int_0^T dr_3 \int_{r_3}^T dr_4 e^{y_1(r_1-r_2)} e^{y_2(r_3-r_4)} \langle\langle \dot{x}(r_1)\dot{x}(r_2)\dot{x}(r_3)\dot{x}(r_4)\rangle\rangle_{(0,m)} \tag{176}$$

and

$$D(\tau, T) = \frac{1}{2D} \int_{-\infty}^{\infty} dm \int_0^{\Lambda} dy_1 dy_2 \int_0^T dr_1 \int_{r_1}^T ds \int_s^T dr_2 e^{y_1(r_1-s)} e^{y_2(s-r_2)} \langle\langle \dot{x}(r_1)\dot{x}(r_2)\rangle\rangle_{(0,m)}. \tag{177}$$

These amplitudes can be expressed in terms of the conditional propagator $\mathbb{Z}_T$ in Eq. (160), and then an explicit result can be derived following an analysis similar to that of the linear-order term in Sec. VIII C. Here we give their final expression, and defer their derivation to the Appendix J.

The double Laplace transform of the amplitude of the diagram D in Fig. 21 can be written as

$$\widetilde{D}(\kappa\, s, s) = \frac{\widetilde{\mathcal{D}}(1+\kappa)}{s\sqrt{1+\kappa}}, \tag{178}$$

where

$$\widetilde{\mathcal{D}}(z) = \frac{2}{(1+\sqrt{z})} \int_0^{\Lambda/s} \frac{dy_1 dy_2}{y_1 y_2} \left\{ \frac{y_2\, \mathfrak{h}(1, z, y_1)}{(y_2 - y_1)} + \frac{y_1\, \mathfrak{h}(1, z, y_2)}{(y_1 - y_2)} \right\}, \tag{179}$$

with

$$\mathfrak{h}(s_1, s_2, y) = \frac{(\sqrt{s_2+y} - \sqrt{s_1+y})[\sqrt{s_2(s_1+y)} - \sqrt{s_1(s_2+y)}]}{(\sqrt{s_1+y} + \sqrt{s_1})(\sqrt{s_2+y} + \sqrt{s_2})}. \tag{180}$$

The double Laplace transform for the diagram C in Fig. 21 is

$$\widetilde{C}(\kappa\, s, s) = \frac{\widetilde{\mathcal{C}}(1+\kappa)}{s\sqrt{1+\kappa}}, \tag{181}$$

with

$$\widetilde{\mathcal{C}}(z) = \frac{4}{(1+\sqrt{z})} \int_0^{\Lambda/s} \frac{dy_1 dy_2}{y_1 y_2} \left\{ \mathfrak{f}(1, z, y_1, y_2) + \mathfrak{f}(z, 1, y_1, y_2) + \frac{\mathfrak{g}(1, z, y_1, y_2) + \mathfrak{g}(z, 1, y_1, y_2)}{y_1} \right\}, \tag{182}$$

where we define

$$\begin{aligned} \mathfrak{g}(s_1, s_2, y_1, y_2) = {} & \sqrt{s_1+y_1+y_2}\, (\sqrt{s_2+y_1+y_2} - \sqrt{s_1+y_1+y_2}) \\ & \times (\sqrt{s_1+y_1} + \sqrt{s_1+y_2} - \sqrt{s_1} + \sqrt{s_2+y_1+y_2} - \sqrt{s_2+y_1} - \sqrt{s_2+y_2} + \sqrt{s_2}) \\ & \times \left[\frac{(\sqrt{s_1} + \sqrt{s_2})(-\sqrt{s_1} - \sqrt{s_2+y_1} + \sqrt{s_2})}{(\sqrt{s_1+y_1} + \sqrt{s_2+y_1})(\sqrt{s_1+y_1+y_2} + \sqrt{s_1+y_1})} + \frac{\sqrt{s_1}}{\sqrt{s_1+y_1+y_2} + \sqrt{s_1}} \right] \end{aligned}$$

$$+ (s_1+y_2)(\sqrt{s_1+y_2}-\sqrt{s_2+y_2})\left[\frac{(\sqrt{s_1}+\sqrt{s_2})(-\sqrt{s_1}-\sqrt{s_2+y_1}+\sqrt{s_2})}{(\sqrt{s_1+y_1}+\sqrt{s_2+y_1})(\sqrt{s_1+y_1}+\sqrt{s_1+y_2})}+\frac{\sqrt{s_1}}{\sqrt{s_1+y_2}+\sqrt{s_1}}\right]$$
$$+\frac{1}{4}(s_2-s_1)(\sqrt{s_1+y_1}+\sqrt{s_1}-\sqrt{s_2+y_1}-\sqrt{s_2})$$
$$+\frac{\sqrt{s_1}(\sqrt{s_1+y_1}-\sqrt{s_2+y_1})[\sqrt{s_1}(\sqrt{s_2+y_1}-\sqrt{s_2})+2s_1+y_1]}{\sqrt{s_1+y_1}+\sqrt{s_1}}, \tag{183}$$

and

$$\mathfrak{f}(s_1,s_2,y_1,y_2)=\frac{(s_1+y_2)}{y_2}(\sqrt{s_2+y_2}-\sqrt{s_1+y_2})\left[\frac{(\sqrt{s_1}+\sqrt{s_2})(\sqrt{s_2}-\sqrt{s_1}-\sqrt{s_2+y_1})}{(\sqrt{s_1+y_1}+\sqrt{s_2+y_1})(\sqrt{s_1+y_1}+\sqrt{s_1+y_2})}+\frac{\sqrt{s_1}}{\sqrt{s_1+y_2}+\sqrt{s_1}}\right]$$
$$+\frac{(\sqrt{s_2}-\sqrt{s_1})}{4y_2}\left[1+\frac{2(\sqrt{s_1}+\sqrt{s_2})(\sqrt{s_2}-\sqrt{s_1}-\sqrt{s_2+y_1})}{(\sqrt{s_1+y_1}+\sqrt{s_1})(\sqrt{s_1+y_1}+\sqrt{s_2+y_1})}\right]$$
$$\times(2\sqrt{s_1}\sqrt{s_2+y_2}-2\sqrt{s_1}\sqrt{s_2}-2\sqrt{s_1}\sqrt{s_1+y_2}-y_2)$$
$$+\frac{\sqrt{s_1}(\sqrt{s_2+y_1}-\sqrt{s_1+y_1})(\sqrt{s_2}-\sqrt{s_1}-\sqrt{s_2+y_1})}{2(\sqrt{s_1+y_1}+\sqrt{s_1})^2}. \tag{184}$$

Adding contribution of these two diagrams we get the double Laplace transform of the second order term

$$\widetilde{W}_2(\lambda,s)=\widetilde{C}(\lambda,s)+\widetilde{D}(\lambda,s).$$

The expressions in Eqs. (183) and (184) are given in the supplemental Mathematica notebook [78] for their numerical evaluation.

E. Result for $\mathcal{F}^{\rm pos}(\kappa,H)$

Rest of the analysis is very similar to that for $t_{\rm last}$ and $t_{\rm max}$. We write the amplitude $\widetilde{W}(\lambda,s)$ in Eq. (156) in an exponential form such that

$$\widetilde{W}(s\kappa,s)=\frac{e^{\widetilde{\mathcal{W}}(\kappa)}}{s\sqrt{1+\kappa}}, \tag{185}$$

where $\widetilde{\mathcal{W}}=\varepsilon\,\widetilde{\mathcal{W}}_1+\varepsilon^2\,\widetilde{\mathcal{W}}_2+\cdots$, with

$$\widetilde{\mathcal{W}}_1(\kappa)=\widetilde{\mathcal{A}}(1+\kappa), \tag{186a}$$
$$\widetilde{\mathcal{W}}_2(\kappa)=\widetilde{\mathcal{C}}(1+\kappa)+\widetilde{\mathcal{D}}(1+\kappa)-\tfrac{1}{2}\widetilde{\mathcal{A}}(1+\kappa)^2. \tag{186b}$$

Considering the normalization in Eq. (155) we get the Laplace transform of the distribution of $t_{\rm pos}$ in Eq. (67) with

$$\widetilde{\mathcal{F}}^{\rm pos}(\kappa,H)=\widetilde{\mathcal{W}}(\kappa)-\widetilde{\mathcal{W}}(0). \tag{187}$$

One can verify that $\widetilde{\mathcal{W}}(0)=0$ up to the second order in the perturbation expansion, and this means in the expansion Eq. (70a),

$$\widetilde{\mathcal{F}}_1^{\rm pos}(\kappa)=\widetilde{\mathcal{W}}_1(\kappa)\quad\text{and}\quad\widetilde{\mathcal{F}}_2^{\rm pos}(\kappa)=\widetilde{\mathcal{W}}_2(\kappa). \tag{188}$$

Comparing with Eq. (145) we see that $\widetilde{\mathcal{F}}_1^{\rm pos}(\kappa)$ is exactly same as $\widetilde{\mathcal{F}}_1^{\rm max}(\kappa)$, and therefore we get

$$\mathcal{F}_1^{\rm pos}(\vartheta)=\mathcal{F}_1^{\rm max}(\vartheta) \tag{189}$$

given in Eq. (148).

The difference with the distribution for $t_{\rm max}$ comes in the second order term. This is given by

$$\mathcal{F}_2^{\rm pos}(\vartheta)=-\tfrac{1}{2}[\mathcal{F}_1^{\rm pos}(\vartheta)-\mathcal{R}^{\rm pos}(\vartheta)]^2$$
$$+\mathcal{K}^{-1}_{\kappa\to\vartheta}\odot\left[\widetilde{\mathcal{F}}_2^{\rm pos}(\kappa)+\tfrac{1}{2}\widetilde{\mathcal{F}}_1^{\rm pos}(\kappa)^2\right]. \tag{190}$$

Following a similar analysis as used for Eq. (153) we get our result

$$\mathcal{F}_2^{\rm pos}(\vartheta)=-\frac{1}{2}\psi_2\left(\sqrt{\frac{\vartheta}{1-\vartheta}}\right)^2+\mathcal{K}^{-1}_{\kappa\to\vartheta}$$
$$\odot\left[\widetilde{\mathcal{C}}(1+\kappa)+\widetilde{\mathcal{D}}(1+\kappa)-\frac{1}{2}\widetilde{\mathcal{A}}(1+\kappa)^2\right] \tag{191}$$

with Eq. (152).

It is difficult to analytically do the integration for the amplitudes in the second term in Eq. (191). We have numerically verified that the term remains finite for $\Lambda\to\infty$. For an explicit formula in terms of ϑ we exchange the order of $\mathcal{K}^{-1}_{\kappa\to\vartheta}$-transformation and the integration. This allows us to write

$$\mathcal{F}_2^{\rm pos}(\vartheta)=-\frac{1}{2}\psi_2\left(\sqrt{\frac{\vartheta}{1-\vartheta}}\right)^2$$
$$+2\int_0^\infty\frac{dy_1dy_2}{y_1^2y_2^2}\,\Psi^{\rm pos}\left(y_1,y_2,\frac{1-\vartheta}{\vartheta}\right). \tag{192}$$

Expression for $\Psi^{\rm pos}$ is lengthy and it is given in the Appendix K. Our result for $\mathcal{F}_2^{\rm pos}(\vartheta)$ is plotted in Fig. 7, which agrees well with our computer simulation result. For this we evaluated both the $\mathcal{K}^{-1}$-transformation and the y-integration numerically.

IX. SUMMARY

We found a generalization of the three arcsine laws of Brownian motion for an fBm. Unlike in the Brownian motion, the probabilities are different and given in Eqs. (39) and (38).

These results are obtained using a perturbation expansion around the Brownian motion, and by a scaling argument for divergences near $\vartheta \to 0$ and 1. Our numerical simulations confirm these highly nontrivial predictions accurately. We find a very good convergence to the numerical results for the entire range of ϑ even for large ε. Most realizations of fBm found in practical applications fall within the range $H \simeq \frac{1}{2} \pm 0.25$ where our formulas yield high-precision predictions.

Our perturbation approach offers a systematic framework to obtain analytical results for other observables of an fBm, of which very few are available so far. For example, distribution of Area under a Brownian excursion is known to have an Airy distribution [79]. Corresponding generalization for an fBm is yet unavailable. On simpler examples, a closed form expression for an fBm propagator with absorbing and reflecting boundary is desirable.

ACKNOWLEDGMENTS

T.S. acknowledges support of the Department of Atomic Energy, Government of India, under Project Identification No. RTI-4002. K.J.W. thanks PSL for support by Grant No. ANR-10-IDEX-0001-02-PSL. It is a pleasure to thank M. Delorme for his contributions to the early stages of this work, and J. U. Klamser for her help with figures.

APPENDIX A: PERTURBATION EXPANSION OF THE FBM ACTION

Writing $H = \frac{1}{2} + \varepsilon$ in the expression for $G^{-1}(t_1, t_2) = \langle X_{t_1} X_{t_2} \rangle$ given in Eq. (1) and expanding in powers of small ε we get

$$G^{-1}(t_1, t_2) = K_0(t_1, t_2) + \varepsilon K_1(t_1, t_2) + \varepsilon^2 K_2(t_1, t_2) + \cdots,$$

where

$$K_0(t_1, t_2) \equiv G_0^{-1}(t_1, t_2) = 2 \min(t_1, t_2),$$

and, for $n \geqslant 1$,

$$K_n(t_1, t_2) = \frac{2^n}{n!}[t_1 \ln^n t_1 \quad + t_2 \ln^n t_2 - |t_1 - t_2| \ln^n |t_1 - t_2|]. \tag{A1}$$

For G related by $G^{-1}\, G(t_1, t_2) = G\, G^{-1}(t_1, t_2) = \delta(t_1 - t_2)$, this is equivalent[1] to a perturbation expansion

$$G(t_1, t_2) = G_0(t_1, t_2) + \varepsilon\, G_1(t_1, t_2) + \varepsilon^2\, G_2(t_1, t_2) + \cdots,$$

with

$$G_0(t_1, t_2) = -\tfrac{1}{2}\delta''(t_1 - t_2), \tag{A2a}$$

and for $n \geqslant 1$,

$$G_n(t_1, t_2) = -\sum_{q=1}^{n} G_0 K_q G_{n-q}(t_1, t_2). \tag{A2b}$$

(Here we denote

$$AB(t_1, t_2) = \int_0^T ds\, A(t_1, s) B(s, t_2), \tag{A3}$$

for any two bivariate functions A and B.)

It will be convenient for our analysis to write G_n in Eq. (A2) as

$$G_n = G_0 \Sigma_n G_0 \tag{A4}$$

for all positive integers n, such that

$$\Sigma_0 = K_0, \quad \Sigma_1 = -K_1, \quad \Sigma_2 = -K_2 + K_1 G_0 K_1,$$
$$\Sigma_3 = -K_3 + K_2 G_0 K_1 + K_1 G_0 K_2 - K_1 G_0 K_1 G_0 K_1, \tag{A5}$$

and so on. In terms of this perturbation expansion, action Eq. (5) is written as

$$S = S_0 + \varepsilon\, \mathcal{L}_1 + \varepsilon^2 \mathcal{L}_2 + \cdots, \tag{A6}$$

where S_0 is in Eq. (8a) and for $n \geqslant 1$,

$$\mathcal{L}_n = \int_0^T dt_1 \int_0^T dt_2\, \dot{x}(t_1) \left\{ \frac{1}{8} \partial_{t_1} \partial_{t_2} \Sigma_n(t_1, t_2) \right\} \dot{x}(t_2), \tag{A7}$$

obtained by integration by parts.

For their explicit expression we use the following results obtained from Eq. (A1): for $t_2 \geqslant t_1$,

$$\frac{1}{4} \partial_{t_1} \partial_{t_2} K_1 = (1 + \ln \omega) \delta(t_1 - t_2) + \frac{1}{2} \frac{1}{(t_2 - t_1)}, \tag{A8a}$$

$$\frac{1}{4} \partial_{t_1} \partial_{t_2} K_2 = \left(\frac{\pi^2}{6} + 2 \ln \omega + \ln^2 \omega \right) \delta(t_1 - t_2) + \frac{1 + \ln \omega}{(t_2 - t_1)} + \frac{1}{2} \int_{t_1 + \omega}^{t_2 - \omega} \frac{ds}{(t_2 - s)(s - t_1)}, \tag{A8b}$$

where singularities are regularized by introducing an infinitesimally small ultraviolet cutoff $\omega > 0$ in time, such that terms like $\delta(t_1 - t_2) \ln(t_2 - t_1) \simeq \delta(t_1 - t_2) \ln \omega$ and

$$\frac{\ln(t_2 - t_1)}{(t_2 - t_1)} \simeq \frac{\ln \omega}{(t_2 - t_1)} + \frac{\pi^2}{6} \delta(t_1 - t_2) + \frac{1}{2} \int_{t_1 + \omega}^{t_2 - \omega} \frac{ds}{(t_2 - s)(s - t_1)}, \tag{A8c}$$

which are used for writing Eq. (A8b). Similarly, for $t_2 \geqslant t_1$,

$$\frac{1}{4} \partial_{t_1} \partial_{t_2} K_1 G_0 K_1 = 2(1 + \ln \omega)^2 \delta(t_1 - t_2) + \frac{2(1 + \ln \omega)}{(t_2 - t_1)} + \frac{1}{2} \int_0^T \frac{ds}{|t_1 - s||t_2 - s|}. \tag{A8d}$$

Using Eq. (A8) in Eqs. (A5) and (A7) it is easy to see that

$$\mathcal{L}_1 = -2(1 + \ln \omega) S_0 - \frac{1}{2} S_1, \tag{A9a}$$

$$\mathcal{L}_2 = \left[2\left(1 - \frac{\pi^2}{6}\right) + 2(1 + \ln \omega)^2 \right] S_0 + (1 + \ln \omega) S_1 + S_2, \tag{A9b}$$

where S_0, S_1, and S_2 are defined in Eq. (8). The expansion (A6) with Eq. (A9) gives Eq. (7).

[1] To see this one can verify that $K_0 \cdot G_0(r, s) = G_0\, K_0(r, s) = \delta(r - s)$ and then use $\sum_{q=0}^{n} K_q\, G_{n-q} = 0$ for all $n \geqslant 1$, which can be seen from Eq. (A2b).

APPENDIX B: ALTERNATE DERIVATION OF THE ACTION

Here we give an elegant and short derivation of the action in Eqs. (7) and (8) in a normal-ordered form. Using integration by parts, Eq. (5) gives

$$S[X_t] = \frac{1}{2}\int_0^T dt_1 \int_0^T dt_2\, \dot{X}_{t_1} C^{-1}(t_1,t_2)\dot{X}_{t_2}, \tag{B1}$$

with the correlation

$$C(t_1,t_2) = \langle \dot{X}_{t_1}\dot{X}_{t_2}\rangle = 4H|t_1-t_2|^{2H-1}\delta(t_1-t_2) + 2H(2H-1)|t_1-t_2|^{2(H-1)}. \tag{B2}$$

An expansion in $\varepsilon = H - \frac{1}{2}$ gives

$$C(t_1,t_2) = 2\widehat{D}\left[\delta(t_1-t_2) + \varepsilon\frac{1}{|t_1-t_2|} + \varepsilon^2\frac{2\ln\frac{|t_1-t_2|}{\omega}}{|t_1-t_2|} + \cdots\right], \tag{B3}$$

with $\widehat{D} = 2H\omega^{2H-1} = (1+2\varepsilon)\omega^{2\varepsilon}$, and ω being an ultraviolet cutoff in time. This implies

$$C^{-1}(t_1,t_2) = \frac{1}{2\widehat{D}}\left[\delta(t_1-t_2) - \frac{\varepsilon}{|t_1-t_2|} - \varepsilon^2\frac{2\ln\frac{|t_1-t_2|}{\omega}}{|t_1-t_2|} + \varepsilon^2\int ds\frac{1}{|s-t_1||s-t_2|} + \cdots\right].$$

Substituting in Eq. (B1) and defining a normal-ordered form (noncontact terms only) in Eq. (17) we get

$$\mathcal{S}^{(n)}[X_t] = \frac{1}{2\widehat{D}}\int_{t1<t_2} dt_1 dt_2 \dot{X}_{t_1}\dot{X}_{t_2}\left[\delta(t_1-t_2) - \frac{\varepsilon}{|t_1-t_2|} - 2\varepsilon^2\frac{\ln\frac{|t_1-t_2|}{\omega}}{|t_1-t_2|} + \cdots\right]. \tag{B4}$$

Using the integral representation Eq. (A8c) this gives

$$\mathcal{S}^{(n)}[X_t] = \frac{1}{2D}\int_{t1<t_2} dt_1 dt_2 \dot{X}_{t_1}\dot{X}_{t_2}\left[\delta(t_1-t_2) - \frac{\varepsilon}{|t_1-t_2|} - \varepsilon^2\int_{t_1}^{t_2} ds\frac{1}{|s-t_1||s-t_2|} + \cdots\right], \tag{B5}$$

with D given in Eq. (9). Comparing with Eqs. (7) and (8) one can see that the both leading and subleading terms are same whereas the ε^2 order term includes only contact-less terms. An integral representation of the normal-ordered second-order term is in Eq. (18).

APPENDIX C: THE FBM PROPAGATOR

Here, we verify Eq. (19) using the perturbation expansion of the action Eq. (A6) to all orders. In terms of this expansion, Eq. (21a) can be written as

$$W_H(m,T) = \left\langle e^{-\sum_{n\geqslant 1}\varepsilon^n\mathcal{L}_n}\right\rangle, \tag{C1}$$

where by the angular brackets we denote (definition restricted only for this Appendix)

$$\langle O[x]\rangle \equiv \int_{x(0)=0}^{x(T)=m}\mathcal{D}[x]\, e^{-S_0}O[x]. \tag{C2}$$

Then, using a result for the multitime correlation given later in Eq. (M13) for $D=1$ and the propagator Eq. (21a) leads to

$$\mathcal{G}_H(m,T) = e^{F(T)\partial_m^2}\mathcal{G}(m,T), \tag{C3}$$

with

$$F(T) = \frac{1}{2}\int_0^T dt_1\int_0^T dt_1 \sum_{n\geqslant 1}\varepsilon^n\partial_{t_1}\partial_{t_2}K_n(t_1,t_2), \tag{C4}$$

where we used Eq. (A5) and Eq. (A7).

Remark. In Eq. (C3), the contribution from terms like $K_1G_0K_1$, etc., in Eq. (A5) are canceled from the terms in normalization N_T in Eq. (19). One may explicitly verify this at lower orders in perturbation expansion.

Using Eq. (A1) in Eq. (C4), it is easy to see that

$$F(T) = T\sum_{n\geqslant 1}\frac{(2\varepsilon\ln T)^n}{n!} = T(T^{2\varepsilon}-1), \tag{C5}$$

which in Eq. (C3) leads to

$$\mathcal{G}_H(m,T) = e^{(T^{2H}-T)\partial_m^2}\mathcal{G}(m,T), \tag{C6}$$

where we used $1+2\varepsilon = 2H$. Using the expression of $\mathcal{G}(m,T)$ in Eq. (24), it is now easy to obtain Eq. (19).

APPENDIX D: NUMERICAL SIMULATION OF AN fBm

Efficient computer simulation of an fBm trajectory is a delicate task. A vast literature has been published on this subject. For a comparative study of many of the sampling methods for an fBm see the review [80] and references therein. In general these algorithms generate the full trajectory. If one is only interested in a specific observable, as the first-passage time, not all points need to be generated, allowing for tremendous gains both in memory usage and execution speed [68,74,75].

In our work, we use a discrete-time sampling method following the Davis and Harte procedure [72] (also known as the Wood and Chan procedure [81]) as described in Ref. [73]. The basic idea is to construct fBm paths from a discrete-time sampling of stationary, Gaussian-distributed, increments ΔX_n for integers $n = 0, 1, \cdots, N-1$, with mean $\langle \Delta X_n\rangle = 0$ and covariance

$$\langle \Delta X_m \Delta X_n\rangle = \gamma(m-n) = (m-n+1)^{2H} + (m-n-1)^{2H} - 2(m-n)^{2H}, \tag{D1}$$

for positive integers $n \leqslant m < N$. For large N with $t = n/N$, one can see that $N^{2-2H}\gamma(Nt-Ns)$ converge to the covariance Eq. (2). This means, the cumulated sum $N^{-H}\sum_{i=0}^{n}\Delta X_i$ for large N gives an fBm path X_t with $X_0 = 0$ in a time window [0,1].

The Davis and Harte procedure is an efficient algorithm for generating samples of ΔX_n with a computational efficiency $\mathcal{O}(N\ln N)$ (compared to $\mathcal{O}(N^3)$ for Choleski decomposition method [80]). The algorithm involves the following simple

steps. We construct two linear arrays $\{W_n\}$ and $\{\lambda_n\}$ of length $2N$ with index $n = 0, 1, \cdots, 2N-1$. Elements of the first array are generated from a set of $2N$ independent Gaussian random numbers $V_0, V_1, \cdots, V_{2N-1}$, with $\langle V_n \rangle = 0$ and $\langle V_m V_n \rangle = \delta_{m,n}$. We define

$$W_0 = V_0, \quad W_n = \frac{1}{\sqrt{2}}(V_n + i\, V_{2N-n}), \tag{D2}$$

for $n = 1, \cdots, N-1$, whereas

$$W_N = V_N, \quad W_n = \frac{(-i)}{\sqrt{2}}(V_n + i\, V_{2N-n}), \tag{D3}$$

for $n = N+1, \cdots, 2N-1$. This construction ensures that $\langle W_n \rangle = 0$ and

$$\langle W_k W_{k'} \rangle = \delta_{k,0}\delta_{k',0} + \delta_{k+k',2N}, \tag{D4}$$

for indices $0 \leqslant k \leqslant 2N-1$.

Elements of the second array are defined by

$$\lambda_n = \sum_{k=0}^{2N-1} \Gamma_k \, e^{i\,\pi \frac{nk}{N}} \tag{D5}$$

for integers $0 \leqslant n \leqslant 2N-1$, where $\Gamma_k = \gamma(k)$ for $0 \leqslant k \leqslant N$ and $\Gamma_k = \gamma(2N-k)$ for $N+1 \leqslant k \leqslant 2N-1$ with covariance in Eq. (D1). This means,

$$\lambda_{2N-n} = \lambda_n \tag{D6}$$

and the inversion formula

$$\Gamma_k = \frac{1}{2N} \sum_{n=0}^{2N-1} \lambda_n \, e^{-i\,\pi \frac{nk}{N}}. \tag{D7}$$

The set of increments for a discrete fBm are obtained from

$$\Delta X_n = \frac{1}{\sqrt{2N}} \sum_{k=0}^{2N-1} W_k \, \sqrt{\lambda_k} \, e^{i\pi \frac{nk}{N}} \tag{D8}$$

for $0 \leqslant n \leqslant N-1$. In comparison, we shall see that the set of increments for $N \leqslant n \leqslant 2N-1$ do not have the covariance Eq. (D1) and they are discarded.

It is simple to verify that this construction Eq. (D8) indeed generates Gaussian random numbers with covariance Eq. (D1). The simplest is to see that $\langle \Delta X_n \rangle = 0$ from $\langle W_n \rangle = 0$. Moreover, X_n is a linear combination of Gaussian random variables W_n, and therefore its distribution remains Gaussian. For the covariance, using Eq. (D8) we write

$$\langle \Delta X_m \Delta X_n \rangle = \frac{1}{2N} \sum_{k,k'=0}^{2N-1} \langle W_k W_{k'} \rangle \, \sqrt{\lambda_k \lambda_{k'}} \, e^{\frac{i\pi}{N}(nk+mk')},$$

which using Eq. (D4) gives

$$\langle \Delta X_m \Delta X_n \rangle = \frac{1}{2N} \left\{ \lambda_0 + \sum_{k=1}^{2N-1} \sqrt{\lambda_k \lambda_{2N-k}} \, e^{-i\frac{\pi}{N}(m-n)k} \right\}, \tag{D9}$$

for $n \leqslant m$. Using the symmetry in Eq. (D6) the above expression simplifies to

$$\langle \Delta X_m \Delta X_n \rangle = \frac{1}{2N} \sum_{k=1}^{2N-1} \lambda_k \, e^{-i\frac{\pi}{N}(m-n)k},$$
$$= \Gamma_{m-n} \tag{D10}$$

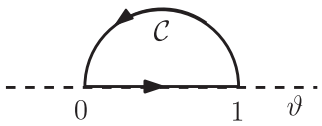

FIG. 22. Contour C for the complex integral (E).

for $m \geqslant n$, where in the last step we used the inverse Fourier transformation Eq. (D7). It is clear from Eq. (D10) that

$$\langle \Delta X_m \Delta X_n \rangle = \gamma(m-n) \quad \text{for } m-n \leqslant N, \tag{D11}$$

which includes all $0 \leqslant n \leqslant m \leqslant N-1$. For indices $\geqslant N$, such that $m - n > N$, the covariance is $\gamma(2N-m+n)$, and therefore ΔX_n for $n \geqslant N$ are discarded.

The mathematics behind this algorithm is clearly explained in Refs. [73,80]. It involves calculating square root of a positive matrix by embedding it in a circulant matrix. We shall not repeat the discussion this here. Reader may find details in Refs. [73,80].

APPENDIX E: A DERIVATION OF THE INVERSE TRANSFORM

The inverse transformation in Eq. (64) can be derived using complex analysis by writing Eq. (63) as

$$\widetilde{p}(z) = \oint_C d\ell \, \frac{p(\ell)}{1+z\ell},$$

where C is a simple closed contour drawn in Fig. 22. In an alternative representation

$$\frac{1}{2\pi i} \oint_C d\ell \, \frac{p(\ell)}{\ell - z} = f(z) := \frac{1}{2\pi i}\left(-\frac{1}{z}\right)\widetilde{p}\left(-\frac{1}{z}\right). \tag{E1}$$

The *Sokhotski-Plemlj* formula of complex analysis gives the inverse transformation

$$p(\ell) = f_+(\ell) - f_-(\ell) \tag{E2}$$

for any point ℓ on the contour C, where $f_\pm(\ell) = \lim_{z \to \ell} f(z)$ with the limit taken from the domain *inside* (+) and *outside* (-) the contour C, respectively. For $\ell = \vartheta$ on the real axis,

$$f_\pm(\vartheta) = -\frac{1}{2\pi i\, \vartheta} \lim_{\delta \to 0} \widetilde{p}\left(-\frac{1}{\vartheta} \pm i\delta\right) \tag{E3}$$

and this gives Eq. (64).

APPENDIX F: A LIST OF USEFUL $\mathcal{K}^{-1}$ TRANSFORMS

Here, we give functions, which are related by the transformation Eq. (69) and its inverse transformation Eq. (71). These relations, indicated below by $\leftrightarrow$, are useful for our analysis.

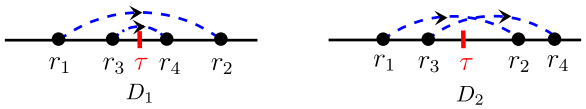

FIG. 23. Two distinct cases of the two-loop diagram D in Fig. 14 for distribution of t_{last}, categorized according to whether loops intersect (for D_1) or not (for D_2). The time variables r's remain on the same side of τ as indicated.

They can be numerically verified in Mathematica. A trivial, but useful result is $1 \leftrightarrow 1$.

Among others,

$$-2\ln[1+\sqrt{1+\kappa}] \leftrightarrow \ln\vartheta, \tag{F1}$$

$$-2\ln\left[1+\frac{1}{\sqrt{1+\kappa}}\right] \leftrightarrow \ln(1-\vartheta), \tag{F2}$$

which using linearity of the transformation leads to

$$\ln(1+\kappa) - 4\ln[1+\sqrt{1+\kappa}] \leftrightarrow \ln\vartheta(1-\vartheta), \tag{F3}$$

and

$$-\ln(1+\kappa) \leftrightarrow \ln\frac{\vartheta}{1-\vartheta}. \tag{F4}$$

Additionally,

$$[\ln(1+\kappa)]^2 \leftrightarrow \left(\ln\frac{\vartheta}{1-\vartheta}\right)^2 - \pi^2. \tag{F5}$$

We get

$$\frac{\ln(1+\sqrt{1+\kappa})}{\sqrt{1+\kappa}} \leftrightarrow x\arctan\frac{1}{x}, \tag{F6}$$

and

$$\sqrt{1+\kappa}\ln(1+\frac{1}{\sqrt{1+\kappa}}) \leftrightarrow \frac{1}{x}\arctan x, \tag{F7}$$

where $x=\sqrt{\frac{\vartheta}{1-\vartheta}}$. A linear combination of Eqs. (F2), (F6), and (F7) gives

$$-(1+\sqrt{1+\kappa})\ln(1+\kappa) + \frac{2(1+\sqrt{1+\kappa})^2}{\sqrt{1+\kappa}} \times \ln(1+\sqrt{1+\kappa}) \leftrightarrow \psi(x) - \ln\vartheta(1-\vartheta), \tag{F8}$$

with Eq. (41c) and the same definition for x. A related result about square of the above function is

$$\left[-(1+\sqrt{1+\kappa})\ln(1+\kappa) + \frac{2(1+\sqrt{1+\kappa})^2}{\sqrt{1+\kappa}}\ln(1+\sqrt{1+\kappa})\right]^2 \leftrightarrow [\psi(x) - \ln\vartheta(1-\vartheta)]^2 - \psi_2(x)^2. \tag{F9}$$

with Eqs. (41c) and (152).

Other results, useful for verifying Eqs. (43), (44), and (45), are

$$\frac{\Gamma\left(\frac{n}{2}\right)}{\sqrt{\pi}}\,{}_2F_1\left(\frac{1}{2},\frac{n-1}{2},\frac{n+1}{2},-\kappa\right) \leftrightarrow (\vartheta)^{\frac{n-1}{2}}, \tag{F10}$$

$$\frac{\sqrt{1+\kappa}\,\Gamma\left(\frac{n}{2}\right)}{\sqrt{\pi}}\,{}_2F_1\left(\frac{1}{2},1,\frac{n+1}{2},-\kappa\right) \leftrightarrow (1-\vartheta)^{\frac{n-1}{2}}, \tag{F11}$$

and their product

$$\frac{\sqrt{1+\kappa}\,\Gamma\left(\frac{n}{2}\right)^2}{\sqrt{\pi}}\,{}_2F_1\left(1,\frac{n}{2},n,-\kappa\right) \leftrightarrow [\vartheta(1-\vartheta)]^{\frac{n-1}{2}}, \tag{F12}$$

for $n \geqslant 1$, where ${}_2F_1(a,b,c,z)/\Gamma(c)$ is regularized hypergeometric function and it can be evaluated to arbitrary numerical precision in Mathematica.

APPENDIX G: AMPLITUDE OF THE TWO-LOOP DIAGRAMS FOR $t_{\rm last}$

Here, we give a detailed derivation of the amplitudes of two-loop diagrams shown in Fig. 14.

1. Nontrivial diagram D contributing to $\mathcal{F}^{\rm last}$

Amplitude of the diagram D in Fig. 14 is given by

$$D(\tau,T) = \frac{1}{4D^2}\int_0^\infty dm\int_0^\Lambda dy_1dy_2\int_0^\tau dr_1\int_\tau^T dr_2\int_0^\tau dr_3\int_\tau^T dr_4\, e^{y_1(r_1-r_2)}e^{y_2(r_3-r_4)}\langle\langle\dot{x}(r_1)\dot{x}(r_2)\dot{x}(r_3)\dot{x}(r_4)\rangle\rangle_m,$$

with the angular brackets defined in Eq. (80). Considering order of the time variables, the possible cases are illustrated in Fig. 23. Their amplitude can be expressed in terms of J and J^+ defined in Eq. (90). Adding them, we write

$$D(\tau,T) = \frac{2}{4D^2}\int_0^\infty dm\int_0^\Lambda dy_1dy_2e^{-\tau(y_1+y_2)}J_\tau(0,x_0;-y_1,-y_2)[J^+_{T-\tau}(x_0,m;y_2,y_1)+J^+_{T-\tau}(x_0,m;y_1,y_2)],$$

where the prefactor 2 is due to interchange of pairs (r_1,r_2) with (r_3,r_4).

Its double Laplace transformation in Eq. (61) gives

$$\widetilde{D}(\lambda,s) = \frac{1}{2D^2}\int_0^\infty dm\int_0^\Lambda dy_1dy_2\widetilde{J}_{s+\lambda+y_1+y_2}(0,x_0;-y_1,-y_2)\big[\widetilde{J}^+_s(x_0,m;y_2,y_1)+\widetilde{J}^+_s(x_0,m;y_1,y_2)\big].$$

It is convenient to write the expression in a form such that the integrand is symmetric in y_1 and y_2. We write

$$\widetilde{D}(\lambda,s) = \frac{1}{4D^2}\int_0^\Lambda dy_1dy_2[\widetilde{J}_{s+\lambda+y_1+y_2}(0,x_0;-y_1,-y_2)+\widetilde{J}_{s+\lambda+y_1+y_2}(0,x_0;-y_2,-y_1)] \times\int_0^\infty dm[\widetilde{J}^+_s(x_0,m;y_2,y_1)+\widetilde{J}^+_s(x_0,m;y_1,y_2)]. \tag{G1}$$

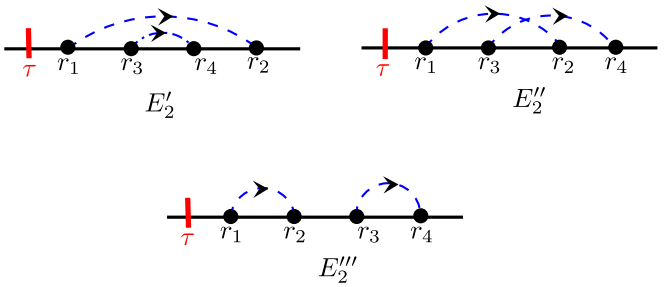

FIG. 24. Diagram E_2 of Fig. 14 is made of three cases according to relative order of time variables with $r_1 < r_2$ and $r_3 < r_4$, remaining on the side of τ as indicated.

We show that (a derivation given in Appendix N)

$$\widetilde{J}_s(m_1, m_2; y_1, y_2) = \frac{2\sqrt{D}}{y_1 y_2 (y_1 + y_2)} [y_1 \sqrt{s}\, e^{-z\sqrt{s}} + y_2 \sqrt{s + y_1 + y_2}\, e^{-z\sqrt{s+y_1+y_2}} - (y_1 + y_2)\sqrt{s + y_2}\, e^{-z\sqrt{s+y_2}}], \tag{G2}$$

where $z = \frac{|m_1 - m_2|}{\sqrt{D}}$ and

$$\int_0^\infty dm_2 \widetilde{J}_s^+(m_1, m_2; y_1, y_2) = \frac{4D}{y_1 y_2} \sqrt{\frac{s + y_2}{s}} \left[e^{-m_1\sqrt{\frac{s+y_2}{D}}} - e^{-m_1\sqrt{\frac{s+y_1+y_2}{D}}}\right] + \frac{4D}{(y_1 + y_2) y_2} \left[e^{-m_1\sqrt{\frac{s+y_1+y_2}{D}}} - e^{-m_1\sqrt{\frac{s}{D}}}\right]. \tag{G3}$$

Using the asymptotic of Eq. (G2) for small x_0, we obtain

$$\widetilde{J}_s(0, x_0; -y_1, -y_2) + \widetilde{J}_s(0, x_0; -y_2, -y_1) \simeq \frac{2\sqrt{D}}{y_1 y_2} (\sqrt{s} - \sqrt{s - y_2} - \sqrt{s - y_1} + \sqrt{s - y_1 - y_2}),$$

and similarly from Eq. (G3) we get for small x_0,

$$\int_0^\infty dm \{\widetilde{J}_s^+(x_0, m; y_2, y_1) + \widetilde{J}_s^+(x_0, m; y_1, y_2)\} \simeq -\frac{4x_0\sqrt{D}}{y_1 y_2} \times \frac{\sqrt{s + y_1 + y_2}}{\sqrt{s}} (\sqrt{s + y_1 + y_2} - \sqrt{s + y_1} - \sqrt{s + y_2} + \sqrt{s}). \tag{G4}$$

Using these asymptotics in Eq. (G1) we get, for small x_0,

$$\widetilde{D}(\lambda, s) \simeq -\frac{2x_0}{D} \int_0^\Lambda \frac{dy_1 dy_2}{y_1^2 y_2^2} \times \frac{\sqrt{s + y_1 + y_2}}{\sqrt{s}} (\sqrt{s + y_1 + y_2} - \sqrt{s + y_1} - \sqrt{s + y_2} + \sqrt{s}) \times (\sqrt{s + \lambda + y_1 + y_2} - \sqrt{s + \lambda + y_1} - \sqrt{s + \lambda + y_2} + \sqrt{s + \lambda}).$$

This leads to the result in terms of rescaled arguments in Eqs. (98) and (99).

2. Two-loop diagrams contributing to simple scaling

a. Diagrams E_1 and E_2

We begin with the diagram E_2 in Fig. 14, whose amplitude is given by

$$E_2(\tau, T) = \frac{1}{4D^2} \int_0^\infty dm \int_0^\Lambda dy_1 dy_2 \int_\tau^T dr_1 \int_{r_1}^T dr_2 \int_\tau^T dr_3 \int_{r_3}^T dr_4\, e^{y_1(r_1 - r_2)} e^{y_2(r_3 - r_4)} \langle\langle \dot{x}(r_1)\dot{x}(r_2)\dot{x}(r_3)\dot{x}(r_4)\rangle\rangle_m,$$

with the angular brackets defined in Eq. (80).

The expression can be written in three parts according to relative order of times r.

$$E_2(\tau, T) = E_2'(\tau, T) + E_2''(\tau, T) + E_2'''(\tau, T),$$

as shown in Fig. 24. Their amplitude can be written in terms of propagator Z in Eq. (24) and J^+ in Eq. (90). Adding their amplitudes, we write

$$E_2(\tau, T) = \frac{2}{4D^2} Z_\tau(0, x_0) \int_0^\Lambda dy dy' \int_0^\infty dm [J^+_{T-\tau}(x_0, m; -y, -y', y', y) + J^+_{T-\tau}(x_0, m; -y, -y', y, y') + J^+_{T-\tau}(x_0, m; -y, y, -y', y')].$$

[The prefactor 2 comes from interchange of pairs (r_1, r_2) and (r_3, r_4).]

Corresponding double Laplace transformation gives

$$\widetilde{E}_2(\lambda,s)=\frac{1}{2D^2}\,\widetilde{Z}_{s+\lambda}(0,x_0)\int_0^\Lambda dydy'\int_0^\infty dm[\widetilde{J}_s^+(x_0,m;-y,y,-y',y')+\widetilde{J}_s^+(x_0,m;-y,-y',y',y)+\widetilde{J}_s^+(x_0,m;-y,-y',y,y')].$$

To evaluate the expressions we use $\widetilde{Z}_s(0,x_0)$ from Eq. (85b), and

$$\begin{aligned}\int_0^\infty dm\,\widetilde{J}_s^+(x_0,m;y_1,y_2,y_3,y_4)=\frac{16D^2}{s}\Bigg[&\frac{s^3(e^{-s_4z}-e^{-sz})}{(s^2-s_1^2)(s^2-s_2{}^2)(s^2-s_3{}^2)(s^2-s_4{}^2)}+\frac{s_1{}^3(e^{-s_4z}-e^{-s_1z})}{(s_1{}^2-s^2)(s_1{}^2-s_2{}^2)(s_1{}^2-s_3{}^2)(s_1{}^2-s_4{}^2)}\\&+\frac{s_2{}^2(ss_1+s_2{}^2)(e^{-s_4z}-e^{-s_2z})}{(s+s_1)(s_2{}^2-s^2)(s_2{}^2-s_1{}^2)(s_2{}^2-s_3{}^2)(s_2{}^2-s_4{}^2)}\\&+\frac{s_3((s_1s_2+s_3{}^2)(s^2s_1+s_2s_3{}^2)+ss_3{}^2(s_1+s_2)^2)(e^{-s_4z}-e^{-s_3z})}{(s+s_1)(s+s_2)(s_1+s_2)(s_3{}^2-s^2)(s_3{}^2-s_1{}^2)(s_3{}^2-s_2{}^2)(s_3{}^2-s_4{}^2)}\Bigg],\end{aligned}\tag{G5}$$

derived later in Eq. (N19), where we denote $z=\frac{x_0}{\sqrt{D}}$, $s_1=\sqrt{s+y_4}$, $s_2=\sqrt{s+y_3+y_4}$, $s_3=\sqrt{s+y_2+y_3+y_4}$, $s_4=\sqrt{s+y_1+y_2+y_3+y_4}$.

Using these two results for small x_0, we get the asymptotics

$$\widetilde{E}_2(\lambda,s)\simeq\frac{1}{2D}\times\frac{x_0}{\sqrt{s(s+\lambda)}}\int_0^\Lambda\frac{dy_1dy_2}{y_1^2y_2^2}\,e(s,y_1,y_2),$$

where we define

$$\begin{aligned}e(s,y_1,y_2)=&-(s+y_1)(s+y_2)+\sqrt{s}(\sqrt{s}-\sqrt{s+y_1}-\sqrt{s+y_2})[2(\sqrt{s+y_1+y_2}-\sqrt{s+y_1}-\sqrt{s+y_2}+\sqrt{s})^2\\&-(\sqrt{s}-\sqrt{s+y_1}-\sqrt{s+y_2})^2-\sqrt{s+y_1}(\sqrt{s}-\sqrt{s+y_1})-\sqrt{s+y_2}(\sqrt{s}-\sqrt{s+y_2})].\end{aligned}\tag{G6}$$

Comparing the two diagrams E_1 and E_2 in Fig. 14, one can see that, for small x_0,

$$\widetilde{E}_1(\lambda,s)\simeq\frac{1}{2D}\times\frac{x_0}{\sqrt{s(s+\lambda)}}\int_0^\Lambda\frac{dy_1dy_2}{y_1^2y_2^2}\,e(s+\lambda,y_1,y_2),$$

with Eq. (G6). (This we have also explicitly verified.) Adding the two amplitudes we get Eq. (101).

Remark. Interestingly the integral in $\widetilde{E}_{1(2)}(\lambda,s)$ can be evaluated:

$$\int_0^\Lambda\frac{dy_1dy_2}{y_1^2y_2^2}\,e(s,y_1,y_2)=-\ln^2\left(\frac{\Lambda}{s}\right)+2[1+2\ln 2]\ln\left(\frac{\Lambda}{s}\right)+(1+2\ln 2)^2-2-\frac{3}{2}\pi^2$$

(we have verified this numerically). This result along with results Eq. (G7) and Eq. (G20) given later, helps recognize the linear combination of diagrams in Eq. (114) where divergences for $\Lambda\to\infty$ cancels.

b. Diagram A

Amplitude of the diagram A in Fig. 14 is given by

$$A(\tau,T)=\frac{1}{4D^2}\int_0^\infty dm\int_0^\Lambda dy_1dy_2\int_0^\tau dr_1\int_{r_1}^\tau dr_2\int_\tau^T dr_3\int_{r_3}^T dr_4\;e^{y_1(r_1-r_2)}e^{y_2(r_3-r_4)}\langle\langle\dot{x}(r_1)\dot{x}(r_2)\dot{x}(r_3)\dot{x}(r_4)\rangle\rangle_m$$

with the angular brackets defined in Eq. (80). In terms of J in Eq. (90) and its analog J^+ in presence of absorbing boundary, we write

$$A(\tau,T)=\frac{2}{4D^2}\int_0^\Lambda dy_1dy_2J_\tau(0,x_0;-y_1,y_1)\int_0^\infty dmJ^+_{T-\tau}(x_0,m;-y_2,y_2),$$

where the prefactor 2 is the degeneracy from the interchange of pair of indices (1,2) and (3,4). The double Laplace transformation Eq. (61) gives

$$\widetilde{A}(\lambda,s)=\frac{1}{2D^2}\int_0^\Lambda dy_1dy_2\widetilde{J}_{s+\lambda}(0,x_0;-y_1,y_1)\int_0^\infty dm\widetilde{J}_s^+(x_0,m;-y_2,y_2).$$

Using Eqs. (G2) and (G3) for small x_0, we get

$$\widetilde{A}(\lambda,s)\simeq-\frac{x_0}{D\sqrt{s(s+\lambda)}}\int_0^\Lambda\frac{dy_1dy_2}{y_1^2y_2^2}(\sqrt{s+y_2}-\sqrt{s})^2(\sqrt{s+\lambda}-\sqrt{s+\lambda+y_1})^2.$$

In terms of rescaled variables this gives Eq. (103).

Remark. The y integration in $\widetilde{A}$ can be evaluated explicitly using

$$\int_0^\Lambda \frac{dy}{y^2}\left(\sqrt{s+y}-\sqrt{s}\right)^2 = \ln\left(\frac{\Lambda}{s}\right) - 1 - 2\ln 2. \tag{G7}$$

c. Diagrams G_1 and G_2

Diagrams G_1 and G_2 in Fig. 14 has a contracted point s. Their amplitude is given by

$$G_1(\tau,T) = \frac{1}{D}\int_0^\infty dm \int_0^\Lambda dy_1 dy_2 \int_0^\tau dr_1 \int_{r_1}^\tau ds \int_s^\tau dr_2 e^{y_1(r_1-s)} e^{y_2(s-r_2)} \langle\langle \dot{x}(r_1)\dot{x}(r_2)\rangle\rangle_m$$

and

$$G_2(\tau,T) = \frac{1}{D}\int_0^\infty dm \int_0^\Lambda dy_1 dy_2 \int_\tau^T dr_1 \int_{r_1}^T ds \int_s^T dr_2 e^{y_1(r_1-s)} e^{y_2(s-r_2)} \langle\langle \dot{x}(r_1)\dot{x}(r_2)\rangle\rangle_m$$

with the angular brackets defined in Eq. (80). (Their difference is in the range of integration for time variables.)

We write these amplitudes in terms of the fBm propagators defined in Eqs. (24) and (81).

$$G_1(\tau,T) = \frac{1}{D}\int_0^\Lambda dy_1 dy_2\, \mathscr{L}_\tau(0,x_0;-y_1,y_1-y_2,y_2)\int_0^\infty dm Z^+_{T-\tau}(x_0,m)$$

and

$$G_2(\tau,T) = \frac{1}{D}\int_0^\Lambda dy_1 dy_2 Z(0,x_0,\tau)\int_0^\infty dm\, \mathscr{L}^+_{T-\tau}(x_0,m;-y_1,y_1-y_2,y_2),$$

where we define

$$\mathscr{L}_t(m_1,m_2;y_1,z,y_2) = \int_0^t dr_1 \int_{r_1}^t ds \int_s^t dr_2 e^{-y_1 r_1 - z s - y_2 r_2} \langle \dot{x}(r_1)\dot{x}(r_2)\rangle_{(m_1,m_2)} \tag{G8}$$

and its analog $\mathscr{L}^+_t$ in presence of an absorbing line. The angular brackets denote average with standard Brownian measure $e^{-\frac{S_0}{D}}$ starting at position m_1 and ending at position m_2.

Their double Laplace transformation Eq. (61) is given by

$$\widetilde{G}_1(\lambda,s) = \frac{1}{D}\int_0^\Lambda dy_1 dy_2 \int_0^\infty dm \widetilde{\mathscr{L}}_{s+\lambda}(0,x_0;-y_1,y_1-y_2,y_2)\,\widetilde{Z}^+_s(x_0,m) \tag{G9}$$

and

$$\widetilde{G}_2(\lambda,s) = \frac{1}{D}\int_0^\Lambda dy_1 dy_2 \int_0^\infty dm \widetilde{Z}_{s+\lambda}(0,x_0)\,\widetilde{\mathscr{L}}^+_s(x_0,m;-y_1,y_1-y_2,y_2). \tag{G10}$$

Expressions of $\widetilde{Z}$ and $\widetilde{Z}^+$ are in Eq. (85) and the integral of the latter is in Eq. (L5).

For Laplace transform $\widetilde{\mathscr{L}}$ of Eq. (G8) we note that

$$\widetilde{\mathscr{L}}_s(m_1,m_2;y_1,z,y_2) = \frac{1}{z}\{\widetilde{J}_s(m_1,m_2;y_1+z,y_2) - \widetilde{J}_s(m_1,m_2;y_1,y_2+z)\} \tag{G11}$$

with Eq. (90), and a similar relation for $\widetilde{\mathscr{L}}^+$ in terms of $\widetilde{J}^+_s$. This is easy to see from Eqs. (G8) and (90) and taking their Laplace transformation.

Then, using Eqs. (G2) and (G3) we get

$$\widetilde{\mathscr{L}}_s(0,x_0;-y_1,y_1-y_2,y_2) = \sqrt{\frac{D}{s}} \times \frac{h_s\left(\frac{x_0}{\sqrt{D}},y_1,y_2\right)}{y_1^2 y_2^2} \tag{G12}$$

and

$$\int_0^\infty dm\, \widetilde{\mathscr{L}}^+_s(x_0,m;-y_1,y_1-y_2,y_2) = \frac{2D}{\sqrt{s}} \times \frac{h^+_s\left(\frac{x_0}{\sqrt{D}},y_1,y_2\right)}{y_1^2 y_2^2}, \tag{G13}$$

where we define

$$h_s(z,y_1,y_2) = e^{-z\sqrt{s}}\, y_1 y_2 - \frac{2\sqrt{s}}{(y_1-y_2)}\{y_1^2(\sqrt{s+y_2}\; e^{-z\sqrt{s+y_2}} - \sqrt{s}\; e^{-z\sqrt{s}}) - y_2^2(\sqrt{s+y_1}\; e^{-z\sqrt{s+y_1}} - \sqrt{s}\; e^{-z\sqrt{s}})\}, \tag{G14}$$

and

$$h_s^+(z,y_1,y_2) = -z\, y_1 y_2 e^{-z\sqrt{s}} + \frac{2}{y_1-y_2}\Big\{y_2^2\sqrt{s+y_1}\big(e^{-z\sqrt{s+y_1}} - e^{-z\sqrt{s}}\big) - y_1^2\sqrt{s+y_2}\big(e^{-z\sqrt{s+y_2}} - e^{-z\sqrt{s}}\big)\Big\}. \tag{G15}$$

In terms of these functions in Eqs. (G9) and (G10), we write

$$\widetilde{G}_1(\lambda,s) = \frac{1-e^{-x_0\sqrt{\frac{s}{D}}}}{s\sqrt{D(s+\lambda)}}\int_0^\Lambda \frac{dy_1dy_2}{y_1^2y_2^2}\, h_{s+\lambda}\left(\frac{x_0}{\sqrt{D}}, y_1, y_2\right)$$

and

$$\widetilde{G}_2(\lambda,s) = \frac{e^{-x_0\sqrt{\frac{s+\lambda}{D}}}}{\sqrt{Ds(s+\lambda)}}\int_0^\Lambda \frac{dy_1dy_2}{y_1^2y_2^2} h_s^+\left(\frac{x_0}{\sqrt{D}}, y_1, y_2\right).$$

For small z, the expressions in Eqs. (G14) and (G15) have the asymptotics

$$h_s(z,y_1,y_2) \simeq \frac{(\sqrt{s+y_2}-\sqrt{s})^2y_1^2 - (\sqrt{s+y_1}-\sqrt{s})^2y_2^2}{(y_1-y_2)}$$

and

$$h_s^+(z,y_1,y_2) \simeq z\, h_s(z,y_1,y_2). \tag{G16}$$

Substituting this in the expression for $\widetilde{G}_1$ and $\widetilde{G}_2$ in the small x_0 limit, we get

$$\widetilde{G}_1(\lambda,s) \simeq \frac{x_0}{D\sqrt{s(s+\lambda)}}\, g(s+\lambda) \tag{G17}$$

and

$$\widetilde{G}_2(\lambda,s) \simeq \frac{x_0}{D\sqrt{s(s+\lambda)}}\, g(s), \tag{G18}$$

where

$$g(s) = \int_0^\Lambda \frac{dy_1dy_2}{y_1^2y_2^2}\left[\frac{(\sqrt{s+y_2}-\sqrt{s})^2y_1^2 - (\sqrt{s+y_1}-\sqrt{s})^2y_2^2}{(y_1-y_2)}\right]. \tag{G19}$$

In terms of rescaled variables, we get Eq. (104).

Remark. The integral in Eq. (G19) can be evaluated analytically,

$$g(s) = \left[\ln\left(\frac{\Lambda}{s}\right) - 1 - 2\ln 2\right]^2 + 1 + \frac{\pi^2}{3}. \tag{G20}$$

d. Diagrams B and C

Amplitude of B_1 and B_2 in Fig. 14 is given by

$$B_1(\tau,T) = \frac{1}{D}\int_0^\infty dm \int_0^\Lambda dy_1dy_2 \int_0^\tau dr_1 \int_{r_1}^\tau ds \int_\tau^T dr_2 e^{y_1(r_1-s)}e^{y_2(s-r_2)}\langle\langle \dot{x}(r_1)\dot{x}(r_2)\rangle\rangle_m$$

and

$$B_2(\tau,T) = \frac{1}{D}\int_0^\infty dm \int_0^\Lambda dy_1dy_2 \int_0^\tau dr_1 \int_\tau^T ds \int_s^T dr_2 e^{y_1(r_1-s)}e^{y_2(s-r_2)}\langle\langle \dot{x}(r_1)\dot{x}(r_2)\rangle\rangle_m.$$

Their difference is in the limit of the time integrals.

Amplitude of these diagrams are of order x_0^2 or higher, for small x_0, and therefore they do not contribute in the leading order amplitude in Eq. (106). To see this let us consider B_2, which we write as

$$B_2(\tau,T) = \frac{1}{D}\int_0^\Lambda dy_1dy_2 J_\tau(0,x_0;-y_1)e^{-y_1\tau}\int_0^\infty dm \mathscr{L}^+_{T-\tau}(x_0,m;y_1-y_2,y_2),$$

where, similar to Eq. (G8), we define

$$\mathscr{L}^+_t(m_1,m_2;y_1,y_2) = \int_0^t dr_1 \int_{r_1}^t dr_2 e^{-y_1r_1-y_2r_2}\langle\dot{x}(r_2)\rangle^+.$$

The double Laplace transformation of B_2 is then given by

$$\widetilde{B}_2(\lambda,s) = \frac{1}{D}\int_0^\Lambda dy_1dy_2 \widetilde{J}_{s+\lambda+y_1}(0,x_0;-y_1)\int_0^\infty dm \widetilde{\mathscr{L}}^+_s(x_0,m;y_1-y_2,y_2). \tag{G21}$$

From the definition in Eq. (90) it is easy to see that

$$\mathscr{L}_t^+(m_1, m_2; y_1, y_2) = \frac{1}{y_1}[J_t^+(m_1, m_2; y_2) - J_t^+(m_1, m_2; y_1 + y_2)]$$

and similar for their Laplace transformation. Then using Eq. (N7) we see that, for small x_0,

$$\int_0^\infty dm\, \widetilde{\mathscr{L}}_s^+(x_0, m; y_1 - y_2, y_2) \sim x_0$$

and similarly, $\widetilde{J}_s(0, x_0; y) \sim x_0$ from Eq. (N1). This means $\widetilde{B}_2 \sim x_0^2$ for small x_0.

Following a very similar calculation one can verify that $\widetilde{B}_1$ is also of order x_0^2 for small x_0. These are easy to see using the argument given in the remark below Eq. (92).

The argument can be used to show that the diagram C is also of order x_0^2. We have as well verified this explicitly using their amplitude

$$C_1(\tau, T) = \frac{1}{4D^2}\int_0^\infty dm \int_0^\Lambda dy_1 dy_2 \int_0^\tau dr_1 \int_{r_1}^\tau dr_2 \int_0^\tau dr_3 \int_\tau^T dr_4\, e^{y_1(r_1-r_2)} e^{y_2(r_3-r_4)} \langle\langle \dot{x}(r_1)\dot{x}(r_2)\dot{x}(r_3)\dot{x}(r_4)\rangle\rangle_m$$

and

$$C_2(\tau, T) = \frac{1}{4D^2}\int_0^\infty dm \int_0^\Lambda dy_1 dy_2 \int_0^\tau dr_1 \int_\tau^T dr_2 \int_\tau^T dr_3 \int_{r_3}^T dr_4\, e^{y_1(r_1-r_2)} e^{y_2(r_3-r_4)} \langle\langle \dot{x}(r_1)\dot{x}(r_2)\dot{x}(r_3)\dot{x}(r_4)\rangle\rangle_m$$

as indicated in the diagram Fig. 14.

APPENDIX H: AMPLITUDE OF TWO-LOOP DIAGRAMS FOR $t_{\max}$

All diagrams in Fig. 14 for distribution of $t_{\max}$ are of order x_0^2 for small x_0. Among these, the diagrams E and A contribute to the scaling term in Eq. (38), and the rest D, B, C, and G contribute to the nontrivial function $\mathcal{F}^{\max}$.

1. Diagrams for scaling term

a. Diagrams E_1 and E_2

We begin with the diagram E_2 in Fig. 14, whose amplitude for the problem of $t_{\max}$ is given by

$$E_2(\tau, T) = \frac{1}{8D^2}\int_0^\infty dm_1 dm_2 \int_0^\Lambda dy_1 dy_2 \int_\tau^T dr_1 \int_{r_1}^T dr_2 \int_\tau^T dr_3 \int_{r_3}^T dr_4 e^{y_1(r_1-r_2)} \times e^{y_2(r_3-r_4)} \langle\langle \dot{x}(r_1)\dot{x}(r_2)\dot{x}(r_3)\dot{x}(r_4)\rangle\rangle_{(m_1,m_2)}, \tag{H1}$$

with the angular brackets defined in Eq. (125). Considering relative order of times r we write the amplitude in three parts as indicated in Fig. 24. Their net amplitude can be written together as

$$E_2(\tau, T) = \frac{2}{8D^2}\int_0^\Lambda dy_1 dy_2 \int_0^\infty dm_1 Z_\tau^+(m_1, x_0) \int_0^\infty dm_2 [J_{T-\tau}^+(x_0, m_2; -y_1, -y_2, y_2, y_1) + J_{T-\tau}^+(x_0, m_2; -y_1, -y_2, y_1, y_2) + J_{T-\tau}^+(x_0, m_2; -y_1, y_1, -y_2, y_2)],$$

where the propagator Z^+ is in Eq. (81) and J^+ is an analog of (90) with absorbing boundary. The prefactor 2 is the degeneracy from interchange of pair of indices (1,2) and (3,4) in Fig. 24.

A double Laplace transformation Eq. (61) of the amplitude is

$$\widetilde{E}_2(\lambda, s) = \frac{1}{4D^2}\int_0^\Lambda dy_1 dy_2 \int_0^\infty dm_1 \widetilde{Z}_{s+\lambda}^+(m_1, x_0) \int_0^\infty dm_2 [\widetilde{J}_s^+(x_0, m_2; -y_1, -y_2, y_2, y_1) + \widetilde{J}_s^+(x_0, m_2; -y_1, -y_2, y_1, y_2) + \widetilde{J}_s^+(x_0, m_2; -y_1, y_1, -y_2, y_2)].$$

Expression of $\tilde{Z}^+$ is in Eq. (85b) and integral of $\widetilde{J}^+$ is in Eq. (G5). Using these results we get, for small x_0,

$$\widetilde{E}_2(\lambda, s) \simeq \frac{1}{2D}\frac{x_0^2}{\sqrt{s(s+\lambda)}}\int_0^\Lambda \frac{dy_1 dy_2}{y_1^2 y_2^2}\, e(s, y_1, y_2),$$

with $e(s, y_1, y_2)$ in Eq. (G6).

Amplitude of the diagram E_1 for $t_{\max}$ is

$$E_1(\tau, T) = \frac{1}{8D^2}\int_0^\infty dm_1 dm_2 \int_0^\Lambda dy_1 dy_2 \int_0^\tau dr_1 \int_{r_1}^\tau dr_2 \int_0^\tau dr_3 \int_{r_3}^\tau dr_4\, e^{y_1(r_1-r_2)} e^{y_2(r_3-r_4)} \langle\langle \dot{x}(r_1)\dot{x}(r_2)\dot{x}(r_3)\dot{x}(r_4)\rangle\rangle_{(m_1,m_2)}. \tag{H2}$$

Comparing with Eq. (H1), we see that for small x_0, the double Laplace transformation of the amplitude E_1 is

$$\widetilde{E}_1(\lambda, s) \simeq \frac{1}{2D} \times \frac{x_0^2}{\sqrt{s(s+\lambda)}} \int_0^\Lambda \frac{dy_1 dy_2}{y_1^2 y_2^2}\, e(s+\lambda, y_1, y_2).$$

We note that amplitude of $\widetilde{E}_1$ and $\widetilde{E}_2$ for small x_0 are almost identical for both problems ($t_{\rm last}$ and $t_{\rm max}$). In terms of rescaled variables we get Eq. (135).

b. Diagram A

Amplitude of the diagram A in Fig. 14 for $t_{\rm max}$ is given by

$$A(\tau, T) = \frac{1}{8D^2} \int_0^\infty dm_1 dm_2 \int_0^\Lambda dy_1 dy_2 \int_0^\tau dr_1 \int_{r_1}^\tau dr_2 \int_\tau^T dr_3 \int_{r_3}^T dr_4\, e^{y_1(r_1-r_2)} e^{y_2(r_3-r_4)} \langle\langle \dot{x}(r_1)\dot{x}(r_2)\dot{x}(r_3)\dot{x}(r_4)\rangle\rangle_{(m_1,m_2)}, \tag{H3}$$

with the angular brackets defined in Eq. (125). In terms of J^+ in Eq. (90), we write

$$A(\tau, T) = \frac{2}{8D^2} \int_0^\Lambda dy_1 dy_2 \int_0^\infty dm_1 J_\tau^+(m_1, x_0; -y_1, y_1) \int_0^\infty dm_2 J_{T-\tau}^+(x_0, m_2; -y_2, y_2),$$

where the prefactor 2 is the degeneracy from the interchange of pair of indices (1,2) and (3,4).

The double Laplace transformation Eq. (61) of the amplitude can be written as

$$\widetilde{A}(\lambda, s) = \frac{1}{4D^2} \int_0^\Lambda dy_1 dy_2 \int_0^\infty dm_1 \widetilde{J}_{s+\lambda}^+(m_1, x_0; -y_1, y_1) \int_0^\infty dm_2\, \widetilde{J}_s^+(x_0, m_2; -y_2, y_2).$$

We use the results of integrals in Eq. (G3) and

$$\int_0^\infty dm_1 \widetilde{J}_s^+(m_1, m_2; y_1, y_2) = \frac{4D}{y_1 y_2} \sqrt{\frac{s+y_2}{s+y_1+y_2}} \Big[e^{-m_2\sqrt{\frac{s+y_2}{D}}} - e^{-m_2\sqrt{\frac{s}{D}}}\Big] + \frac{4D}{(y_1+y_2)y_1} \Big[e^{-m_2\sqrt{\frac{s}{D}}} - e^{-m_2\sqrt{\frac{s+y_1+y_2}{D}}}\Big]. \tag{H4}$$

Their derivation is in Appendix N. Substituting the results, we get, for small x_0,

$$\widetilde{A}(\lambda, s) \simeq \frac{x_0^2}{D} \times \frac{1}{\sqrt{s(s+\lambda)}} \int_0^\Lambda \frac{dy_1 dy_2}{y_1^2 y_2^2} (\sqrt{s+\lambda+y_1} - \sqrt{s+\lambda})^2 (\sqrt{s+y_2} - \sqrt{s})^2.$$

In terms of rescaled variables this gives Eq. (136).

2. Nontrivial diagrams contributing to $\mathcal{F}^{\rm max}$

a. Diagram D

Amplitude of the diagram D in Fig. 14 for $t_{\rm max}$ is given by

$$\begin{aligned} D(\tau, T) = \frac{1}{8D^2} \int_0^\infty dm_1 dm_2 \int_0^\Lambda dy_1 dy_2 \int_0^\tau dr_1 \int_\tau^T dr_2 \int_0^\tau dr_3 \int_\tau^T dr_4\, e^{y_1(r_1-r_2)} \\ \times\, e^{y_2(r_3-r_4)} \langle\langle \dot{x}(r_1)\dot{x}(r_2)\dot{x}(r_3)\dot{x}(r_4)\rangle\rangle_{(m_1,m_2)}, \end{aligned} \tag{H5}$$

with the angular brackets defined in Eq. (125).

Analysis for this amplitude is similar to the analysis in Appendix G 1. It is straightforward to get

$$D(\tau, T) = \frac{1}{4D^2} \int_0^\Lambda dy_1 dy_2\, e^{-y_1\tau - y_2\tau} \int_0^\infty dm_1 J_\tau^+(m_1, x_0; -y_1, -y_2) \int_0^\infty dm_2 [J_{T-\tau}^+(x_0, m_2; y_2, y_1) + J_{T-\tau}^+(x_0, m_2; y_1, y_2)],$$

with J^+ in Eq. (90). Taking the double Laplace transformation Eq. (61) we get

$$\widetilde{D}(\lambda, s) = \frac{1}{4D^2} \int_0^\Lambda dy_1 dy_2 \int_0^\infty dm_1 \widetilde{J}_{s+\lambda+y_1+y_2}^+(m_1, x_0; -y_1, -y_2) \Big[\int_0^\infty dm_2 \widetilde{J}_s^+(x_0, m_2; y_2, y_1) + \widetilde{J}_s^+(x_0, m_2; y_1, y_2)\Big].$$

It is more convenient to write the expression in a symmetric form

$$\begin{aligned} \widetilde{D}(\lambda, s) = \frac{1}{8D^2} \int_0^\Lambda dy_1 dy_2 \int_0^\infty dm_1 \big[\widetilde{J}_{s+\lambda+y_1+y_2}^+(m_1, x_0; -y_1, -y_2) + \widetilde{J}_{s+\lambda+y_1+y_2}^+(m_1, x_0; -y_2, -y_1)\big] \\ \times \int_0^\infty dm_2 [\widetilde{J}_s^+(x_0, m_2; y_1, y_2) + \widetilde{J}_s^+(x_0, m_2; y_2, y_1)]. \end{aligned} \tag{H6}$$

For evaluating the expression we use the results for integrals in Eqs. (G3) and (H4). This leads to, for small x_0,

$$\int_0^\infty dm_1\big[\widetilde{J}_s^+(m_1,x_0;y_1,y_2)+\widetilde{J}_s^+(m_1,x_0;y_2,y_1)\big]\simeq-\frac{x_0\,4\sqrt{D}}{y_1y_2}\times\frac{\sqrt{s}}{\sqrt{s+y_1+y_2}}(\sqrt{s+y_1+y_2}-\sqrt{s+y_1}-\sqrt{s+y_2}+\sqrt{s})$$

and an analogous formula Eq. (G4).

More explicitly, for the integrals in Eq. (H6) we get for small x_0,

$$\int_0^\infty dm_1\big\{\widetilde{J}^+_{s+\lambda+y_1+y_2}(m_1,x_0;-y_1,-y_2)+\widetilde{J}^+_{s+\lambda+y_1+y_2}(m_1,x_0;-y_2,-y_1)\big\}$$
$$\simeq-\frac{2^2\sqrt{D}\,x_0}{y_1y_2}\times\frac{\sqrt{s+\lambda+y_1+y_2}}{\sqrt{s+\lambda}}(\sqrt{s+\lambda}-\sqrt{s+\lambda+y_2}-\sqrt{s+\lambda+y_1}+\sqrt{s+\lambda+y_1+y_2}).$$

Using this with Eq. (G4) we get an explicit expression for $\widetilde{D}$ in Eq. (H6). For small x_0 limit,

$$\widetilde{D}(\lambda,s)\simeq\frac{1}{D}\times\frac{x_0^2}{\sqrt{s(s+\lambda)}}\int_0^\Lambda\frac{dy_1dy_2}{y_1^2y_2^2}\,d(s,s+\lambda,y_1,y_2),$$

where we define

$$d(s_1,s_2,y_1,y_2)=2\sqrt{s_1+y_1+y_2}\,\sqrt{s_2+y_1+y_2}(\sqrt{s_1+y_1+y_2}-\sqrt{s_1+y_1}-\sqrt{s_1+y_2}+\sqrt{s_1})$$
$$\times\,(\sqrt{s_2+y_1+y_2}-\sqrt{s_2+y_1}-\sqrt{s_2+y_2}+\sqrt{s_2}).\tag{H7}$$

In terms of rescaled variables, this gives the amplitude in Eq. (138).

b. Diagram C

One can see that for $t_{\max}$, amplitude of the diagrams C_1 in Fig. 14 is

$$C_1(\tau,T)=\frac{2}{8D^2}\int_0^\Lambda dy_1dy_2\int_0^\infty dm_1dm_2\int_0^\tau dr_1\int_{r_1}^\tau dr_2\int_0^\tau dr_3\int_\tau^T dr_4\,e^{y_1(r_1-r_2)}e^{y_2(r_3-r_4)}\langle\langle\dot{x}(r_1)\dot{x}(r_2)\dot{x}(r_3)\dot{x}(r_4)\rangle\rangle_{(m_1,m_2)},\tag{H8}$$

with the angular brackets defined in Eq. (125). (The prefactor 2 is the degeneracy from interchange of pair of indices (1,2) and (3,4).) The amplitude can be expressed in terms of J^+ in Eq. (90), giving

$$C_1(\tau,T)=\frac{1}{4D^2}\int_0^\Lambda dy_1dy_2\int_0^\infty dm_1dm_2\,e^{-y_2\tau}\mathscr{I}_\tau^+(m_1,x_0;-y_1,y_1,-y_2)\,J^+_{T-\tau}(x_0,m_2;y_2),\tag{H9}$$

where we define

$$\mathscr{I}_\tau^+(m_1,m_2;y_1,y_2,y_3)=\int_0^\tau dr_1\int_{r_1}^\tau dr_2\int_0^\tau dr_3e^{-y_1r_1-y_2r_2-y_3r_3}\langle\dot{x}(r_1)\dot{x}(r_2)\dot{x}(r_3)\rangle^+_{(m_1,m_2)},\tag{H10}$$

for $m_1>0$ and $m_2>0$. For an explicit evaluation one can use that $\mathscr{I}_\tau^+$ is related to J^+ [an absorbing-boundary-analogue of Eq. (90)] by

$$\mathscr{I}_\tau^+(m_1,m_2;y_1,y_2,y_3)=J_\tau^+(m_1,m_2;y_1,y_2,y_3)+J_\tau^+(m_1,m_2;y_1,y_3,y_2)+J_\tau^+(m_1,m_2;y_3,y_1,y_2).\tag{H11}$$

A double Laplace transform Eq. (61) of the amplitude in Eq. (H9) gives

$$\widetilde{C}_1(\lambda,s)=\frac{1}{4D^2}\int_0^\Lambda dy_1dy_2\int_0^\infty dm_1dm_2\widetilde{\mathscr{I}}^+_{s+\lambda+y_2}(m_1,x_0;-y_1,y_1,-y_2)\widetilde{J}_s^+(x_0,m_2;y_2).\tag{H12}$$

To evaluate the integrals, we use a result from Eq. (N7) which, for small x_0, gives

$$\int_0^\infty dm_2\,\widetilde{J}_s^+(x_0,m_2;y_2)\simeq\frac{2x_0}{\sqrt{s}}\left(\frac{\sqrt{s+y_2}-\sqrt{s}}{y_2}\right).\tag{H13}$$

Similarly, using Eq. (H11) and the integration result Eq. (N16), for small x_0, we get

$$\int_0^\infty dm_1\widetilde{\mathscr{I}}^+_{s+\lambda+y_2}(m_1,x_0;-y_1,y_1,-y_2)\simeq-\frac{4Dx_0}{\sqrt{s+\lambda}\,y_1^2y_2}\times c(s+\lambda,y_2,y_1),\tag{H14}$$

where we define

$$c(s,y_1,y_2)=\sqrt{s+y_1}\,(\sqrt{s+y_1+y_2}-\sqrt{s+y_1}-\sqrt{s+y_2}+\sqrt{s})^2.\tag{H15}$$

Using Eqs. (H13) and (H14) for the integrals in the expression Eq. (H12) we get the amplitude

$$\widetilde{C}_1(\lambda, s) = \frac{2x_0^2}{D} \times \frac{1}{\sqrt{s(s+\lambda)}} \int_0^\Lambda \frac{dy_1 dy_2}{y_1^2\, y_2^2} (\sqrt{s} - \sqrt{s+y_1})\, c(s+\lambda, y_1, y_2),$$

for small x_0, where we exchanged the dummy variables y_1 and y_2.

Analysis for the diagram C_2 in Fig. 14 is similar. Its amplitude

$$C_2(\tau, T) = \frac{2}{8D^2} \int_0^\Lambda dy_1 dy_2 \int_0^\infty dm_1 dm_2 \int_0^\tau dr_1 \int_\tau^T dr_2 \int_\tau^T dr_3 \int_{r_3}^T dr_4\; e^{y_1(r_1-r_2)} e^{y_2(r_3-r_4)} \langle\langle \dot{x}(r_1)\dot{x}(r_2)\dot{x}(r_3)\dot{x}(r_4)\rangle\rangle_{(m_1,m_2)} \tag{H16}$$

and the asymptotics for the corresponding double Laplace transformation for small x_0 is

$$\widetilde{C}_2(\lambda, s) \simeq \frac{2x_0^2}{D} \times \frac{1}{\sqrt{s(s+\lambda)}} \int_0^\Lambda \frac{dy_1 dy_2}{y_1^2\, y_2^2} (\sqrt{s+\lambda} - \sqrt{s+\lambda+y_1}) c(s, y_1, y_2). \tag{H17}$$

Adding the results for $\widetilde{C}_1$ and $\widetilde{C}_2$ gives Eq. (142) in terms of rescaled variables.

c. Diagram B

For $t_{\max}$, amplitude of B_1 and B_2 in Fig. 14 is

$$B_1(\tau, T) = \frac{1}{2D} \int_0^\infty dm_1 dm_2 \int_0^\Lambda dy_1 dy_2 \int_0^\tau dr_1 \int_{r_1}^\tau ds \int_\tau^T dr_2\; e^{y_1(r_1-s)} e^{y_2(s-r_2)} \langle\langle \dot{x}(r_1)\dot{x}(r_2)\rangle\rangle_{(m_1,m_2)} \tag{H18}$$

and

$$B_2(\tau, T) = \frac{1}{2D} \int_0^\infty dm_1 dm_2 \int_0^\Lambda dy_1 dy_2 \int_0^\tau dr_1 \int_\tau^T ds \int_s^T dr_2 e^{y_1(r_1-s)}\; e^{y_2(s-r_2)} \langle\langle \dot{x}(r_1)\dot{x}(r_2)\rangle\rangle_{(m_1,m_2)}, \tag{H19}$$

with the angular brackets defined in Eq. (125). Their difference is in the limit of the time integrals.

These expressions can be written in terms of J^+ in Eq. (90). We write

$$B_1(\tau, T) = \frac{1}{2D} \int_0^\Lambda dy_1 dy_2 \int_0^\infty dm_1 dm_2 \mathbb{L}_\tau^+(m_1, x_0; -y_1, y_1 - y_2)\; e^{-y_2\tau} J_{T-\tau}^+(x_0, m_2; y_2), \tag{H20}$$

where we define

$$\mathbb{L}_\tau^+(m_1, m_2; y_1, y_2) = \int_0^\tau dr_1 \int_{r_1}^\tau dr_2 e^{-y_1 r_1 - y_2 r_2} \langle \dot{x}(r_1)\rangle^+.$$

This function can be evaluated in terms of J^+ in Eq. (90),

$$\mathbb{L}_t^+(m_1, m_2; y_1, y_2) = \frac{1}{y_2}\{J_t^+(m_1, m_2; y_1 + y_2) - e^{-y_2\tau} J_t^+(m_1, m_2; y_1)\}. \tag{H21}$$

In a similar way, we write Eq. (H19) by

$$B_2(\tau, T) = \frac{1}{2D} \int_0^\Lambda dy_1 dy_2 \int_0^\infty dm_1 dm_2 J_\tau^+(m_1, x_0; -y_1)\; e^{-y_1\tau}\; \mathscr{L}_{T-\tau}^+(x_0, m_2; y_1 - y_2, y_2), \tag{H22}$$

with J^+ defined in Eq. (90) and $\mathscr{L}^+$ defined in Eq. (G8). The last quantity can also be expressed in terms of J^+ by their analog of Eq. (G11) with absorbing boundary.

A double Laplace transformation Eq. (61) of the amplitudes Eqs. (H20) and (H22) are

$$\widetilde{B}_1(\lambda,s) = \frac{1}{2D} \int_0^\Lambda dy_1 dy_2 \int_0^\infty dm_1 dm_2 \widetilde{\mathbb{L}}_{s+\lambda+y_2}^+(m_1, x_0; -y_1, y_1 - y_2)\; \widetilde{J}_s^+(x_0, m_2; y_2)$$

and

$$\widetilde{B}_2(\lambda, s) = \frac{1}{2D} \int_0^\Lambda dy_1 dy_2 \int_0^\infty dm_1 dm_2 \widetilde{J}_{s+\lambda+y_1}^+(m_1, x_0; -y_1)\; \widetilde{\mathscr{L}}_s^+(x_0, m_2; y_1 - y_2, y_2),$$

where

$$\widetilde{\mathbb{L}}_s^+(m_1, m_2; y_1, y_2) = \frac{1}{y_2}\{\widetilde{J}_s^+(m_1, m_2; y_1 + y_2) - \widetilde{J}_{s+y_2}^+(m_1, m_2; y_1)\}$$

and

$$\widetilde{\mathscr{L}}_s^+(m_1,m_2;y_1,y_2)=\frac{1}{y_1}\{\widetilde{J}_1^+(m_1,m_2,y_2,s)-\widetilde{J}_1^+(m_1,m_2,y_1+y_2,s)\}.$$

For an explicit evaluation of the amplitudes we use Eq. (N6) that for small x_0 leads to

$$\int_0^\infty dm_1\widetilde{\mathbb{L}}^+_{s+y_2}(m_1,x_0;-y_1,y_1-y_2)\simeq\frac{2x_0}{\sqrt{s}}\times\frac{(\sqrt{s+y_1}-\sqrt{s})y_2-(\sqrt{s+y_2}-\sqrt{s})y_1}{y_1y_2(y_1-y_2)}.$$

Similarly, using Eq. (G3) we get, for small x_0,

$$\int_0^\infty dm_2\,\widetilde{\mathscr{L}}_s^+(x_0,m_2;y_1-y_2,y_2)\simeq\frac{2x_0}{\sqrt{s}}\times\frac{(\sqrt{s+y_2}-\sqrt{s})y_1-(\sqrt{s+y_1}-\sqrt{s})y_2}{y_1y_2(y_1-y_2)}.$$

Using these asymptotics, along with Eqs. (N6) and (N7) we get the amplitudes, for small x_0,

$$\widetilde{B}_1(\lambda,s)\simeq\frac{2x_0^2}{D\sqrt{s(s+\lambda)}}\int_0^\Lambda dy_1dy_2\,\frac{(\sqrt{s+y_2}-\sqrt{s})}{y_1y_2^2(y_1-y_2)}[(\sqrt{s+\lambda+y_1}-\sqrt{s+\lambda})y_2-(\sqrt{s+\lambda+y_2}-\sqrt{s+\lambda})y_1]$$

and

$$\widetilde{B}_2(\lambda,s)\simeq\frac{2x_0^2}{D\sqrt{s(s+\lambda)}}\int_0^\Lambda dy_1dy_2\,\frac{(\sqrt{s+\lambda+y_2}-\sqrt{s+\lambda})}{y_1y_2^2(y_1-y_2)}[(\sqrt{s+y_1}-\sqrt{s})y_2-(\sqrt{s+y_2}-\sqrt{s})y_1],$$

where in the expression for $\widetilde{B}_2$ we exchanged the dummy variables y_1 and y_2.

Sum of the two amplitudes has a simpler expression, given by

$$\widetilde{B}(\lambda,s)=\widetilde{B}_1(\lambda,s)+\widetilde{B}_2(\lambda,s)=\frac{1}{D}\times\frac{x_0^2}{\sqrt{s(s+\lambda)}}\times b(s,s+\lambda),$$

where we define

$$b(s_1,s_2)=2\int_0^\Lambda\frac{dy_1dy_2}{y_1^2y_2^2(y_1-y_2)}\big[(\sqrt{s_1+y_1}-\sqrt{s_1})(\sqrt{s_2+y_1}-\sqrt{s_2})y_2^2-(\sqrt{s_1+y_2}-\sqrt{s_1})(\sqrt{s_2+y_2}-\sqrt{s_2})y_1^2\big].$$

In terms of rescaled variables this result gives Eq. (140).

Remark. We have numerically verified the asymptotic divergence for large Λ,

$$b(s_1,s_2)=-2\ln^2(\Lambda)+\frac{2\ln\Lambda}{\sqrt{s_1s_2}}[2(\sqrt{s_1}+\sqrt{s_2})^2\ln(\sqrt{s_1}+\sqrt{s_2})-s_1\ln(s_1)-s_2\ln(s_2)+2\sqrt{s_1s_2}(1-2\ln 2)]+\cdots. \quad \text{(H23)}$$

d. Diagrams G_1 and G_2

For $t_{\max}$, amplitude of G_1 and G_2 in Fig. 14 are

$$G_1(\tau,T)=\frac{1}{2D}\int_0^\Lambda dy_1dy_2\int_0^\infty dm_1dm_2\int_0^\tau dr_1\int_{r_1}^\tau ds\int_s^\tau dr_2\,e^{y_1(r_1-s)}e^{y_2(s-r_2)}\langle\langle\dot{x}(r_1)\dot{x}(r_2)\rangle\rangle_{(m_1,m_2)}$$

and

$$G_2(\tau,T)=\frac{1}{2D}\int_0^\Lambda dy_1dy_2\int_0^\infty dm_1dm_2\int_\tau^T dr_1\int_{r_1}^T ds\int_s^T dr_2\,e^{y_1(r_1-s)}e^{y_2(s-r_2)}\langle\langle\dot{x}(r_1)\dot{x}(r_2)\rangle\rangle_{(m_1,m_2)},$$

with the angular brackets defined in Eq. (125).

These expressions can be written as

$$G_1(\tau,T)=\frac{1}{2D}\int_0^\Lambda dy_1dy_2\int_0^\infty dm_1dm_2\mathscr{L}_\tau^+(m_1,x_0;-y_1,y_1-y_2,y_2)Z^+_{T-\tau}(x_0,m_2)$$

and

$$G_2(\tau,T)=\frac{1}{2D}\int_0^\Lambda dy_1dy_2\int_0^\infty dm_1dm_2Z_\tau^+(m_1,x_0)\mathscr{L}^+_{T-\tau}(x_0,m_2;-y_1,y_1-y_2,y_2),$$

where Z_t^+ is in Eq. (81) and $\mathscr{L}^+$ is an analog of (G8) in presence of absorbing boundary.

A double Laplace transformation Eq. (61) of the amplitudes are

$$\widetilde{G}_1(\lambda,s)=\frac{1}{2D}\int_0^\Lambda dy_1dy_2\int_0^\infty dm_1dm_2\widetilde{\mathscr{L}}^+_{s+\lambda}(m_1,x_0;-y_1,y_1-y_2,y_2)\widetilde{Z}_s^+(x_0,m_2) \quad \text{(H24)}$$

and

$$\widetilde{G}_2(\lambda, s) = \frac{1}{2D}\int_0^\Lambda dy_1 dy_2 \int_0^\infty dm_1 dm_2 \widetilde{Z}^+_{s+\lambda}(m_1, x_0)\widetilde{\mathscr{L}}^+_s(x_0, m_2; -y_1, y_1 - y_2, y_2), \tag{H25}$$

where the Laplace transformation of $\mathscr{L}^+$ is expressed in terms of $\widetilde{J}^+$ in an analogous relation of Eq. (G11). From this relation and using the results in Eqs. (G3) and (H4) we see that

$$\int_0^\infty dm_2\ \widetilde{\mathscr{L}}^+_s(x_0, m_2; -y_1, y_1 - y_2, y_2) = \int_0^\infty dm_1 \widetilde{\mathscr{L}}^+_s(m_1, x_0; -y_1, y_1 - y_2, y_2),$$

with an expression for the latter in Eq. (G13). This gives

$$\int_0^\infty dm\ \widetilde{\mathscr{L}}^+_s(x_0, m; -y_1, y_1 - y_2, y_2) = \frac{2D}{\sqrt{s}\, y_1^2 y_2^2} \times h^+_s\left(\frac{x_0}{\sqrt{D}}, y_1, y_2\right), \tag{H26}$$

with h^+_s in Eq. (G15).

Result for the integral of $\widetilde{Z}^+$ is in Eq. (L5). Using these results in Eq. (H24) we get

$$\widetilde{G}_1(\lambda, s) = \mathfrak{h}(s, s + \lambda), \tag{H27}$$

$$\widetilde{G}_2(\lambda, s) = \mathfrak{h}(s + \lambda, s), \tag{H28}$$

where

$$\mathfrak{h}(s_1, s_2) = \frac{(1 - e^{-x_0\sqrt{\frac{s_1}{D}}})}{s_1\sqrt{s_2}} \int_0^\Lambda \frac{dy_1 dy_2}{y_1^2 y_2^2}\ h^+_{s_2}\left(\frac{x_0}{\sqrt{D}}, y_1, y_2\right). \tag{H29}$$

For small x_0, using the asymptotic Eq. (G16) we get

$$\widetilde{G}_1(\lambda, s) \simeq \frac{x_0^2}{D\sqrt{s(s + \lambda)}} \times g(s + \lambda) \tag{H30}$$

and

$$\widetilde{G}_2(\lambda, s) \simeq \frac{x_0^2}{D\sqrt{s(s + \lambda)}} \times g(s), \tag{H31}$$

with $g(x)$ defined in Eq. (G19). Beside the x_0^2 prefactor, amplitudes are similar to asymptotics in Eqs. (H30) and (H31) for t_{last}.

In terms of rescaled variables, we get Eq. (137).

APPENDIX I: EXPRESSION FOR $\Psi^{\max}$

The expression for $\Psi^{\max}$ in Eq. (154) can be written as

$$\Psi^{\max}(y_1, y_2, z) = \mathfrak{d} + \mathfrak{b} + \mathfrak{c} - \mathfrak{a}, \tag{I1}$$

where the terms on the right-hand side are associated to the amplitudes in Eq. (149) and given by

$$\begin{aligned}
\mathfrak{d} = {} & \sqrt{y_1 + y_2 + 1}(\sqrt{y_1 + y_2 + 1} - \sqrt{y_1 + 1} - \sqrt{y_2 + 1} + 1) \\
& \times (-\sqrt{y_1 + y_2 + 1}(\sqrt{y_1 + y_2 + 1} - \sqrt{y_1 + 1} - \sqrt{y_2 + 1} + 1) + \sqrt{|y_1 + y_2 - z|} \\
& \times \{\sqrt{|z - y_1|}\ [\Theta(z - y_1) - \Theta(y_1 + y_2 - z)] + \sqrt{|z - y_2|}\ [\Theta(z - y_2) - \Theta(y_1 + y_2 - z)] \\
& + \sqrt{|y_1 + y_2 - z|}\ [\Theta(y_1 + y_2 - z) - \Theta(z - y_1 - y_2)] + \sqrt{|z|}\ [\Theta(y_1 + y_2 - z) - \Theta(z)]\}),
\end{aligned} \tag{I2}$$

$$\begin{aligned}
\mathfrak{b} = {} & \frac{1}{y_1 - y_2}\big[y_2^2(\sqrt{y_1 + 1} - 1)(\sqrt{y_1 - z}\ \Theta(y_1 - z) - \sqrt{y_1 + 1} + 1) \\
& - y_1^2(\sqrt{y_2 + 1} - 1)(\sqrt{y_2 - z}\ \Theta(y_2 - z) - \sqrt{y_2 + 1} + 1)\big],
\end{aligned} \tag{I3}$$

$$\begin{aligned}
\mathfrak{c} = {} & \sqrt{y_1 + 1}(\sqrt{y_1 + y_2 + 1} - \sqrt{y_1 + 1} - \sqrt{y_2 + 1} + 1)^2(-\sqrt{y_1 - z}\ \Theta(y_1 - z) + \sqrt{y_1 + 1} - 1) \\
& - (1 - \sqrt{y_1 + 1})(\sqrt{y_1 + 1}(\sqrt{y_1 + y_2 + 1} - \sqrt{y_1 + 1} - \sqrt{y_2 + 1} + 1)^2 + \sqrt{|y_1 - z|}\ \Theta(z - y_1) \\
& \times \Theta(y_2 - z)\ \Theta(y_1 + y_2 - z)[(\sqrt{y_1 + y_2 - z} - \sqrt{z - y_1} - \sqrt{y_2 - z} + \sqrt{z})^2 - 2(\sqrt{z} - \sqrt{z - y_1})^2] \\
& + \sqrt{|y_1 - z|}\ \Theta(y_1 + y_2 - z)\{\Theta(y_1 - z)\Theta(y_2 - z)[z - (\sqrt{y_1 + y_2 - z} - \sqrt{y_1 - z} - \sqrt{y_2 - z})^2] \\
& + \Theta(z - y_1)\ \Theta(y_2 - z)[(\sqrt{z} - \sqrt{z - y_1})^2 - (\sqrt{y_2 - z} - \sqrt{y_1 + y_2 - z})^2]
\end{aligned}$$

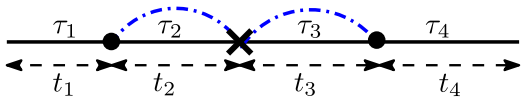

FIG. 25. An illustration for a change of variables in the amplitude Eq. (J1) of the diagram D in Fig. 21 to write the expression in Eq. (J2). Inside each time window t_i the process is conditioned to stay a net τ_i amount of time on positive side.

$$
\begin{aligned}
&- 2\Theta(z-y_1)\,\Theta(z-y_2)\sqrt{y_1+y_2-z}(\sqrt{z-y_1}+\sqrt{z-y_2}-\sqrt{z}) \\
&+ \Theta(y_1-z)\,\Theta(z-y_2)[(\sqrt{z}-\sqrt{z-y_2})^2-(\sqrt{y_1-z}-\sqrt{y_1+y_2-z})^2]]\}),
\end{aligned} \tag{I4}
$$

and

$$
\begin{aligned}
\mathfrak{a} = {} & (1-\sqrt{y_1+1})(1-\sqrt{y_2+1})^2[1-\sqrt{y_1+1}+\sqrt{y_1-z}\,\Theta(y_1-z)]+(1-\sqrt{y_1+1})(1-\sqrt{y_2+1}) \\
& \times\{\sqrt{y_1-z}\,\sqrt{y_2-z}\,\Theta(y_1-z)\,\Theta(y_2-z)-[\sqrt{z}-\sqrt{z-y_1}\,\Theta(z-y_1)][\sqrt{z}-\sqrt{z-y_2}\,\Theta(z-y_2)]\} \\
& +(1-\sqrt{y_1+1})\{y_2\sqrt{y_1-z}\,\Theta(y_1-z)-2\sqrt{z}\sqrt{y_1-z}\,\Theta(y_1-z)[\sqrt{z}-\sqrt{z-y_2}\,\Theta(z-y_2)] \\
& -2\sqrt{z}\sqrt{y_2-z}\,\Theta(y_2-z)[\sqrt{z}-\sqrt{z-y_1}\,\Theta(z-y_1)]\}.
\end{aligned} \tag{I5}
$$

Here $\Theta(x)$ is the Heaviside step function. These expressions are also given in the supplemental Mathematica notebook [78] for their numerical evaluation.

APPENDIX J: TWO-LOOP DIAGRAMS FOR DISTRIBUTION OF $t_{\rm pos}$

Among the two diagrams in Fig. 21 which contribute to second order, the diagram D is simpler to evaluate. Corresponding amplitude is in Eq. (177), which can be expressed in terms of conditional propagator Eq. (159) using the correlation in Eq. (170):

$$
\begin{aligned}
D(\tau,T) = {} & \frac{2^2D^2}{2D}\int_0^\Lambda dy_1dy_2\int_0^T dr_1\int_{r_1}^T ds\int_s^T dr_2\int_0^{r_1}d\tau_1\int_0^{r_2-r_1}d\tau_2\int_0^{T-r_2}d\tau_3\int_{-\infty}^\infty dx_1\,dx_2\,dm \\
& \times\,\delta(\tau-\tau_1-\tau_2-\tau_3)\,e^{y_1(r_1-s)}e^{y_2(s-r_2)}\,\mathbb{Z}_{r_1}(0,x_1|\tau_1)\partial_{x_1}\mathbb{Z}_{r_2-r_1}(x_1,x_2|\tau_2)\,\partial_{x_2}\mathbb{Z}_{T-r_2}(x_2,m|\tau_3).
\end{aligned} \tag{J1}
$$

For reasons that will be clear shortly, we make a change of variables (see illustration in Fig. 25), and write

$$
\begin{aligned}
D(\tau,T) = {} & 2D\int_0^\Lambda dy_1dy_2\int_0^\infty dt_1dt_2dt_3dt_4\int_0^{t_1}d\tau_1\int_0^{t_2}d\tau_2\int_0^{t_3}d\tau_3\int_0^{t_4}d\tau_4\int_{-\infty}^\infty dx_1dx_2dx_3dm \\
& \times\,\delta(T-t_1-t_2-t_3-t_4)\,\delta(\tau-\tau_1-\tau_2-\tau_3-\tau_4)e^{-y_1t_2-y_2t_3}\,\mathbb{Z}_{t_1}(0,x_1|\tau_1)\,\partial_{x_1}\mathbb{Z}_{t_2}(x_1,x_2|\tau_2) \\
& \times\,\mathbb{Z}_{t_3}(x_2,x_3|\tau_3)\,\partial_{x_3}\mathbb{Z}_{t_4}(x_3,m|\tau_4),
\end{aligned} \tag{J2}
$$

where in the last two lines of the expression we used $\mathbb{Z}_{t_2+t_3}(x_1,x_3|\tau_2+\tau_3)=\int dx_2\mathbb{Z}_{t_2}(x_1,x_2|\tau_2)\mathbb{Z}_{t_3}(x_2,x_3|\tau_3)$.

A double Laplace transformation Eq. (61) of the amplitude gives a simpler expression

$$
\widetilde{D}(\lambda,s) = 2D\int_0^\Lambda dy_1dy_2\int_{-\infty}^\infty dx_1dx_2dx_3dm\;\widetilde{\mathbb{Z}}_s(0,x_1|\lambda)\partial_{x_1}\,\widetilde{\mathbb{Z}}_{s+y_1}(x_1,x_2|\lambda)\,\widetilde{\mathbb{Z}}_{s+y_2}(x_2,x_3|\lambda)\,\partial_{x_3}\widetilde{\mathbb{Z}}_s(x_3,m|\lambda),
$$

with $\widetilde{\mathbb{Z}}$ defined in Eq. (167).

Results for spatial integration of $\widetilde{\mathbb{Z}}_s$ are derived in Appendix P and successively using them we get (a lengthy but straightforward algebra) an explicit expression for the amplitude,

$$
\widetilde{D}(\lambda,s) = \frac{2}{\sqrt{s(s+\lambda)}\big(\sqrt{s}+\sqrt{s+\lambda}\big)}\int_0^\Lambda\frac{dy_1dy_2}{y_1y_2}\left\{\frac{y_2\,\mathfrak{h}(1,z,y_1)}{(y_2-y_1)}+\frac{y_1\,\mathfrak{h}(1,z,y_2)}{(y_1-y_2)}\right\}, \tag{J3}
$$

where $\mathfrak{h}(s_1,s_2,y)$ is defined in Eq. (180). In terms of rescaled variables, Eq. (J3) gives Eq. (178).

For the diagram C in Fig. 21, we write the amplitude Eq. (176) in three parts according to the order of time variables (associated diagrams are indicated in Fig. 26). For example, amplitude of diagram C_1 is

$$
C_1(\tau,T) = \frac{2}{8D^2}\int_{-\infty}^\infty dm\int_0^\Lambda dy_1dy_2\int_0^T dr_1\int_{r_1}^T dr_2\int_{r_2}^T dr_3\int_{r_3}^T dr_4\;e^{y_1(r_1-r_2)}e^{y_2(r_3-r_4)}\langle\langle\dot{x}(r_1)\dot{x}(r_2)\dot{x}(r_3)\dot{x}(r_4)\rangle\rangle_{(0,m)}, \tag{J4}
$$

where the prefactor 2 is the degeneracy for exchange of pairs (r_1,r_2) and (r_3,r_4) for the diagram C_1 in Fig. 26.

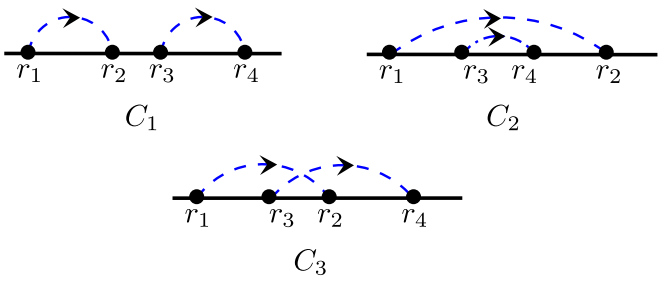

FIG. 26. The diagram C in Fig. 21 is split into three parts according to relative position of the loops. For these diagrams we choose $r_2 > r_1$ and $r_4 > r_3$, as indicated by the arrowheads.

Similar to the diagram D, these amplitudes can be expressed in terms of conditional propagator Eq. (159). The four point correlation in the conditional case is given by, for $r_1 < r_2 < r_3 < r_4 < T$,

$$\begin{aligned}\langle\langle \dot{x}(r_1)\dot{x}(r_2)\dot{x}(r_3)\dot{x}(r_4)\rangle\rangle_{(m_1,m_2)} = 2^4D^4 \int_{-\infty}^{\infty} dx_1dx_2dx_3dx_4 \int_0^{r_1} d\tau_1 \int_0^{r_2-r_1} d\tau_2 \int_0^{r_3-r_2} d\tau_3 \int_0^{r_4-r_3} d\tau_4 \int_0^{T-r_4} d\tau_5 \\ \times \delta(\tau-\tau_1-\tau_2-\tau_3-\tau_4-\tau_5)\mathbb{Z}_{r_1}(m_1,x_1|\tau_1)\partial_{x_1}\mathbb{Z}_{r_2-r_1}(x_1,x_2|\tau_2)\partial_{x_2}\mathbb{Z}_{r_3-r_2}(x_2,x_3|\tau_3) \\ \times \partial_{x_3}\mathbb{Z}_{r_4-r_3}(x_3,x_4|\tau_4)\partial_{x_4}\mathbb{Z}_{T-r_4}(x_4,m_2|\tau_5),\end{aligned} \tag{J5}$$

where the conditional average is defined in Eq. (158). This is analogous to Eq. (M8) without a condition on positive time and can be derived following a similar analysis given in Appendix M.

Following this result Eq. (J5) and the amplitude in Eq. (J4) we write the

$$\begin{aligned}C_1(\tau,T) = 2\times\frac{2^4D^4}{8D^2}\int_0^{\Lambda}dy_1dy_2\int_0^{\infty}dt_1dt_2dt_3dt_4dt_5\int_0^{t_1}d\tau_1\int_0^{t_2}d\tau_2\int_0^{t_3}d\tau_3\int_0^{t_4}d\tau_4\int_0^{t_5}d\tau_5 \\ \times\int_{-\infty}^{\infty}dx_1dx_2dx_3dx_4dm\,\delta(T-t_1-t_2-t_3-t_4-t_5)\delta(\tau-\tau_1-\tau_2-\tau_3-\tau_4-\tau_5)\,e^{-y_1t_2-y_2t_4} \\ \times\,\mathbb{Z}_{t_1}(0,x_1|\tau_1)\partial_{x_1}\mathbb{Z}_{t_2}(x_1,x_2|\tau_2)\partial_{x_2}\mathbb{Z}_{t_3}(x_2,x_3|\tau_3)\partial_{x_3}\mathbb{Z}_{t_4}(x_3,x_4|\tau_4)\partial_{x_4}\mathbb{Z}_{t_4}(x_4,m|\tau_4),\end{aligned} \tag{J6}$$

where we have made a change of integration variables similar to that used for the diagram D in Eq. (J2).

Following a very similar analysis we find that amplitude of other two diagrams in Fig. 26 are almost same as in Eq. (J6), with only the term $e^{-y_1r_2-y_2r_4}$ replaced by $e^{-y_1(t_2+t_3+t_4)-y_2t_3}$ for C_2 and by $e^{-y_1(t_2+t_3)-y_2(t_3+t_4)}$ for C_3.

A double Laplace transformation Eq. (61) of the amplitudes integrates the delta functions and lead to a simpler formula,

$$\widetilde{C}_1(\lambda,s) = 4D^2\int_0^{\Lambda}dy_1dy_2\int_{-\infty}^{\infty}dx_1dx_2dx_3dx_4dm\widetilde{\mathbb{Z}}_s(0,x_1|\lambda)\partial_{x_1}\widetilde{\mathbb{Z}}_{s+y_1}(x_1,x_2|\lambda)\partial_{x_2}\widetilde{\mathbb{Z}}_s(x_2,x_3|\lambda)\partial_{x_3}\widetilde{\mathbb{Z}}_{s+y_2}(x_3,x_4|\lambda)\partial_{x_4}\widetilde{\mathbb{Z}}_s(x_4,m|\lambda), \tag{J7}$$

with $\widetilde{\mathbb{Z}}$ defined in Eq. (167). The other two amplitudes

$$\begin{aligned}\widetilde{C}_2(\lambda,s) = 4D^2\int_0^{\Lambda}dy_1dy_2\int_{-\infty}^{\infty}dx_1dx_2dx_3dx_4dm\widetilde{\mathbb{Z}}_s(0,x_1\lambda)\partial_{x_1}\widetilde{\mathbb{Z}}_{s+y_1}(x_1,x_2|\lambda)\partial_{x_2}\widetilde{\mathbb{Z}}_{s+y_1+y_2}(x_2,x_3|\lambda) \\ \times\,\partial_{x_3}\widetilde{\mathbb{Z}}_{s+y_1}(x_3,x_4|\lambda)\partial_{x_4}\widetilde{\mathbb{Z}}_s(x_4,m|\lambda)\end{aligned} \tag{J8}$$

and

$$\begin{aligned}\widetilde{C}_3(\lambda,s) = 4D^2\int_0^{\Lambda}dy_1dy_2\int_{-\infty}^{\infty}dx_1dx_2dx_3dx_4dm\widetilde{\mathbb{Z}}_s(0,x_1|\lambda)\partial_{x_1}\widetilde{\mathbb{Z}}_{s+y_1}(x_1,x_2|\lambda)\partial_{x_2}\widetilde{\mathbb{Z}}_{s+y_1+y_2}(x_2,x_3|\lambda) \\ \times\,\partial_{x_3}\widetilde{\mathbb{Z}}_{s+y_2}(x_3,x_4|\lambda)\partial_{x_4}\widetilde{\mathbb{Z}}_s(x_4,m|\lambda).\end{aligned} \tag{J9}$$

Difference in Eqs. (J8) and (J9) are in the subscript of a single $\widetilde{\mathbb{Z}}$ term.

Spatial integrals in these amplitudes can be evaluated by successively applying results from Appendix P. It follows a lengthy but straightforward algebra. We write their final expression as follows:

$$\widetilde{C}_1(\lambda,s) = \frac{4}{\sqrt{s(s+\lambda)}\,(\sqrt{s}+\sqrt{s+\lambda})}\int_0^{\Lambda}\frac{dy_1dy_2}{y_1y_2}[\mathfrak{f}(s,s+\lambda,y_1,y_2)+\mathfrak{f}(s+\lambda,s,y_1,y_2)], \tag{J10}$$

with $\mathfrak{f}$ in Eq. (184). Amplitudes of C_2 and C_3 are similar,

$$\widetilde{C}_2(\lambda, s) + \widetilde{C}_3(\lambda, s) = \frac{4}{\sqrt{s(s+\lambda)}\,(\sqrt{s}+\sqrt{s+\lambda})} \int_0^\Lambda \frac{dy_1 dy_2}{y_1^2 y_2} [\mathfrak{g}(s, s+\lambda, y_1, y_2) + \mathfrak{g}(s+\lambda, s, y_1, y_2)], \tag{J11}$$

with $\mathfrak{g}$ in Eq. (183). Writing them together in terms of rescaled variables we get Eq. (142).

Remark. We have verified the expression in Eqs. (J3), (J10), and (J11) using the formula Eq. (167) in Eqs. (J7), (J8), and (J9) and then numerically integrating in Mathematica.

APPENDIX K: EXPRESSION FOR $\Psi^{\rm pos}$

Similar to the Eq. (I1) for $t_{\max}$ we write $\Psi^{\rm pos}$ in Eq. (192) as a combination of three terms,

$$\Psi^{\rm pos}(y_1, y_2, z) = \mathfrak{c} + \mathfrak{d} - \tfrac{1}{4}\mathfrak{a}, \tag{K1}$$

where the terms on the right-hand side corresponds to amplitudes in Eq. (191). Expression for $\mathfrak{c}(y_1, y_2, z)$ is cumbersome to write here and it is given in the Supplemental Material Mathematica notebook [78]. In comparison, $\mathfrak{d}$ and $\mathfrak{a}$ have simpler expression, given below. Their numerical verification is also given in the Mathematica notebook.

$$\mathfrak{d}(y_1, y_2, z) = y_1 y_2 + \frac{y_2^2\, r(y_1, z) - y_1^2\, r(y_2, z)}{y_1 - y_2}, \tag{K2}$$

with

$$r(y, z) = -\sqrt{z(z-y)}\,\Theta(z-y) + (\sqrt{y+1}-1)\sqrt{y-z}\,\Theta(y-z) + \sqrt{y+1} + z - 1. \tag{K3}$$

Here $\Theta(x)$ is the Heaviside step function.

$$\mathfrak{a}(y_1, y_2, z) = u(y_1, y_2, z) + u(y_2, y_1, z), \tag{K4}$$

with

$$\begin{aligned}
u(y_1, y_2, z) = {} & 2 - 4z + \frac{z^2}{2} + \frac{y_1 y_2}{2} - y_1 z + 2y_1 + [6z - 4 - 2y_2 + 2(1-z)\sqrt{y_2+1}]\sqrt{y_1+1} \\
& + |y_1 - z|[\Theta(y_1 - z) - \Theta(z - y_1)][2 + y_2 - z - 2\sqrt{y_2+1} - 2\sqrt{y_2+1}\sqrt{y_2 - z}\,\Theta(y_2 - z)] \\
& + 2\sqrt{|y_2 - z|}(\Theta(y_2 - z)\{z(2\sqrt{y_1+1} + \sqrt{y_2+1} - 3) + y_1(1 - \sqrt{y_2+1}) \\
& + 2[1 - \sqrt{y_1+1} - \sqrt{y_2+1} + \sqrt{(y_1+1)(y_2+1)}]\} \\
& + \sqrt{z}\,\Theta(z - y_2)[2\sqrt{(y_1+1)(y_2+1)} - 4\sqrt{y_1+1} - 2\sqrt{y_2+1} + y_1 - z + 4]) \\
& + 2|y_1 - z|\sqrt{|y_2 - z|}[\Theta(y_1 - z) - \Theta(z - y_1)][\Theta(y_2 - z) + \sqrt{z}\,\Theta(z - y_2)] \\
& + \frac{1}{2}|y_1 - z||y_2 - z|[\Theta(y_1 - z) - \Theta(z - y_1)][\Theta(y_2 - z) - \Theta(z - y_2)] \\
& - 2\sqrt{|y_1 - z|}\sqrt{|y_2 - z|}\{\sqrt{z}(\sqrt{y_1+1} + \sqrt{y_2+1} - 2)[\Theta(y_1 - z)\Theta(z - y_2) + \Theta(z - y_1)\Theta(y_2 - z)] \\
& + [z - 1 + \sqrt{y_1+1} + \sqrt{y_2+1} - \sqrt{(y_1+1)(y_2+1)}][\Theta(y_1 - z)\Theta(y_2 - z) - \Theta(z - y_1)\Theta(z - y_2)]\}.
\end{aligned} \tag{K5}$$

APPENDIX L: A LIST OF INTEGRALS FOR THE BROWNIAN PROPAGATOR

The Brownian propagator $Z_t(m_1, m_2)$ in Eq. (24) is symmetric under exchange of m_1 and m_2, and therefore

$$\partial_{m_1} Z_t(m_1, m_2) = -\partial_{m_2} Z_t(m_1, m_2) \tag{L1}$$

and its Laplace transformation Eq. (85),

$$\partial_{m_1} \widetilde{Z}_s(m_1, m_2) = -\partial_{m_2} \widetilde{Z}_s(m_1, m_2). \tag{L2}$$

There is an analogous formula for the propagator $\widetilde{Z}_s^+$ in presence of absorbing line,

$$\partial_{m_1} \widetilde{Z}_s^+(m_1, m_2) = -\partial_{m_2} \widetilde{Z}_s^+(m_1, m_2) + \frac{1}{D} e^{-\sqrt{\frac{s}{D}}(m_1 + m_2)}. \tag{L3}$$

We list the following results for the integral of the propagators, which are frequently used in this paper. They can be numerically verified in Mathematica.

$$\int_{-\infty}^{\infty} dm_2 \widetilde{Z}_s(m_1, m_2) = \frac{1}{s} \tag{L4}$$

and its analog with absorbing boundary

$$\int_0^{\infty} dm_2 \widetilde{Z}_s^+(m_1, m_2) = \frac{1}{s}(1 - e^{-m_1\sqrt{\frac{s}{D}}}). \tag{L5}$$

Another useful result

$$\int_0^{\infty} dm_2 \widetilde{Z}_{s+y}^+(m_1, m_2) e^{-m_2\sqrt{\frac{s}{D}}} = \frac{1}{y}\left(e^{-m_1\sqrt{\frac{s}{D}}} - e^{-m_1\sqrt{\frac{s+y}{D}}}\right). \tag{L6}$$

Due to a symmetry $\widetilde{Z}_s(m_1,m_2)=\widetilde{Z}_s(m_2,m_1)$ an integral over m_1 yields the same results as above.

For product of two propagators we get

$$\int_{-\infty}^{\infty} dx \widetilde{Z}_r(m_1,x)\widetilde{Z}_s(x,m_2) = \begin{cases} \frac{\widetilde{Z}_s(m_1,m_2)}{r-s}+\frac{\widetilde{Z}_r(m_1,m_2)}{s-r} & \text{if } s\neq r, \\ \frac{1+\sqrt{\frac{s}{D}}|m_1-m_2|}{2s}\,\widetilde{Z}_s(m_1,m_2) & \text{if } r=s, \end{cases} \tag{L7}$$

and for its analog with absorbing boundary

$$\int_0^{\infty} dx \widetilde{Z}^+_r(m_1,x)\widetilde{Z}^+_s(x,m_2) = \begin{cases} \frac{\widetilde{Z}^+_s(m_1,m_2)}{r-s}+\frac{\widetilde{Z}^+_r(m_1,m_2)}{s-r} & \text{if } s\neq r, \\ \frac{1+\sqrt{\frac{s}{D}}|m_1-m_2|}{2s}\,\widetilde{Z}^+_s(m_1,m_2) & \text{if } r=s, \\ -\frac{\min\{m_1,m_2\}}{2s}e^{-(m_1+m_2)\sqrt{\frac{s}{D}}} & \end{cases} \tag{L8}$$

For product of three propagators, corresponding formula is

$$\int_{-\infty}^{\infty} dx \int_{-\infty}^{\infty} dy \widetilde{Z}_r(m_1,x)\widetilde{Z}_s(x,y)\widetilde{Z}_t(y,m_2) = \begin{cases} \frac{\widetilde{Z}_r(m_1,m_2)}{(s-r)(t-r)}+\frac{\widetilde{Z}_s(m_1,m_2)}{(r-s)(t-s)}+\frac{\widetilde{Z}_t(m_1,m_2)}{(r-t)(s-t)} & \text{if } r\neq s\neq t \\ \left[\frac{1+\sqrt{\frac{r}{D}}|m_1-m_2|}{2r}-\frac{1}{s-r}\right]\frac{\widetilde{Z}_r(m_1,m_2)}{s-r} & \\ \quad +\frac{\widetilde{Z}_s(m_1,m_2)}{(r-s)^2} & \text{if } r=t\neq s \\ \left[\frac{1+\sqrt{\frac{r}{D}}|m_1-m_2|}{2r}-\frac{1}{t-r}\right]\frac{\widetilde{Z}_r(m_1,m_2)}{t-r} & \\ \quad +\frac{\widetilde{Z}_t(m_1,m_2)}{(r-t)^2} & \text{if } r=s\neq t \end{cases} \tag{L9}$$

and its counterpart in presence of absorbing line,

$$\int_0^{\infty} dx \int_0^{\infty} dy \widetilde{Z}^+_r(m_1,x)\widetilde{Z}^+_s(x,y)\widetilde{Z}^+_t(y,m_2) = \begin{cases} \frac{\widetilde{Z}^+_r(m_1,m_2)}{(s-r)(t-r)}+\frac{\widetilde{Z}^+_s(m_1,m_2)}{(r-s)(t-s)}+\frac{\widetilde{Z}^+_t(m_1,m_2)}{(r-t)(s-t)} & \text{if } r\neq s\neq t \\ \left[\frac{1+\sqrt{\frac{r}{D}}|m_1-m_2|}{2r}-\frac{1}{s-r}\right]\frac{\widetilde{Z}^+_r(m_1,m_2)}{s-r} & \\ \quad +\frac{\widetilde{Z}^+_s(m_1,m_2)}{(r-s)^2}-\frac{\min(m_1,m_2)}{2r(s-r)}e^{-(m_1+m_2)\sqrt{\frac{r}{D}}} & \text{if } r=t\neq s \\ \left[\frac{1+\sqrt{\frac{r}{D}}|m_1-m_2|}{2r}-\frac{1}{t-r}\right]\frac{\widetilde{Z}^+_r(m_1,m_2)}{t-r} & \\ \quad +\frac{\widetilde{Z}^+_t(m_1,m_2)}{(r-t)^2}-\frac{\min(m_1,m_2)}{2r(t-r)}e^{-(m_1+m_2)\sqrt{\frac{r}{D}}} & \text{if } r=s\neq t \end{cases} \tag{L10}$$

APPENDIX M: TIME-CORRELATION OF BROWNIAN VELOCITIES

Here, we derive multitime correlations of velocity $\dot{x}(t)$ for a standard Brownian motion with diffusivity D. The first moment is defined by

$$\langle \dot{x}(t)\rangle = \int_{x(0)=m_1}^{x(T)=m_2} \mathcal{D}[x] e^{-\frac{S_0}{D}} \dot{x}(t), \tag{M1}$$

where the angular brackets denote average with a Brownian measure of diffusivity D starting at position $x(0)=m_1$ and finishing at time T at position $x(T)=m_2$. For evaluating the average we consider a small window between time t and $t+\Delta t$ such that

$$\langle \dot{x}(t)\rangle = \lim_{\Delta t\to 0}\int_{-\infty}^{\infty} dx dy\, Z_t(m_1,x) \times \left[\frac{e^{-\frac{(y-x)^2}{4D\Delta t}}}{\sqrt{4\pi D\Delta t}}\left(\frac{y-x}{\Delta t}\right)\right] Z_{T-t-\Delta t}(y,m_2), \tag{M2}$$

where the Brownian propagator Z is in Eq. (24) and we use Eq. (8a) for small Δt. Writing

$$\frac{e^{-\frac{(y-x)^2}{4D\Delta t}}}{\sqrt{4\pi D\Delta t}}\left(\frac{y-x}{\Delta t}\right) = -2D\,\partial_y\left[\frac{e^{-\frac{(y-x)^2}{4D\Delta t}}}{\sqrt{4\pi D\Delta t}}\right]$$

and using integration by parts for y variable, we get

$$\langle \dot{x}(t)\rangle = 2D\int_{-\infty}^{\infty} dx dy\, Z_t(m_1,x) \times \lim_{\Delta t\to 0}\left[\frac{e^{-\frac{(y-x)^2}{4D\Delta t}}}{\sqrt{4\pi D\Delta t}}\right]\partial_y Z_{T-t-\Delta t}(y,m_2).$$

In the $\Delta t\to 0$ limit, it gives an expression

$$\langle \dot{x}(t)\rangle = 2D\int_{-\infty}^{\infty} dx\, Z_t(m_1,x)\partial_x Z_{T-t}(x,m_2), \tag{M3}$$

which can be explicitly evaluated using Eq. (24).

For two-time correlation one can similarly show that

$$\langle \dot{x}(r_1)\dot{x}(r_2)\rangle = 2^2D^2\mathscr{C}(r_1,r_2) + 2D\,\delta(r_1-r_2)Z_T(m_1,m_2), \tag{M4}$$

where $\mathscr{C}(r_1,r_2)$ is a symmetric function given by

$$\mathscr{C}(r_1,r_2) = \int_{-\infty}^{\infty} dx_1 dx_2 Z_{r_1}(m_1,x_1) \times \partial_{x1}Z_{r_2-r_1}(x_1,x_2)\partial_{x2}Z_{T-r_2}(x_2,m_2), \tag{M5}$$

for $r_2>r_1$. The integral remains finite for $r_1\to r_2$ limit.

A generalization of Eq. (M4) in an analogy of Wick's theorem gives multitime correlations. For example, we get

$$\langle \dot{x}(r_1)\dot{x}(r_2)\dot{x}(r_3)\rangle = 2^3D^3\mathscr{C}(r_1,r_2,r_3) + 2D\sum_{\text{pairs}}\delta(r_i-r_j)\langle \dot{x}(r_k)\rangle, \quad \text{(M6)}$$

where $\mathscr{C}(r_1,r_2,r_3)$ is a symmetric function under permutation of its arguments and given by

$$\mathscr{C}(r_1,r_2,r_3) = \int_{-\infty}^{\infty} dx_1dx_2dx_3 Z_{r_1}(m_1,x_1) \times \partial_{x_1}Z_{r_2-r_1}(x_1,x_2)\,\partial_{x_2}Z_{r_3-r_2}(x_2,x_3)\partial_{x_3}Z_{T-r_3}(x_3,m_2), \quad \text{(M7)}$$

for $r_3 > r_1 > r_1$.

For the four-time correlation, we get

$$\langle \dot{x}(r_1)\dot{x}(r_2)\dot{x}(r_3)\dot{x}(r_4)\rangle = 2^4D^4\mathscr{C}(r_1,r_2,r_3,r_4) + 2D\sum_{\text{pairs}}\delta(r_i-r_j)\langle \dot{x}(r_k)\dot{x}(r_\ell)\rangle, \quad \text{(M8)}$$

with

$$\mathscr{C}(r_1,r_2,r_3,r_4) = \int_{-\infty}^{\infty} dx_1dx_2dx_3dx_4 Z_{r_1}(m_1,x_1) \times \partial_{x_1}Z_{r_2-r_1}(x_1,x_2)\partial_{x_2}Z_{r_3-r_2}(x_2,x_3) \times \partial_{x_3}Z_{r_4-r_3}(x_3,x_4)\partial_{x_4}Z_{T-r_4}(x_4,m_2), \quad \text{(M9)}$$

for $r_1 < r_2 < r_3 < \cdots < r_4$.

Expression for these correlations can be further simplified. For the first moment Eq. (M3), using Eq. (L1) and then integrating over x, we get

$$\langle \dot{x}(t)\rangle = \big(-2D\partial_{m_2}\big)Z_T(m_1,m_2). \quad \text{(M10)}$$

Similarly, from Eq. (M4) we get

$$\langle \dot{x}(r_1)\dot{x}(r_2)\rangle = \big[2^2D^2\partial_{m_2}^2 + 2D\delta(r_1-r_2)\big]Z_T(m_1,m_2), \quad \text{(M11)}$$

and for three-time correlation in Eq. (M6) we get

$$\langle \dot{x}(r_1)\dot{x}(r_2)\dot{x}(r_3)\rangle = \big(-2D\,\partial_{m_2}\big)\Big[2^2D^2\partial_{m_2}^2 + 2D\sum_{\text{pairs}}\delta(r_i-r_j)\Big]Z_T(m_1,m_2). \quad \text{(M12)}$$

More generally, for $r_1 < r_2 < \cdots < r_{2n}$ we see that

$$\langle \dot{x}(r_1)\cdots\dot{x}(r_{2n})\rangle = 2^{2n}D^{2n}\partial_{m_2}^{2n}Z_T(m_1,m_2), \quad \text{(M13)}$$

which is used for a derivation of Eq. (C3).

Remark. Formulas in Eqs. (M11) and (M12) are mentioned earlier in Eqs. (25) and (29).

Remark. In presence of an absorbing wall, correlations have a very similar formula as in Eqs. (M3), (M4), (M6), and (M8), where one need to substitute the propagator Z by Z^+. However, they can not be simplified like in Eqs. (M10)–(M12).

APPENDIX N: IDENTITIES FOR J_t IN EQ. (90)

In this section, we give a list of results for J_t in Eq. (90) and its analog J_t^+ with absorbing boundary. These results are used in our analysis.

1. $J_t(m_1, m_2; y)$

Using Eq. (M10) in Eq. (90) we write

$$J_t(m_1,m_2;y) = 2D\,\partial_{m_2}Z_t(m_1,m_2)\left\{\frac{e^{-yt}-1}{y}\right\}.$$

Its Laplace transform is

$$\widetilde{J}_s(m_1,m_2;y) = \frac{2D}{y}\partial_{m_2}[\widetilde{Z}_{s+y}(m_1,m_2) - \widetilde{Z}_s(m_1,m_2)],$$

and using Eq. (85b) it leads to

$$\widetilde{J}_s(m_1,m_2;y) = \frac{\text{sgn}(m_1-m_2)}{y} \times \Big[e^{-|m_1-m_2|\sqrt{\frac{s+y}{D}}} - e^{-|m_1-m_2|\sqrt{\frac{s}{D}}}\Big]. \quad \text{(N1)}$$

Here $\text{sgn}(x)$ gives the sign of x.

2. $J_t^+(m_1, m_2; y)$

An analog of J_t in presence of absorbing line is

$$J_t^+(m_1,m_2;y) = \int_0^t dr\; e^{-yr}\langle \dot{x}(r)\rangle^+, \quad \text{(N2)}$$

with the average $\langle\cdot\rangle^+$ defined as in Eq. (M1) with absorbing boundary at origin. Using the analogous formula of Eq. (M3) for absorbing boundary and taking Laplace transformation we get

$$\widetilde{J}_s^+(m_1,m_2;y) = 2D\int_0^\infty dx\widetilde{Z}_{s+y}^+(m_1,x)\partial_x\widetilde{Z}_s^+(x,m_2). \quad \text{(N3)}$$

Further, using Eqs. (L3) and (L8) leads to

$$\widetilde{J}_s^+(m_1,m_2;y) = -2D\partial_{m_2}\left[\int_0^\infty dx\widetilde{Z}_{s+y}^+(m_1,x)\widetilde{Z}_s^+(x,m_2)\right] + 2\int_0^\infty dx\widetilde{Z}_{s+y}^+(m_1,x)e^{-\sqrt{\frac{s}{D}}(x+m_2)}. \quad \text{(N4)}$$

Invoking the explicit expression of $\widetilde{Z}^+$ in Eq. (85b) leads to a small x_0 asymptotic,

$$\widetilde{J}_s^+(m_1,x_0;y) \simeq \frac{2x_0\sqrt{s}}{y\sqrt{D}}\big\{e^{-m_1\sqrt{\frac{s+y}{D}}} - e^{-m_1\sqrt{\frac{s}{D}}}\big\}, \quad \text{(N5)}$$

which has been used many times in our analysis.

Another useful result is for integrals of $\widetilde{J}_s^+$. It is straightforward to see that an integration over m_1 gives

$$\int_0^\infty dm_1\widetilde{J}_s^+(m_1,m_2;y) = \frac{2\sqrt{D}}{y\sqrt{(s+y)}}\big\{e^{-m_2\sqrt{\frac{s+y}{D}}} - e^{-m_2\sqrt{\frac{s}{D}}}\big\}, \quad \text{(N6)}$$

and an integration over m_2 gives

$$\int_0^\infty dm_2 \widetilde{J}_s^+(m_1,m_2;y) = \frac{2\sqrt{D}}{y\sqrt{s}}\left\{e^{-m_1\sqrt{\frac{s}{D}}} - e^{-m_1\sqrt{\frac{s+y}{D}}}\right\}, \tag{N7}$$

where we used Eq. (L6). The same result can also be derived using a symmetry

$$\widetilde{J}_s^+(m_1,m_2;y) = -\widetilde{J}_{s+y}^+(m_2,m_1;-y),$$

which is evident from Eq. (N4) and the symmetry of $\widetilde{Z}_t^+$.

3. $J_t(m_1,m_2;y_1,y_2)$

For $J_t(m_1,m_2;y_1,y_2)$ in Eq. (90) using the correlation Eq. (M11) with the choice of integration Eq. (15) we get

$$J_t(m_1,m_2;y_1,y_2) = 2^2D^2\frac{\partial_{m_2}^2 Z_t(m_1,m_2)}{y_1y_2}\left[\frac{y_1+y_2e^{-t(y_1+y_2)}}{y_1+y_2} - e^{-y_2t}\right].$$

A Laplace transformation gives

$$\widetilde{J}_s(m_1,m_2;y_1,y_2) = \frac{2^2D^2}{y_1y_2(y_1+y_2)}\left[y_1\partial_{m_2}^2\widetilde{Z}_s(m_1,m_2) + y_2\partial_{m_2}^2\widetilde{Z}_{s+y_1+y_2}(m_1,m_2) - (y_1+y_2)\partial_{m_2}^2\widetilde{Z}_{s+y_2}(m_1,m_2)\right].$$

The explicit formula of $\widetilde{Z}$ in Eq. (85b) leads to the result given in Eq. (G2).

A special case of Eq. (G2), used earlier for deriving the result Eq. (91), is

$$\widetilde{J}_s(0,x_0;-y,y) = \frac{\sqrt{D}}{y^2}\left[2\sqrt{s+y}e^{-x_0\sqrt{\frac{s+y}{D}}} - \frac{e^{-x_0\sqrt{\frac{s}{D}}}}{\sqrt{s}}\left(2s+y-yx_0\sqrt{\frac{s}{D}}\right)\right]. \tag{N8}$$

4. $J_t^+(m_1,m_2;y_1,y_2)$

Starting with the definition

$$J_t^+(m_1,m_2;y_1,y_2) = \int_0^t dr_1\int_{r_1}^t dr_2\, e^{-y_1r_1-y_2r_2}\langle\dot{x}(r_1)\dot{x}(r_2)\rangle^+, \tag{N9}$$

with the convention in Eq. (15) for time-integrals and using an analog of Eq. (M4) for correlations with absorbing boundary, we write

$$J_t^+(m_1,m_2;y_1,y_2) = \int_{-\infty}^\infty dx_1dx_2\int_0^t dr_1\int_{r_1}^t dr_2\, e^{-y_1r_1-y_2r_2} \times Z_{r_1}(m_1,x_1)\partial_{x_1}Z_{r_2-r_1}(x_1,x_2)\partial_{x_2}Z_{T-r_2}(x_2,m_2).$$

Its Laplace transformation (in $t\to s$ variable) is

$$\widetilde{J}_s^+(m_1,m_2;y_1,y_2) = 2^2D^2\int_0^\infty dx_1dx_2 \times \widetilde{Z}_{s+y_1+y_2}^+(m_1,x_1)\partial_{x_1}\widetilde{Z}_{s+y_2}^+(x_1,x_2)\partial_{x_2}\widetilde{Z}_s^+(x_2,m_2). \tag{N10}$$

An explicit expression can be derived using the result in Eq. (85b).

Analysis gets simplified realizing that

$$\widetilde{J}_s^+(m_1,m_2;y_1,y_2) = 2D\int_0^\infty dx\widetilde{Z}_{s+y_1+y_2}^+(m_1,x)\partial_x\widetilde{J}_s^+(x,m_2,y_2), \tag{N11}$$

with $\widetilde{J}_s^+(x,m_2,y_2)$ in Eq. (N3). Using this, for example, one can derive a useful asymptotic for small x_0 by using Eq. (N5) and Eq. (85b), which gives

$$\widetilde{J}_s^+(m_1,x_0;y_1,y_2) \simeq 4x_0\left\{\frac{s}{y_2(y_1+y_2)}\left(e^{-m_1\sqrt{\frac{s}{D}}} - e^{-m_1\sqrt{\frac{s+y_1+y_2}{D}}}\right) - \frac{\sqrt{s(s+y_2)}}{y_1y_2}\left(e^{-m_1\sqrt{\frac{s+y_2}{D}}} - e^{-m_1\sqrt{\frac{s+y_1+y_2}{D}}}\right)\right\}. \tag{N12}$$

For an analogous formula of Eq. (N7) we evaluate the integration in Eq. (N11) using Eq. (L5), a symmetry $\widetilde{Z}_s^+(m_1,m_2) = \widetilde{Z}_s^+(m_2,m_1)$, the results in Eqs. (L2), (L6), (L8), and using integration by parts. This way it is straightforward to get the result in Eq. (G3).

In a similar way we derive the integral over m_1, and the result is given in Eq. (H4). Alternatively, one can use a symmetry

$$\widetilde{J}_s^+(m_1,m_2;y_1,y_2) = \widetilde{J}_{s+y_1+y_2}^+(m_2,m_1;-y_2,-y_1),$$

which is evident from Eq. (N14) using the symmetry $\widetilde{Z}_s^+(x_1,x_2) = \widetilde{Z}_s^+(x_2,x_1)$.

A special case of Eq. (G3), which is used for deriving Eq. (91), is

$$\int_0^\infty dm_2\widetilde{J}_s^+(m_1,m_2;-y,y) = \frac{2\sqrt{D}}{y^2\sqrt{s}}\left\{2\sqrt{(s+y)}\sqrt{D}\left(e^{-m_1\sqrt{\frac{s}{D}}} - e^{-m_1\sqrt{\frac{s+y}{D}}}\right) \times -m_1ye^{-m_1\sqrt{\frac{s}{D}}}\right\}. \tag{N13}$$

5. $J_t^+(m_1,m_2;y_1,y_2,y_3)$

Similar to Eq. (N9) we define $J_t^+(m_1,m_2;y_1,y_2,y_3)$. Using the analog of Eq. (M6) with an absorbing boundary and then taking a Laplace transformation (in $t\to s$ variable) we write

$$\widetilde{J}_s^+(m_1,m_2;y_1,y_2,y_3) = 2^3D^3\int_0^\infty dx_1dx_2dx_3 \times \widetilde{Z}_{s+y_1+y_2+y_3}^+(m_1,x_1)\partial_{x_1}\widetilde{Z}_{s+y_2+y_3}^+(x_1,x_2) \times \partial_{x_2}\widetilde{Z}_{s+y_3}^+(x_2,x_3)\partial_{x_3}\widetilde{Z}_s^+(x_3,m_2). \tag{N14}$$

For an explicit result we note that

$$\widetilde{J}_s^+(m_1,m_2;y_1,y_2,y_3) = 2D\int_0^\infty dx\widetilde{Z}_{s+y_1+y_2+y_3}^+(m_1,x) \times \partial_x\widetilde{J}_s^+(x,m_2;y_2,y_3), \tag{N15}$$

with Eq. (N14). Then, Eqs. (85b) and (N12) can be used to get an asymptotic for small x_0.

Integral of $\widetilde{J}^+_s(m_1, x_0; y_1, y_2, y_3)$ analogous to Eq. (N6) is also straightforward to derive using Eq. (N15). For small x_0,

$$\begin{aligned}\int_0^\infty dm_1 \widetilde{J}^+_s(m_1, x_0; y_1, y_2, y_3) &\simeq 8Dx_0\Big\{\frac{(s+y_3)(\sqrt{s+y_3}-\sqrt{s+y_1+y_2+y_3})}{\sqrt{s}\, y_2(y_1+y_2)y_3} \\ &+ \frac{\sqrt{s+y_2+y_3}[(y_2+y_3)\sqrt{s+y_3}-y_2\sqrt{s}]}{\sqrt{s}\, y_1y_2y_3(y_2+y_3)} \\ &\times (\sqrt{s+y_1+y_2+y_3}-\sqrt{s+y_2+y_3}) \\ &+ \frac{\sqrt{s}(\sqrt{s+y_1+y_2+y_3}-\sqrt{s})}{y_3(y_2+y_3)(y_1+y_2+y_3)}\Big\}, \end{aligned} \tag{N16}$$

which is used for a derivation of Eq. (H14).

For an integral over m_2 variable, one can use a symmetry

$$\widetilde{J}^+_s(m_1, m_2; y_1, y_2, y_3) = -\widetilde{J}^+_{s+y_1+y_2+y_3}(m_2, m_1; -y_3, -y_2, -y_1), \tag{N17}$$

which is evident from Eq. (N14) and $\widetilde{Z}^+_s(m_1, m_2) = \widetilde{Z}^+_s(m_2, m_1)$. The result is useful for a derivation of Eq. (H17).

6. $J^+_t(m_1, m_2; y_1, y_2, y_3, y_4)$

Similar to Eqs. (N11) and (N15),

$$\begin{aligned}J^+_t(m_1, m_2; y_1, y_2, y_3, y_4) &= \int_0^t dr_1 \int_{r_1}^t dr_2 \int_{r_2}^t dr_3 \\ &\times \int_{r_3}^t dr_4 e^{-y_1r_1-y_2r_2-y_3r_3-y_4r_4}\langle \dot{x}(r_1)\dot{x}(r_2)\dot{x}(r_3)\dot{x}(r_4)\rangle^+ \end{aligned} \tag{N18}$$

follows a hierarchy where

$$\begin{aligned}\widetilde{J}^+_s(m_1, m_2; y_1, y_2, y_3, y_4) &= 2D\int_0^\infty dx \widetilde{Z}^+_{s+y_1+y_2+y_3+y_4}(m_1, x) \\ &\times \partial_x \widetilde{J}^+_s(x, m_2; y_2, y_3, y_4), \end{aligned} \tag{N19}$$

which leads to explicit results explicit result for Eq. (N18).

For example, an integral over m_2 variable is given in Eq. (G5). From this one can derive also the integral over m_1 variable using a symmetry relation

$$\widetilde{J}^+_s(m_1, m_2; y_1, y_2, y_3, y_4) = \widetilde{J}^+_{s+y_1+y_2+y_3+y_4}(m_2, m_1; -y_4, -y_3, -y_2, -y_1), \tag{N20}$$

which is evident from Eq. (N19) and a symmetry $\widetilde{Z}^+_s(m_1, m_2) = \widetilde{Z}^+_s(m_2, m_1)$.

APPENDIX O: IDENTITIES FOR $\mathscr{I}^+_\tau$ IN EQ. (H10)

Using Eq. (H11) we get a relation for their Laplace transformation

$$\begin{aligned}\widetilde{\mathscr{I}}^+_s(m_1, m_2; y_1, y_2, y_3) &= \widetilde{J}^+_s(m_1, m_2; y_1, y_2, y_3) + \widetilde{J}^+_s(m_1, m_2; y_1, y_3, y_2) \\ &+ \widetilde{J}^+_s(m_1, m_2; y_3, y_1, y_2). \end{aligned} \tag{O1}$$

This leads to the results we need, namely,

$$\begin{aligned}\int_0^\infty dm_1 \widetilde{\mathscr{I}}^+_{s+\lambda+y_2}(m_1, x_0; -y_1, y_1, -y_2) &= \int_0^\infty dm_1 \big\{\widetilde{J}^+_{s+\lambda+y_2}(m_1, x_0; -y_1, y_1, -y_2) \\ &+ \widetilde{J}^+_{s+\lambda+y_2}(m_1, x_0; -y_1, -y_2, y_1) \\ &+ \widetilde{J}^+_{s+\lambda+y_2}(m_1, x_0; -y_2, -y_1, y_1)\big\}, \end{aligned}$$

which using Eq. (N16) for small x_0 limit gives Eq. (H14). A analogous integral

$$\begin{aligned}\int_0^\infty dm_2 \widetilde{\mathscr{I}}^+_s(x_0, m_2; -y_2, y_2, y_1) &\simeq \frac{4Dx_0\sqrt{s+y_1}}{y_1y_2^2\sqrt{s}}(\sqrt{s+y_1+y_2}-\sqrt{s+y_1} \\ &- \sqrt{s+y_2}+\sqrt{s})^2, \end{aligned} \tag{O2}$$

for small x_0, is derived using Eqs. (O1), (N16), and (N17). It is used for a derivation of Eq. (H17).

APPENDIX P: IDENTITIES FOR CONDITIONAL PROPAGATOR $\mathbb{Z}_t$

In this section we give a list of identities for conditional Brownian propagator $\mathbb{Z}_t$ in Eq. (159). These identities are often used for our analysis in Sec. VIII.

In Eq. (162) we see that

$$\widetilde{\mathbb{A}}_s(0, x|\lambda) = 0 = \widetilde{\mathbb{A}}_s(x, 0|\lambda). \tag{P1}$$

Substituting this and Eq. (165) in Eq. (167) we get

$$\widetilde{\mathbb{Z}}_s(0, x|\lambda) = \widetilde{\mathbb{B}}_s(0, x|\lambda) = \frac{\sqrt{s+\lambda}-\sqrt{s}}{\lambda\sqrt{D}}\, e^{-|x|\sqrt{\frac{s+\lambda\Theta(x)}{D}}}. \tag{P2}$$

The result is used for the zeroth-order amplitude in Eq. (168) and also appears in the linear order amplitude Eq. (172).

For results about integrals of $\widetilde{\mathbb{Z}}_s$ we use that for $\widetilde{\mathbb{A}}$ in Eq. (162),

$$\int_{-\infty}^\infty dx_2\, \widetilde{\mathbb{A}}_s(x_1, x_2|\lambda) = \frac{1-e^{-|x_1|\sqrt{\frac{s+\lambda\Theta(x_1)}{D}}}}{s+\lambda\Theta(x_1)}$$

and for $\widetilde{\mathbb{B}}$ in Eq. (165),

$$\int_{-\infty}^\infty dx_2\, \widetilde{\mathbb{B}}_s(x_1, x_2|\lambda) = \frac{e^{-|x_1|\sqrt{\frac{s+\lambda\Theta(x_1)}{D}}}}{\sqrt{s(s+\lambda)}}.$$

Then Eq. (167) leads to

$$\begin{aligned}\int_{-\infty}^\infty dx_2\, \widetilde{\mathbb{Z}}_s(x_1, x_2|\lambda) &= \frac{1-e^{-|x_1|\sqrt{\frac{s+\lambda\Theta(x_1)}{D}}}}{s+\lambda\Theta(x_1)} + \frac{e^{-|x_1|\sqrt{\frac{s+\lambda\Theta(x_1)}{D}}}}{\sqrt{s(s+\lambda)}}. \end{aligned} \tag{P3}$$

For a related result, we use

$$\int_{-\infty}^{\infty} dx_2 \partial_{x_1} \widetilde{\mathbb{A}}_s(x_1, x_2|\lambda) = \frac{\mathrm{sgn}(x_1) e^{-|x_1|\sqrt{\frac{s+\lambda\Theta(x_1)}{D}}}}{\sqrt{D[s+\lambda\Theta(x_1)]}},$$

and

$$\int_{-\infty}^{\infty} dx_2 \partial_{x_1} \widetilde{\mathbb{B}}_s(x_1, x_2|\lambda) = \frac{\mathrm{sgn}(-x_1)\sqrt{s+\lambda\Theta(x_1)}}{\sqrt{Ds(s+\lambda)}} e^{-|x_1|\sqrt{\frac{s+\lambda\Theta(x_1)}{D}}},$$

to get

$$\int_{-\infty}^{\infty} dx_2 \partial_{x_1} \widetilde{\mathbb{Z}}_s(x_1, x_2|\lambda) = \frac{e^{-|x_1|\sqrt{\frac{s+\lambda\Theta(x_1)}{D}}}[\sqrt{s}-\sqrt{s+\lambda}]}{\sqrt{Ds(s+\lambda)}}, \tag{P4}$$

which appears in the amplitudes Eqs. (172) and (175).

In the rest we list a few more identities which frequently appear for calculating the amplitude Eq. (175). Their derivation is similar to those shown for Eqs. (P3) and (P4). They can be verified numerically in Mathematica using the expressions in Eqs. (162), (165), and (167).

These are as follows:

$$\int_{-\infty}^{\infty} dx_2 \widetilde{\mathbb{Z}}_{s_2}(x_1, x_2|\lambda) e^{-|x_2|\sqrt{\frac{s_1+\lambda\Theta(x_2)}{D}}} = \frac{e^{-|x_1|\sqrt{\frac{s_1+\lambda\Theta(x_1)}{D}}}}{s_2-s_1} - \left(\frac{\sqrt{s_2}-\sqrt{s_2+\lambda}}{\sqrt{s_1}-\sqrt{s_1+\lambda}}\right)\frac{e^{-|x_1|\sqrt{\frac{s_2+\lambda\Theta(x_1)}{D}}}}{s_2-s_1} \tag{P5}$$

and

$$\int_{-\infty}^{\infty} dx_2 \widetilde{\mathbb{Z}}_s(0, x_2|\lambda) \partial_{x_2} e^{-|x_2|\sqrt{\frac{s_1+\lambda\Theta(x_2)}{D}}} = \frac{1}{\sqrt{D}} \times \frac{\sqrt{s_1(s+\lambda)}-\sqrt{s(s_1+\lambda)}}{(\sqrt{s+\lambda}+\sqrt{s})(\sqrt{s}+\sqrt{s_1})(\sqrt{s+\lambda}+\sqrt{s_1+\lambda})}. \tag{P6}$$

An analogous result [difference with Eq. (P6) is in a space derivative] is

$$\int_{-\infty}^{\infty} dx_1 \left[\partial_{x_1} \widetilde{\mathbb{Z}}_{s_1}(0, x_1|\lambda)\right] e^{-|x_1|\sqrt{\frac{s_2+\lambda\Theta(x_1)}{D}}} = \frac{1}{\sqrt{D}} \times \frac{\sqrt{s_1(s_2+\lambda)}-\sqrt{(s_1+\lambda)s_2}}{(\sqrt{s_1+\lambda}+\sqrt{s_1})(\sqrt{s_1}+\sqrt{s_2})(\sqrt{s_1+\lambda}+\sqrt{s_2+\lambda})}. \tag{P7}$$

More identities involving products of $\mathbb{Z}$ are as follows:

$$\int_{-\infty}^{\infty} dx_2 dm \widetilde{\mathbb{Z}}_{s_2}(x_1, x_2|\lambda) \partial_{x_2} \widetilde{\mathbb{Z}}_{s_1}(x_2, m|\lambda) = \frac{1}{s_2-s_1}\frac{1}{\sqrt{D\, s_1(s_1+\lambda)}}\Big[e^{-|x_1|\sqrt{\frac{s_1+\lambda\Theta(x_1)}{D}}}(\sqrt{s_1}-\sqrt{s_1+\lambda}) - e^{-|x_1|\sqrt{\frac{s_2+\lambda\Theta(x_1)}{D}}}(\sqrt{s_2}-\sqrt{s_2+\lambda})\Big] \tag{P8}$$

and

$$\begin{aligned}\int_{-\infty}^{\infty} dx_1 \widetilde{\mathbb{Z}}_s(0, x_1|\lambda) \partial_{x_1} \widetilde{\mathbb{Z}}_{s+y_1}(x_1, x_2|\lambda) &= \frac{1}{Dy_1} \times \frac{1}{\left(\sqrt{\lambda+s}+\sqrt{s}\right)}\Bigg\{\mathrm{sgn}(x_2)\sqrt{\lambda\Theta(x_2)+s}\, e^{-|x_2|\sqrt{\frac{\lambda\Theta(x_2)+s}{D}}} + \Bigg[\frac{(\sqrt{s+y_1}-\sqrt{s})(\sqrt{(\lambda+s)(s+y_1)}-\sqrt{s(\lambda+s+y_1)})}{\left(\sqrt{\lambda+s}+\sqrt{\lambda+s+y_1}\right)(\sqrt{\lambda+s+y_1}+\sqrt{s+y_1})} \\ &- \mathrm{sgn}(x_2)\sqrt{\lambda\Theta(x_2)+s}\Bigg] e^{-|x_2|\sqrt{\frac{\lambda\Theta(x_2)+s+y_1}{d}}}\Bigg\}.\end{aligned} \tag{P9}$$

A last one involving products of four $\mathbb{Z}$,

$$\begin{aligned}&\int_{-\infty}^{\infty} dx_1 dx_2 dx_3 dm\ \widetilde{\mathbb{Z}}_s(0, x_1|\lambda) \partial_{x_1} \widetilde{\mathbb{Z}}_{s+y_1}(x_1, x_2|\lambda) \widetilde{\mathbb{Z}}_{s+y_2}(x_2, x_3|\lambda) \partial_{x_3} \widetilde{\mathbb{Z}}_s(x_3, m|\lambda) \\ &= \frac{1}{D\sqrt{s(s+\lambda)}} \times \frac{1}{(\sqrt{s}+\sqrt{s+\lambda})}\left[\frac{h(s, s+\lambda, y_1)}{y_1(y_2-y_1)} + \frac{h(s, s+\lambda, y_2}{y_2(y_1-y_2)}\right],\end{aligned} \tag{P10}$$

where $h(s_1, s_2, y)$ is defined in Eq. (180). This is used for the amplitude of diagram D in Eq. (178).

APPENDIX Q: UNIFORM DISTRIBUTION OF t_{pos} FOR A BROWNIAN BRIDGE

In Sec. VIII A we used a result that for a Brownian bridge, time spent on positive half has a uniform distribution. Here, we give a derivation of this result.

Our derivation is for a random walk of total $2n$ steps on an infinite chain. The walker is conditioned to take equal number of positive and negative *steps* such that at the final step the walker returns to the starting point, which we choose to be the origin. Continuous limit of the process is a Brownian bridge, and the distribution of positive time for the Random walk gives the distribution for Brownian bridge in the continuous limit.

For our derivation, we define a generating function

$$G(\kappa, \rho) = 1 + \sum_{n=1}^{\infty}\sum_{m=0}^{n} \kappa^n \rho^m \frac{1}{2^{2n}} N(2n, 2m), \tag{Q1}$$

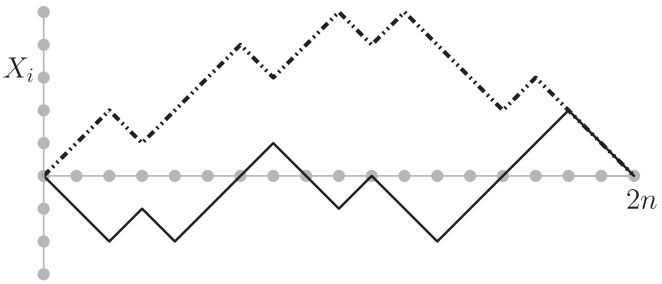

FIG. 27. The zigzag solid line shows a random walk bridge of $2n = 18$ steps that spends $2m = 6$ steps on the positive side. The dashed line shows an excursion of $2n$ steps that is conditioned to stay positive, for the entire duration.

where (κ, ρ) are parameters and $N(2n, 2m)$ gives the total number of Random walk bridges of length $2n$ with $2m$ number of steps spent on the positive side of the chain (see illustration in Fig. 27).

We define a second generating function

$$g(\kappa) = \sum_{n=1}^{\infty} \frac{\kappa^n}{2^{2n}} N^+(2n), \tag{Q2}$$

where $N^+(2n)$ gives the number of random bridges that stay on the positive side of the chain for the entire duration $2n$ (random walk excursion; see illustration in Fig. 27).

Using method of images it is straightforward to show that

$$N^+(2n) = \binom{2n-2}{n-1} - \binom{2n-2}{n} = \frac{(2n-2)!}{n!(n-1)!}, \tag{Q3}$$

leading to

$$g(\kappa) = \frac{1}{2}(1 - \sqrt{1-\kappa}). \tag{Q4}$$

To calculate $G(\kappa, \rho)$ we use a relation

$$\begin{aligned} G(\kappa, \rho) = \; & 1 + [g(\kappa) + g(\kappa\rho)] \\ & + [g(\kappa)^2 + 2g(\kappa)g(\kappa\rho) + g(\kappa\rho)^2] \\ & + [g(\kappa)^3 + 3g(\kappa)^2 g(\kappa\rho) + 3g(\kappa)g(\kappa\rho)^2 + g(\kappa\rho)^3] \\ & + \cdots, \end{aligned} \tag{Q5}$$

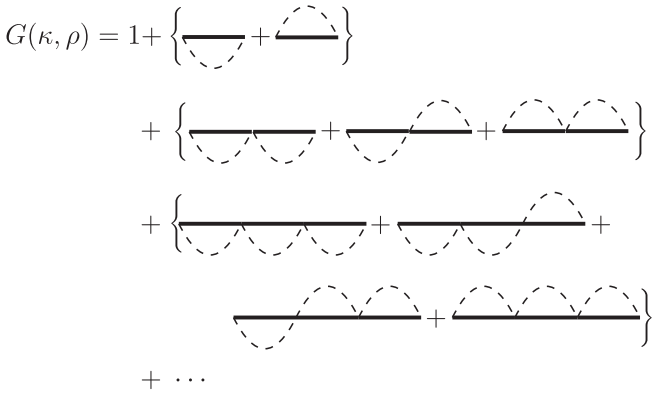

FIG. 28. A graphical representation of the infinite summation in Eq. (Q5). Down-sided excursions represent $g(\kappa)$ and up-sided excursions represent $g(\kappa\rho)$. Relative order of excursions give the degeneracy in Eq. (Q5).

which can be seen by the graphical illustration in Fig. 28. Completing the summation we get

$$G(\kappa, \rho) = \frac{1}{1 - g(\kappa) - g(\kappa\rho)}. \tag{Q6}$$

Using the formula for $g(\kappa)$ in Eq. (Q2) we write

$$G(\kappa, \rho) = 1 + \sum_{n=1}^{\infty} \sum_{m=0}^{n} \kappa^n \rho^m \frac{(2n)!}{2^{2n}(n+1)(n!)^2}. \tag{Q7}$$

Comparing with Eq. (Q1) it is evident that $N(2n, 2m)$ is independent of m. Equivalently, there are equal number of paths for all values of m in a random walk bridge of length $2n$. In the continuous limit, this means that for a Brownian bridge, all values of fractional positive time are equally probable.

[1] L. Decreusefond and A. S. Üstünel, Fractional Brownian motion: Theory and applications, in *ESAIM: Mathematical Modelling and Numerical Analysis* (EDP Sciences, Les Ulis, France, 1998), Vol. 32, pp. 75–86.

[2] H. Qian, Fractional Brownian motion and fractional Gaussian noise, in *Processes with Long-Range Correlations* (Springer, Berlin, 2003).

[3] I. Nourdin, *Selected Aspects of Fractional Brownian Motion* (Bocconi & Springer Series, Berlin, 2012).

[4] G. Shevchenko, Fractional Brownian motion in a nutshell, Int. J. Mod. Phys. **36**, 1560002 (2015).

[5] A. N. Kolmogorov, Wienersche spiralen und einige andere interessante Kurven im Hilbertschen Raum, C. R. (Dokl.) Acad. Sci. URSS **26**, 115 (1940).

[6] B. B. Mandelbrot and J. W. Van Ness, Fractional Brownian motions, fractional noises and applications, SIAM Rev. **10**, 422 (1968).

[7] R. Metzler and J. Klafter, The random walk's guide to anomalous diffusion: A fractional dynamics approach, Phys. Rep. **339**, 1 (2000).

[8] S. Cohen and J. Istas, *Fractional Fields and Applications* (Springer, Berlin, 2013).

[9] V. Kukla, J. Kornatowski, D. Demuth, I. Girnus, H. Pfeifer, L. V. C. Rees, S. Schunk, K. K. Unger, and J. Karger, NMR studies of single-file diffusion in unidimensional channel zeolites, Science **272**, 702 (1996).

[10] Q.-H. Wei, C. Bechinger, and P. Leiderer, Single-file diffusion of colloids in one-dimensional channels, Science **287**, 625 (2000).

[11] L. Lizana, T. Ambjörnsson, A. Taloni, E. Barkai, and M. A. Lomholt, Foundation of fractional Langevin equation: Harmonization of a many-body problem, Phys. Rev. E **81**, 051118 (2010).

[12] P. L. Krapivsky, K. Mallick, and T. Sadhu, Dynamical properties of single-file diffusion, J. Stat. Mech. (2015) P09007.

[13] T. Sadhu and B. Derrida, Large deviation function of a tracer position in single file diffusion, J. Stat. Mech. (2015) P09008.

[14] T. Sadhu and B. Derrida, Correlations of the density and of the current in nonequilibrium diffusive systems, J. Stat. Mech. (2016) 113202.

[15] A. Zoia, A. Rosso, and S. N. Majumdar, Asymptotic Behavior of Self-Affine Processes in Semi-Infinite Domains, Phys. Rev. Lett. **102**, 120602 (2009).

[16] J. L. A. Dubbeldam, V. G. Rostiashvili, A. Milchev, and T. A. Vilgis, Fractional Brownian motion approach to polymer translocation: The governing equation of motion, Phys. Rev. E **83**, 011802 (2011).

[17] V. Palyulin, T. Ala-Nissila, and R. Metzler, Polymer translocation: The first two decades and the recent diversification, Soft Matter **10**, 9016 (2014).

[18] J.-P. Bouchaud and A. Georges, Anomalous diffusion in disordered media: Statistical mechanisms, models and physical applications, Phys. Rep. **195**, 127 (1990).

[19] E. E. Peters, *Chaos and Order in the Capital Markets, Wiley Finance Editions*, 2nd ed. (Wiley, New York, 1996).

[20] N. J. Cutland, P. E. Kopp, and W. Willinger, Stock price returns and the Joseph effect: A fractional version of the Black-Scholes model, *Seminar on Stochastic Analysis, Random Fields and Applications*, edited by E. Bolthausen, M. Dozzi, and F. Russo, Progress in Probability (Birkhäuser, Basel, 1995), Vol. 36, pp. 327–351.

[21] F. Biagini, Y. Hu, B. Oksendal, and T. Zhang, *Stochastic Calculus for Fractional Brownian Motion and Applications* (Springer Verlag, London, 2008).

[22] T. Sottinen, Fractional Brownian motion, random walks and binary market models, Finance Stochast. **5**, 343 (2001).

[23] H. E. Hurst, Long-term storage capacity of reservoirs, Trans. Am. Soc. Civ. Eng. **116**, 770 (1951).

[24] B. B. Mandelbrot and J. R. Wallis, Noah, Joseph, and operational hydrology, Water Resour. Res. **4**, 909 (1968).

[25] S. Gupta, A. Rosso, and C. Texier, Dynamics of a Tagged Monomer: Effects of Elastic Pinning and Harmonic Absorption, Phys. Rev. Lett. **111**, 210601 (2013).

[26] E. Monte-Moreno and M. Hernández-Pajares, Occurrence of solar flares viewed with GPS: Statistics and fractal nature, J. Geophys. Res. **119**, 9216 (2014).

[27] I. Simonsen, Measuring anticorrelations in the nordic electricity spot market by wavelets, Physica A **322**, 597 (2003).

[28] I. Norros, On the use of fractional Brownian motion in the theory of connectionless networks, IEEE J. Sel. A. Commun. **13**, 953 (2006).

[29] K. Burnecki, E. Kepten, J. Janczura, I. Bronshtein, Y. Garini, and A. Weron, Universal algorithm for identification of fractional Brownian motion: A case of telomere subdiffusion, Biophys. J. **103**, 1839 (2012).

[30] J. H. Jeon, V. Tejedor, S. Burov, E. Barkai, C. Selhuber-Unkel, K. Berg-Sørensen, L. Oddershede, and R. Metzler, *In Vivo* Anomalous Diffusion and Weak Ergodicity Breaking of Lipid Granules, Phys. Rev. Lett. **106**, 048103 (2011).

[31] D. Ernst, M. Hellmann, K. Jürgen, and M. Weiss, Fractional Brownian motion in crowded fluids, Soft Matter **8**, 4886 (2012).

[32] G. M. Molchan, Maximum of a fractional Brownian motion: Probabilities of small values, Commun. Math. Phys. **205**, 97 (1999).

[33] J. Krug, H. Kallabis, S. N. Majumdar, S. J. Cornell, A. J. Bray, and C. Sire, Persistence exponents for fluctuating interfaces, Phys. Rev. E **56**, 2702 (1997).

[34] T. Guérin, N. Levernier, O. Bénichou, and R. Voituriez, Mean first-passage times of non-Markovian random walkers in confinement, Nature **534**, 356 (2016).

[35] S. N. Majumdar, Brownian functionals in physics and computer science, Curr. Sci. **89**, 2076 (2005).

[36] T. Hida, Functionals of Brownian motion, in *Transactions of the Seventh Prague Conference on Information Theory, Statistical Decision Functions, Random Processes and of the European Meeting of Statisticians: Held at Prague, from August 18 to 23, 1974*, edited by J. Kožešnik (Springer Netherlands, Dordrecht, 1977), pp. 239–243.

[37] S. Carmi, L. Turgeman, and E. Barkai, On distributions of functionals of anomalous diffusion paths, J. Stat. Phys. **141**, 1071 (2010).

[38] L. Turgeman, S. Carmi, and E. Barkai, Fractional Feynman-Kac Equation for Non-Brownian Functionals, Phys. Rev. Lett. **103**, 190201 (2009).

[39] D. Ruelle, Smooth dynamics and new theoretical ideas in nonequilibrium statistical mechanics, J. Stat. Phys. **95**, 393 (1999).

[40] D. Ruelle, Conversations on nonequilibrium physics with an extraterrestrial, Phys. Today **57**(5), 48 (2004).

[41] J. L. Lebowitz and H. Spohn, A Gallavotti–Cohen-type symmetry in the large deviation functional for stochastic dynamics, J. Stat. Phys. **95**, 333 (1999).

[42] P. Lévy, Sur certains processus stochastiques homogènes, Compositio Mathematica **7**, 283 (1940).

[43] W. Feller, *Introduction to Probability Theory and Its Applications* (John Wiley & Sons, New York, NY, 1950).

[44] P. Mörters and Y. Peres, *Brownian Motion* (Cambridge University Press, Cambridge, UK, 2010).

[45] J. Y. Yen and M. Yor, *Paul Lévy's Arcsine Laws* (Springer International Publishing, Cham, 2013), pp. 43–54.

[46] S. N. Majumdar, J. Randon-Furling, M. J. Kearney, and M. Yor, On the time to reach maximum for a variety of constrained Brownian motions, J. Phys. A **41**, 365005 (2008).

[47] S. N. Majumdar and J. P. Bouchaud, Optimal time to sell a stock in the black-scholes model: Comment on "Thou shalt buy and hold," by A. Shiryaev, Z. Xu, and X. Y. Zhou, Quant. Finance **8**, 753 (2008).

[48] J. Randon-Furling and S. N. Majumdar, Distribution of the time at which the deviation of a Brownian motion is maximum before its first-passage time, J. Stat. Mech. (2007) P10008.

[49] S. N. Majumdar, Universal first-passage properties of discrete-time random walks and Lévy flights on a line: Statistics of the global maximum and records, Physica A **389**, 4299 (2010).

[50] G. Schehr and P. Le Doussal, Extreme value statistics from the real space renormalization group: Brownian motion, Bessel processes, and continuous time random walks, J. Stat. Mech. (2010) P01009.

[51] K. J. Hochberg and E. Orsingher, The arcsine law and its analogs for processes governed by signed and complex measures, Stoch. Proc. App. **52**, 273 (1994).

[52] J. Pitman and M. Yor, Arcsine laws and interval partitions derived from a stable subordinator, Proc. London Math. Soc. **s3-65**, 326 (1992).

[53] P. Carmona, F. Petit, and M. Yor, Some extensions of the arcsine law as partial consequences of the scaling property of Brownian motion, Prob. Theo. Rel. Fields **100**, 1 (1994).

[54] J. Lamperti, An occupation time theorem for a class of stochastic processes, Trans. Am. Math. Soc. **88**, 380 (1958).

[55] M. Barlow, J. Pitman, and M. Yor, Une extension multidimensionnelle de la loi de tare sinus, in *Siminaire de Probabilites XXIII* (Springer, Berlin, 1989), pp. 294–314.

[56] N. H. Bingham, and R. A. Doney, On higher-dimensional analogues of the arcsine law, J. App. Prob. **25**, 120 (1988).

[57] P. A. Ernst and L. Shepp, On occupation times of the first and third quadrants for planar Brownian motion, J. Appl. Prob. **54**, 337 (2017).

[58] D. Charles and W. Rosemarie, The arcsine law and the treasury bill futures market, Financ. Anal. J. **36**, 71 (1980).

[59] J. Baz and G. Chacko, *Financial Derivatives: Pricing, Applications, and Mathematics* (Cambridge University Press, Cambridge, UK, 2004).

[60] A. Clauset, M. Kogan, and S. Redner, Safe leads and lead changes in competitive team sports, Phys. Rev. E **91**, 062815 (2015).

[61] K. J. Wiese, S. N. Majumdar, and A. Rosso, Perturbation theory for fractional Brownian motion in presence of absorbing boundaries, Phys. Rev. E **83**, 061141 (2011).

[62] M. Delorme and K. J. Wiese, Maximum of a Fractional Brownian Motion: Analytic Results from Perturbation Theory, Phys. Rev. Lett. **115**, 210601 (2015).

[63] M. Delorme and K. J. Wiese, Extreme-value statistics of fractional Brownian motion bridges, Phys. Rev. E **94**, 052105 (2016).

[64] M. Delorme and K. J. Wiese, Perturbative expansion for the maximum of fractional Brownian motion, Phys. Rev. E **94**, 012134 (2016).

[65] M. Delorme, A. Rosso, and K. J. Wiese, Pickands' constant at first order in an expansion around Brownian motion, J. Phys. A **50**, 16LT04 (2017).

[66] M. Delorme, Stochastic processes and disordered systems, around Brownian motion, Ph.D. thesis, PSL Research University, 2016.

[67] K. J. Wiese, First passage in an interval for fractional Brownian motion, Phys. Rev. E **99**, 032106 (2019).

[68] M. Arutkin, B. Walter, and K. J. Wiese, Extreme events for fractional Brownian motion with drift: Theory and numerical validation, Phys. Rev. E **102**, 022102 (2020).

[69] T. Sadhu, M. Delorme, and K. J. Wiese, Generalized Arcsine Laws for Fractional Brownian Motion, Phys. Rev. Lett. **120**, 040603 (2018).

[70] M. Kac, On distributions of certain Wiener functionals, Trans. Am. Math. Soc. **65**, 1 (1949).

[71] J. Zinn-Justin, *Quantum Field Theory and Critical Phenomena* (Oxford University Press, Oxford, 1989).

[72] R. B. Davies and D. S. Harte, Tests for Hurst effect, Biometrika **74**, 95 (1987).

[73] A. B. Dieker, Simulation of fractional Brownian motion, Ph.D. thesis, University of Twente, 2004.

[74] B. Walter and K. J. Wiese, Monte Carlo sampler of first passage times for fractional Brownian motion using adaptive bisections: Source code, retrieved from https://hal.archives-ouvertes.fr/hal-02270046hal-02270046 (2019).

[75] B. Walter and K. J. Wiese, Sampling first-passage times of fractional Brownian motion using adaptive bisections, Phys. Rev. E **101**, 043312 (2020).

[76] A. Dhar and S. N. Majumdar, Residence time distribution for a class of Gaussian Markov processes, Phys. Rev. E **59**, 6413 (1999).

[77] D. B. Owen, Orthant probabilities, in *Wiley StatsRef: Statistics Reference Online* (American Cancer Society, Atlanta, GA, 2014).

[78] See Supplemental Material at http://link.aps.org/supplemental/10.1103/PhysRevE.104.054112 for a mathematica notebook which describes certain steps to evaluate the expression for $\mathcal{F}_2$.

[79] S. N. Majumdar and A. Comtet, Airy distribution function: From the area under a Brownian excursion to the maximal height of fluctuating interfaces, J. Stat. Phys. **119**, 777 (2005).

[80] J. F. Coeurjolly, Simulation and identification of the fractional Brownian motion: A bibliographical and comparative study, J. Stat. Softw. **05**, i07 (2000).

[81] A. T. A. Wood and G. Chan, Simulation of stationary Gaussian processes in $[0, 1]^d$, J. Comput. Graph. Stat. **3**, 409 (1994).